

University of Montana

ScholarWorks at University of Montana

Graduate Student Theses, Dissertations, &
Professional Papers

Graduate School

2003

Structure and petrology of Windermere age intrusions in the northern Rocky Mountains

Erik W. Burtis

The University of Montana

Follow this and additional works at: <https://scholarworks.umt.edu/etd>

Let us know how access to this document benefits you.

Recommended Citation

Burtis, Erik W., "Structure and petrology of Windermere age intrusions in the northern Rocky Mountains" (2003). *Graduate Student Theses, Dissertations, & Professional Papers*. 7184.
<https://scholarworks.umt.edu/etd/7184>

This Thesis is brought to you for free and open access by the Graduate School at ScholarWorks at University of Montana. It has been accepted for inclusion in Graduate Student Theses, Dissertations, & Professional Papers by an authorized administrator of ScholarWorks at University of Montana. For more information, please contact scholarworks@mso.umt.edu.

**Structure and Petrology of Windermere Age Intrusions in the Northern Rocky
Mountains**

By

Erik W. Burtis

B. S., Mary Washington College, 1996

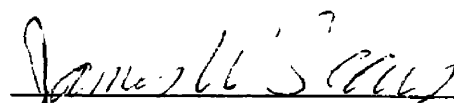
Presented in partial fulfillment of the requirements for the degree of

Master of Science

University Of Montana

2003

Approved by:


Chairperson


Dean, Graduate School

1-6-04
Date

UMI Number: EP37985

All rights reserved

INFORMATION TO ALL USERS

The quality of this reproduction is dependent upon the quality of the copy submitted.

In the unlikely event that the author did not send a complete manuscript and there are missing pages, these will be noted. Also, if material had to be removed, a note will indicate the deletion.



UMI EP37985

Published by ProQuest LLC (2013). Copyright in the Dissertation held by the Author.

Microform Edition © ProQuest LLC.

All rights reserved. This work is protected against unauthorized copying under Title 17, United States Code



ProQuest LLC.
789 East Eisenhower Parkway
P.O. Box 1346
Ann Arbor, MI 48106 - 1346

Structure and Petrology of Windermere Age Intrusions in the Northern Rocky Mountains

Director: James W. Sears

jws

Mafic intrusions within the Mesoproterozoic Belt-Purcell basin of the Northern Rocky Mountains of Montana record important Mesoproterozoic and Neoproterozoic rifting episodes. Previous studies established three major igneous intrusive events. This project focuses on sills and dikes that represent a fourth intrusive event, and establishes their regional extent and relationship to late Proterozoic Windermere rift activity.

These sills and dikes intruded Archean basement rock and the middle Proterozoic formations of the Belt-Purcell Supergroup. They are truncated at the western margin of the basin and are unconformably overlain by Cambrian Flathead Sandstone. When restored on a palinspastic map, the thickest and deepest segments of the sills, along with dike swarms in western Montana and northern Wyoming, are co-linear with the basin axis. The sills and dikes fall on the eastern margin of an en echelon pattern delineated by Windermere rock exposures along the margins of the Laurentian craton.

The sills and dikes are tholeiitic diabase and have locally undergone low-grade metamorphism and alteration. Granophyre is associated with some sills. Geochemical analysis, while not conclusive, is compatible with a single intrusive event. Belt-Purcell xenoliths found in the granophyre show some signs of interaction with the magma, and trends in major and trace elements indicate possible crustal contamination during intrusion.

A preliminary U-Pb zircon age of 763 ± 12 Ma date obtained from granophyre sampled near Rogers Pass, Montana, strongly correlates with the earlier argon dates of previous studies, which indicates the sills have not surpassed the reset temperature of the argon system. This date approximates the Gunbarrel magmatic event (780 Ma) and earliest Windermere rift activity. Recent dates of Windermere rocks in Idaho suggest a westerly shift of the rift axis to establish the eventual western margin of Laurentia.

Windermere-related rocks occur in British Columbia, Washington, and Idaho, but are absent in Montana. The dikes and sills may represent earliest Windermere rift activity and comprise the only such rocks in Montana. Because of this relationship, this study refers to these sills and dikes as the Windermere intrusive group or Windermere sills and dikes.

Table of Contents

Acknowledgements	iv
List of Tables	v
List of Figures	vi
Introduction	1
The Belt-Purcell Basin	2
Magmatism and Rift Zones	6
Large Igneous Provinces	8
Magmatism in the Belt-Purcell Basin	9
Previous Work – Belt-Purcell Intrusive Episodes	10
Plains Sill	10
Purcell-Nichol Creek Lavas	11
Salmon River Intrusives	12
Neoproterozoic Sills and Dikes (Windermere Intrusive Group)	13
Previous Work – Windermere Intrusive Group	13
Northwestern Montana	14
Northern Wyoming	19
Sample Locations	21
Rogers Pass-Wolf Creek Area	24
Milltown-Bonner-Turah	31
Holland Lake	36
McDonald Reservoir	41
Alberton	45
Kootenai National Forest	48
Structure	50
U-Pb Dates	55
Methods	56
Results	57
Geochemical Analysis	58
Methods	58
Geochemical Results	61
Discussion and Conclusions	78
References	84
Appendix I	95
Appendix II	104

Acknowledgments

I would like to thank many people for supporting my graduate school endeavor, including my committee members Jim Sears, Don Hyndman, and Paul Wilson. Their advice was invaluable and their office doors always open. Thanks to Dr. K. Chamberlain at the University of Wyoming and the Washington State University GeoAnalytical Laboratory for analyses. This project would not have been possible without the financial support of the National Science Foundation and the Tobacco Root Geological Society. Thanks also to the Geological Society of America and the Department of Geology at The University of Montana for providing funds for presenting my work at various geological meetings.

In addition, I would like to thank Brian Collins and Michael Hoffman for their help throughout this project and the rest of the Geology graduate students at Montana for their support and enthusiasm. Special thanks are extended to David Curbishley for indirectly introducing me to the field of geology, my wife, Martha, for encouraging me to enter graduate school, and her unwavering support, and to my parents and family for their interest and support of my endeavors.

List of Tables

Sample MT-AI-02 (Alberton)	96
Sample MT-AE-01 (Alberton)	96
Sample MT-KF-01 (Kootenai National Forest)	97
Sample MT-KF-02 (Kootenai National Forest)	97
Sample MT-KF-03 (Kootenai National Forest)	98
Sample MT-MR-01 (McDonald Reservoir)	98
Sample MT-MR-02 (McDonald Reservoir)	99
Sample MT-RPE-04 (Rogers Pass East)	99
Sample MT-RPE-22 (Rogers Pass East)	100
Sample MT-RPM-01 (Rogers Pass Middle)	100
Sample MT-RPM-02 (Rogers Pass Middle)	101
Quartz Sample Blank	101
Granophyre Sample MT-TU-01 (Turah)	102
Granophyre Sample MT-HL-13 (Holland Lake)	102
Granophyre Sample RP-KRC-02-2 (Rogers Pass East)	103
Table 1. XRF data	105
Table 2. ICP-MS data	107
Table 3. Electron microprobe data (plagioclase)	109
Table 4. Electron microprobe data (pyroxene)	111
Table 5. Geochemical data from Eisenbeis (1958)	115
Table 6. Geochemical data from Schmidt (1978)	116
Table 7. Geochemical data from Mueller (1971)	116

List of Figures

Figure 1. Locations of the Belt-Purcell exposures in the western U. S.	1
Figure 2. Block diagram showing structural development of Belt-Purcell basin	3
Figure 3. Major units and formations of the Belt-Purcell Supergroup	4
Figure 4. Block diagram showing Belt-Purcell basin in relation to Laurentia and unknown western craton	5
Figure 5. Belt-Purcell basin in relation to the strontium 0.706 isopleth	5
Figure 6. Mount Moran and Christmas lake dikes and Wolf Creek sill	14
Figure 7. Location of Milltown dam sill	15
Figure 8. Location of Bonner sill	15
Figure 9. Wolf Creek sill	19
Figure 10. Sample sites	22
Figure 11. Sample sites along section lines	23
Figure 12. Sill locations at Rogers Pass	25
Figure 13. Sample site RPM (Rogers Pass)	26
Figure 14a. Exposure of two lower sill contacts (RPM)	26
Figure 14b. Exposure of two lower sill contacts (RPM)	27
Figure 15. Pigeonite lamellae in augite (from Rogers Pass sample)	28
Figure 16. Collection points for RPM	28
Figure 17. Trace of RPE sill to Wolf Creek site	29
Figure 18. Sample locations at RPE	30
Figure 19. Granophyre exposed at RPE	31
Figure 20. Sill exposure near Milltown dam	32
Figure 21. Sill exposure near Bonner	33
Figure 22. Sill exposure at Turah	34
Figure 23. Granophyre exposed at Turah	35
Figure 24. Graphic and micrographic textures seen in thin section of Turah granophyre sample	35

Figure 25. Location of sill at Holland Lake	36
Figure 26. Graphic texture seen in thin section of Holland Lake sample	37
Figure 27. Perthitic texture seen in thin section of Holland Lake sample	38
Figure 28. Cliff exposure of sill at Holland Lake	39
Figure 29. Xenoliths in cliff exposure at Holland Lake	39
Figure 30. Xenoliths at Holland Lake outcrop (close-up)	40
Figure 31a. Top view of xenolith found in Holland Lake sample	40
Figure 31b. Bottom view of xenolith found in Holland Lake sample	41
Figure 32. Sill location at McDonald Reservoir	42
Figure 33. Sill exposure at McDonald Reservoir	42
Figure 34. Possible granophyre boulder from McDonald Reservoir	43
Figure 35. Two xenoliths in possible granophyre boulder found at McDonald Reservoir	44
Figure 36. Possible location of potential granophyre at McDonald Reservoir	44
Figure 37. Sill location near Alberton	45
Figure 38. Sill exposure near Alberton	46
Figure 39. Micrographic texture seen in thin section from Alberton sample	47
Figure 40. Dike exposure near Alberton	48
Figure 41. Sill location in the Kootenai National Forest	49
Figure 42. Sill exposure in the Kootenai National Forest	49
Figure 43. Minimum thickness of Windermere sills on a palinspastic map	52
Figure 44. Minimum depth of Windermere sills on a palinspastic map	53
Figure 45. Schematic cross-section of the Belt-Purcell basin showing potential sill and dikes intrusion paths	53
Figure 46a. Map of Windermere-related rock exposures	54
Figure 46b. An en echelon pattern in the Windermere-related rock exposures	54
Figure 47. Location and ages of Windermere-related rocks	55

Figure 48. Geochronology results from U-Pb analysis	58
Figure 49. REE spidergram	62
Figure 50. Rock/chondrite normalized spidergram	62
Figure 51. Ba vs. Rb graph	63
Figure 52. Ba vs. Zr graph	63
Figure 53. Nb/Y vs. Zr/Y graph	64
Figure 54. Total alkali vs. SiO ₂ graph	65
Figure 55. Na ₂ O/K ₂ O vs. SiO ₂ graph	67
Figure 56. CaO vs. SiO ₂ graph	67
Figure 57. TiO ₂ vs. SiO ₂ graph	69
Figure 58. TiO ₂ vs. Al ₂ O ₃ graph	69
Figure 59. TiO ₂ vs. MgO graph	70
Figure 60. Al ₂ O ₃ vs. MgO graph	70
Figure 61. CaO vs. MgO graph	71
Figure 62. Na ₂ O vs. MgO graph	71
Figure 63. SiO ₂ vs. MgO graph	72
Figure 64. Total alkalis vs. silica graph (microprobe)	73
Figure 65a. TiO ₂ vs. SiO ₂ graph (microprobe)	73
Figure 65b. CaO vs. SiO ₂ graph (microprobe)	73
Figure 66a. Al ₂ O ₃ vs. TiO ₂ graph (microprobe)	74
Figure 66b. Al ₂ O ₃ vs. MgO graph (microprobe)	74
Figure 66c. TiO ₂ vs. MgO graph (microprobe)	74
Figure 66d. TiO ₂ vs. MgO graph (microprobe)	74
Figure 67a. LIL/HFS spidergram with Plains sill	76
Figure 67b. Rock/chondrite spidergram with Plains sill	76
Figure 68. Total alkalis vs. SiO ₂ graph with Plains sill	77
Figure 69a. TiO ₂ vs. SiO ₂ graph with Plains sill	77
Figure 69b. TiO ₂ vs. MgO graph with Plains sill	77

Introduction

The purpose of this study is to determine the age, extent, and tectonic significance of a set of mafic sills within the Belt-Purcell basin of northwestern Montana (Figure 1). The Mesoproterozoic Belt-Purcell basin dominates the Northern Rocky Mountains of Montana. It has been the focus of many geologic studies due to its economic ore deposits as well as its significance for the tectonic history of the northwestern United States. The stratigraphy, structures, and areal configuration of the basin record important Mesoproterozoic (1600-900 Ma) and Neoproterozoic (900-570 Ma) rifting events. Mesozoic and Cenozoic orogenic and extensional events have exposed the Belt-Purcell Supergroup over 130,000 sq. km (Obradovich and Peterman, 1968; Lyons et al., 2000). The evolution of the basin spanned from approximately 1500 to 1350 Ma (Winston, 1993; Anderson and Parrish, 2000; Lydon 2000; Evans et al., 2000). Approaching 18 km in thickness, the Belt-Purcell Supergroup comprises thick units of quartzite, argillite, and argillaceous carbonate (Winston, 1986; Ross et al., 1992; Winston, 1993). The nomenclature of the Belt-Purcell Supergroup is under revision (Winston, 2003).

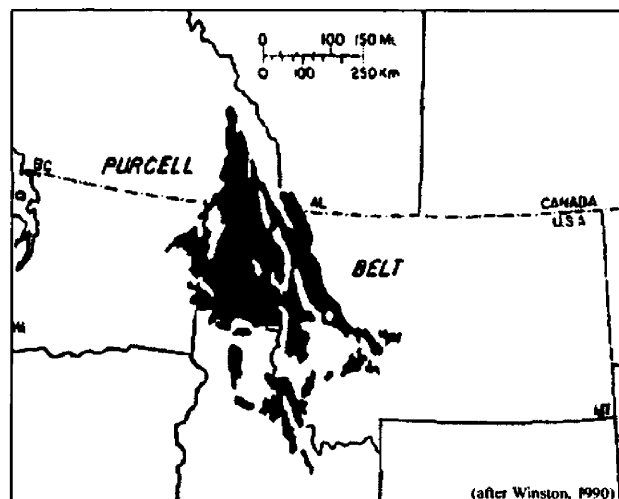


Figure 1. The locations of Belt-Purcell exposures in the western U. S. (after Winston, 1990).

The Belt-Purcell Basin

The tectonic environment of the Belt-Purcell basin is complex and not fully understood. Many theories have been proposed for the tectonic setting of the basin including, intracratonic basin (Walcott, 1910, 1914, 1916; Winston, 1990), marine miogeocline (Price 1964), epicratonic basin (Fenton and Fenton, 1937; Ross, 1963), and impact basin (Sears and Alt, 1989). Harrison (1972) supported the marine miogeocline theory, but this concept does not fully explain the westerly-derived sediments within the Belt-Purcell basin (Winston, 1990). According to Winston (1990, 1993), the Belt-Purcell basin most likely was a failed intracontinental rift basin, as indicated by the westerly-derived sediments and many sedimentary features that argue for a nonmarine depositional environment. Nd isotopic and detrital zircon studies show the source of most of the sediments did not come from North America (Frost and Winston, 1987; Ross et al., 1992) and implies a landmass to the west (present-day coordinates) of the basin (Winston, 1990). Lyons et al. (2000) studied sulfur geochemistry in the Newland Formation of the Lower Belt-Purcell Supergroup and found that, at least during early development, the Belt-Purcell basin may have been a restricted marine environment that was periodically open to seawater. While the debate continues about the tectonic setting of the Belt-Purcell basin, a recent detailed paleo-continental reconstruction (Sears and Price, 2003) supports the theory of the basin being a closed intracratonic rift basin between Laurentia and Siberia that episodically opened to a nearby seaway.

The controls of the basin formation were block-faulting and subsidence (Winston, 1993). Three west-trending extensional faults and one or more northwest-trending faults appear to have broken the Proterozoic crust into five blocks. Four of these blocks then

subsided to form the Belt-Purcell basin (Figure 2) (Winston, 1986). The western margin of the basin was tectonically more active than the eastern side; the sediment that came from the west thins from west to east; minor sediment came from the east and south (Winston, 1986; Ross and Villeneuve, 2003). On the eastern side of the basin, deposition of sediments covered Archean and Proterozoic continental crust (Winston, 1993). Sedimentation within the basin occurred on vast alluvial aprons, sand flats, playas, and perennial lakes (Winston, 1993). Researchers have subdivided the Belt-Purcell Supergroup stratigraphically into four major units, the lower Belt, Ravalli Group, Middle Belt Carbonate, and Missoula Group (Figure 3) (Ross et al., 1992).

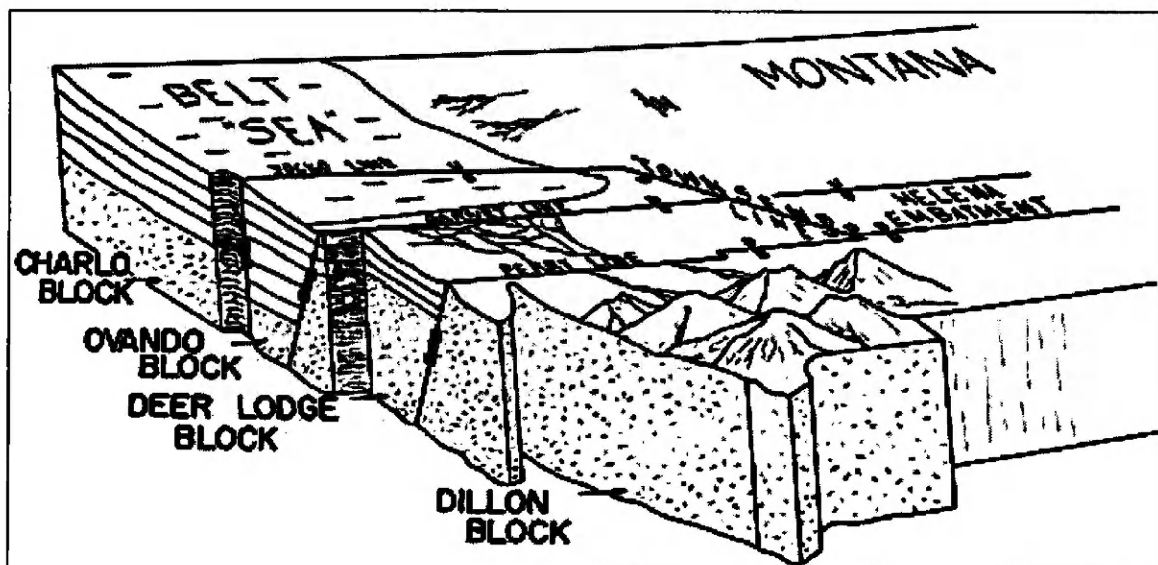


Figure 2. Block diagram showing structural development of Belt-Purcell basin (Winston, 1986).

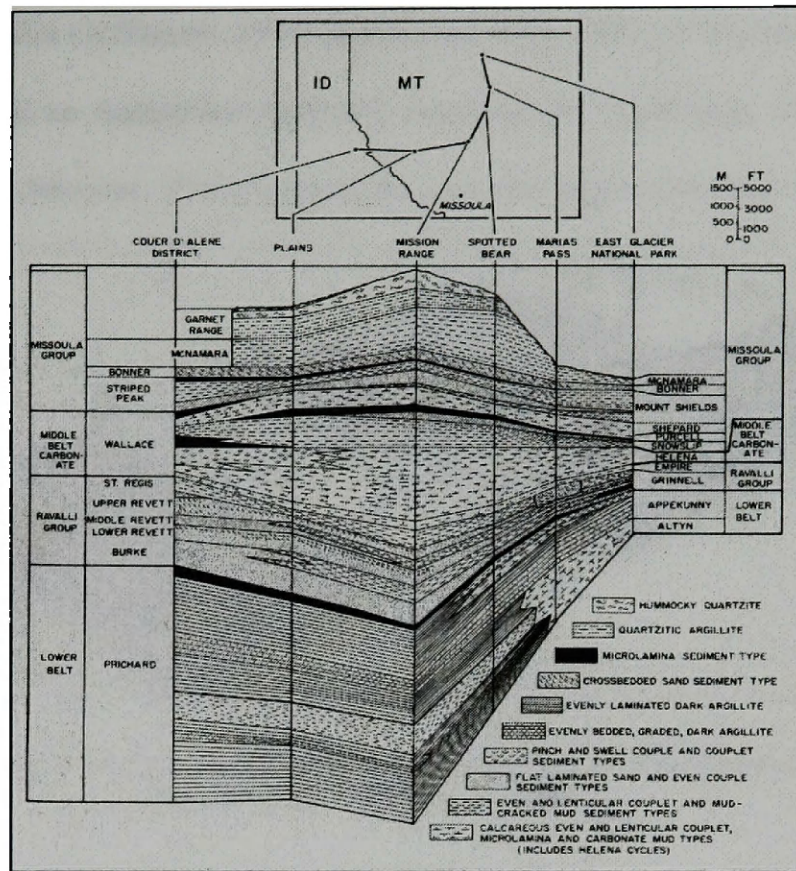


Figure 3. Major units and formations of the Belt-Purcell Supergroup (Winston, 1989).

Structurally, continental crust on the north, east, and south sides of the basin (Winston, 1993) is thought to have been a part of a Mesoproterozoic supercontinent. To the west was an unknown “western craton” (Figure 4). The Belt-Purcell Supergroup crops out east of the initial strontium 0.706 isopleth, which marks the western edge of thick Precambrian crust (Figure 5) (Ross and Villeneuve, 2003). After Belt-Purcell deposition ceased, during the opening of the Paleo-Pacific Ocean, tectonic processes removed the western sediment source for the basin (Ross et al., 1992; Ross and Villeneuve, 2003). The identification of this source area has become the subject of great interest and debate as its identification would lay the foundation for determining plate positions in the Mesoproterozoic and the reconstruction of Rodinia. The current theories

variously place Australia (Jefferson, 1978; Karlstrom et al., 2001), Siberia (Sears and Price, 1978, 2003), and an Antarctica-Australia combination (Jefferson, 1978; Dalziel, 1991; Hoffman, 1991; Moores, 1991) against the western edge of the basin.

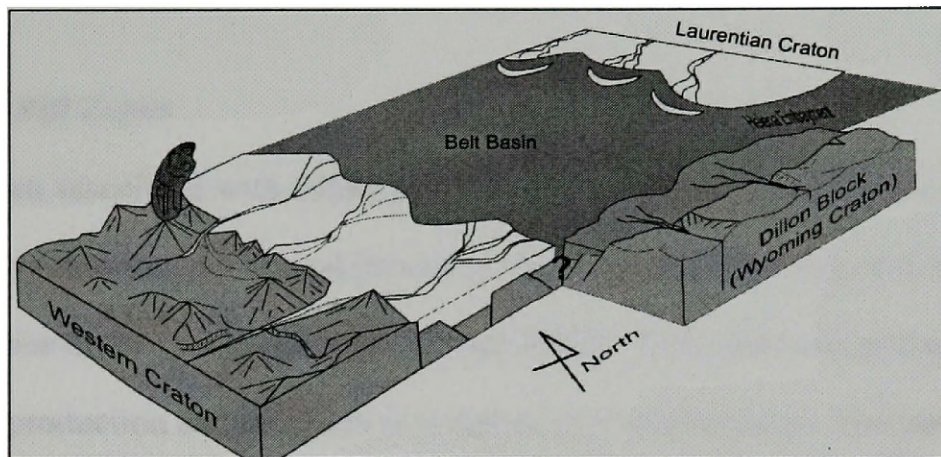


Figure 4. Block diagram showing Belt-Purcell basin in relation to Laurentia and unknown western Craton (After Ross and Villeneuve, 2003).

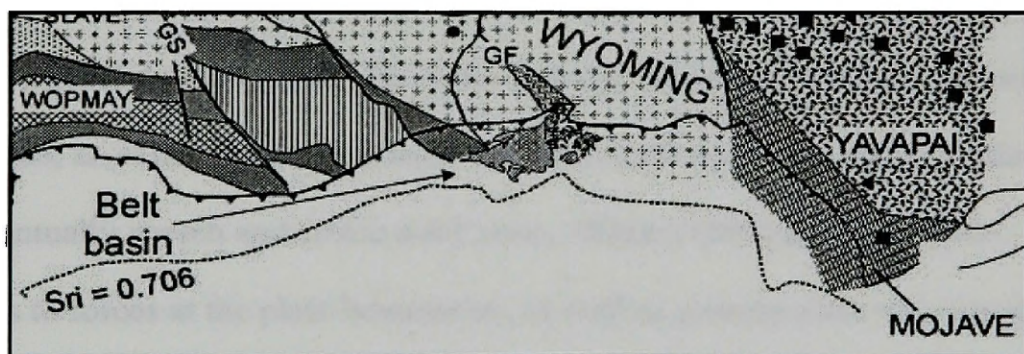


Figure 5. Belt-Purcell basin in relation to the initial strontium 0.706 isopleth (After Ross and Villeneuve, 2003).

Lingering questions about the formation of the Belt-Purcell basin and the identity of the western landmass require further studies. Examination of the Proterozoic igneous intrusions within the basin may provide answers to many of these questions. Dates obtained from igneous rock can help constrain timing and rate of sedimentation, subsidence curves, and tectonic history. Recognition of relationships between

sedimentary units and igneous bodies can also provide additional information about the history of the basin. Piercing points created from igneous bodies split during continent separation are an important tool for reconstructions (c.f. Wingate, 1998).

Magmatism and Rift Zones

Magmatism associated with rifting and the subsequent breakup of continents has been an extremely important geological process in the history of the Earth and the focus of numerous studies in the past (Ernst and Buchan, 2000). Two main competing models describe magma production and intrusion in zones of crustal extension. The passive model (Courtney and White, 1986; White and McKenzie, 1989) attributes continental rifting to the stresses and strains within a continental plate. Bott (1992) suggests that local stresses within the interior of a plate may result from activity along the plate margins, chiefly at subduction zones. He states that if a supercontinent has opposing subduction zones, an extensional stress regime would result within the supercontinent that would eventually stretch and create a rift zone. White (1992) also attributes localized stress to forces at the plate boundaries, as well as general plate movement. No matter what the cause, initiation of extension within a continent and the resulting thinning of the crust produces adiabatic melting within the upper mantle creating a small upwelling or plume (White and McKenzie, 1989; White, 1992). The plume domes the overlying lithosphere, increasing the rate of extension and enhances the adiabatic melting of the asthenosphere (Keen, 1987; Coffin and Eldholm, 1994). With further melting, emplacement of magma within the rift heats the lithosphere, making it more ductile. This system, at first, is dependent on initial extension in the lithosphere, but becomes

codependent on feedback from the resulting plume for continued rifting and plate separation. The amount of magma produced simply depends on the rate of initial rifting, its size, and the nature of the resulting plume.

The “active” model suggests that mantle plumes drive the extension regime (Wilson, 1963; Morgan, 1971, 1981). As a mantle plume develops, whether from deep within the mantle or from shallower depths, it applies pressure on the lithosphere as it rises. Heat and stress transferred from the plume to the base of the lithosphere, lifts the crust, which begins to extend and thin (Coffin and Eldholm, 1994). The thinning of the crust results in adiabatic melting that enhances magma production in the athenosphere. Long-lived plumes result in continued extension and continental separation. In some circumstances, migratory occurrences of extensive magmatism are related to continental break-up (Coffin and Eldholm, 1992). Ernst and Buchan (2000) and Dalziel et al. (2000) proposed that mantle plumes played an active role in plate fragmentation and formation of continental rifts and ocean basins during the breakup of Pangea. Although igneous bodies often comprise some portion of rift structures, their volumes and distribution are not consistent (Zehnder et al., 1990). The amount of igneous material associated with a rift depends on the activity of the plume and rate of crustal thinning.

It may be true that both models are correct and what mechanism actually occurs simply depends on the initial environment. Clarification of these processes requires further studies. The structural and geochemical data collected during this project may assist others working on Neoproterozoic rifting in northwestern North America.

Large Igneous Provinces

Large igneous provinces (LIPs) result from significant magmatic emplacement and are often found in rift zones. Unfortunately, there is no clear definition for the size of LIPs (Coffin and Eldholm, 1992). Ideally, the basis of the definition would depend on the amount of magma emplaced over a specific period of time. Due to the fact that a large percent of their volume is located up to a few kilometers beneath the surface and is inaccessible, extensive dating of LIPs has not taken place (Coffin and Eldholm, 1992, 1994). LIPs are principally massive accumulations of mafic extrusive rock, underlain by intrusive rock, and result from processes other than “normal” seafloor-forming activities (Coffin and Eldholm, 1994). They are second in global volume only to basalts and other intrusive rocks produced at spreading centers and can extend over hundreds or thousands of square kilometers and approach a few thousand cubic kilometers in volume (Coffin and Eldholm, 1994). They are found in many geologic environments, including spreading centers, triple junctions, oceanic lithosphere, passive margins, and cratons (Coffin and Eldholm, 1994). In general, LIPs are thought to result from a mantle plume invading the base of the lithosphere followed by adiabatic melting of atypically hot, upwelled athenosphere (White and McKenzie, 1989; Dalziel et al., 2000). Coffin and Eldholm (1992) suggest that, in terms of volume, emplacement of LIPs occur at a greater rate than present-day mid-ocean ridge systems due to the plume activity.

Studies analyzing the geochemistry of LIP rocks indicate that their source lies in the upper to lower mantle with some regional differences due to mantle heterogeneities and contamination from the crust (Coffin and Eldholm, 1992). Three factors control the volumes of LIPs, the intensity of the plume within the mantle, ease with which the

athensphere can intrude the lithosphere, and the rate at which the plate travels over the source (Coffin and Eldholm, 1992, 1994). The latter does not appear to be as important an influence as structures within the lithosphere; i.e. fracture zones and rifts which may act as channels for magma (Coffin and Eldholm, 1994). While not all rifts are associated with LIPs, they seem to be prevalent during continent separation (Ernst and Buchan, 2000). Alt et al. (1988) and Dalziel et al. (2000) noted that LIPs frequently preceded formation of continental rifts and ocean basins during the breakup of Pangea. Ernst and Buchan (2000) and Dalziel et al. (2000) further suggest that the presence of LIPs at Archean and Proterozoic craton margins indicate that this phenomenon occurred throughout Earth history.

Magmatism in the Belt-Purcell Basin

The Belt-Purcell basin contains abundant mafic intrusions, which are a significant feature that can provide valuable data when analyzing the tectonic history of the basin (Harrison, 1972). These intrusions cut Belt-Purcell rock from the lower-Belt Prichard Formation to the Garnet Range Formation (Winston, 1993), and occurred during discrete episodes, most likely related to extensional tectonics within the basin (Chamberlain et al., 2003). Sills are the dominant mafic intrusive form in eastern Washington, northern Idaho, and northwestern Montana (Winston, 1993). They are comprised of mostly of basalt and some contain granophyric regions or caps (Winston, 1993; Poage, 1997; Poage et al., 2000). Sills intruded the Belt basin from the earliest stages of basin development, and there appear to be four mappable major sill complexes (Sears et al., 1998; Price and Sears, 2000). The geometry of the developing basin seems to have controlled the

emplacement of the earliest sill structures (Burtis et al., 2003a, 2003b). This project focuses on the fourth, or youngest, sill complex and establishes its regional extent and origin as well as linking this event to early Neoproterozoic Windermere rifting.

Previous Work - Belt-Purcell Basin Intrusive Episodes

Plains Sill

The initial set of sills intruded the lower Belt-Purcell Supergroup (Prichard and Aldridge Formations). Twenty-five to thirty-five percent of the thickness of the lower Belt-Purcell comprises mafic sills, which reach a cumulative thickness exceeding 2 km (Cressman, 1989, Winston, 1993). The Plains sill crops out in the Prichard Formation near Perma and Plains, Montana. It consists of 150-300 m thick high-iron tholeiite diabase that is geochemically congruent with melting large volumes of mantle material associated with intracratonic rifting (Poage et al., 2000). Mafic sills comprise approximately ten to twenty-one percent of the Prichard Formation in this area (Cressman, 1985, 1989). Wide areas of granosediment, along with soft-sediment deformation and sedimentary ovoid-structures, occur adjacent to the sills (Höy, 1989; Poage et al., 2000). Buckley and Sears (1993) and Höy (1989) suggest emplacement occurred during sedimentation, based on the sill complex association with syn-sedimentary faulting, sediment boiling, mud diapirism, and black-smoker SEDEX deposition; all indicators that the surrounding rocks were unconsolidated and retained a significant amount of water during sill emplacement. Poage et al. (2000) describe miarolitic cavities present in a granophyre layer, which caps the sill, suggesting a shallow

depth of intrusion. These sills form regular seismic reflectors that indicate an approximately constant stratigraphic depth parallel to the Purcell anticlinorium for greater than 300 km along strike (Cook and Van der Velden, 1995).

Mineralogically, hornblende, which was the result of hydrothermal metamorphism that occurred during crystallization and cooling, dominates the Plains sill and is surrounded by a matrix of fine-grained plagioclase and a minor amount of quartz (Poage et al., 2000). Although approximately equal amounts of clinopyroxene and plagioclase typically characterize diabase, the Plains sill lacks evidence of primary clinopyroxene (Poage et al., 2000). Approximately 150 m of granophyre, originated from the magma, caps the sill in some locations. Biotite comprises twenty-percent of the granophyre along with near equal amounts of anhedral quartz, plagioclase and fine-grained plagioclase-quartz intergrowths (Poage et al., 2000).

U-Pb dating methods on zircon have determined crystallization dates of 1469 ± 2.5 Ma for the Plains Sill and 1455 ± 2.0 Ma for the underlying Paradise Sill (Sears et al., 1998). They are related to the Moyie sills, which comprise thirty percent of the Aldridge Formation in southeastern British Columbia (Höy, 1989), and the Purcell sills, which make up about thirty percent of the Prichard Formation near Crossport, Idaho (Bishop, 1973). Sears et al. (1998) and Poage et al. (2000) use this evidence to suggest that this intrusive episode occurred throughout the basin.

Purcell-Nichol Creek Lavas

The 1443-Ma Purcell-Nichol Creek lavas of Glacier/Waterton National Park and vicinity (U-Pb dated by Evans et al., 2000) and associated dikes represent the second,

next to oldest, mafic complex. Five meters of Snowslip Formation lie between the lower intrusions and the surface flows, which are interbedded with siltite beds of the Snowslip Formation in the vicinity of Glacier National Park (McGimsey, 1985). Near the surface, contacts between the dikes and country rock show signs of being intruded before lithification, and emplacement appears to have occurred from the north (McGimsey, 1985). The mineralogy of the complex is unique and has undergone low-grade metamorphism. Geochemically, the lava flows are very similar to the composition of the underlying dikes. Mejstrick (1975) characterized these intrusions as originally alkaline, which is an indicator of faulting associated with renewed rifting within the basin.

Salmon River Intrusions

Evans and Green (2003) mapped the rocks of the third episode, which intruded the southern part of the Belt-Purcell basin in central Idaho. The diabase sills, which cut the Yellow Jacket Formation and have partially been metamorphosed into the amphibolite facies, are associated with 1370 Ma porphyritic granite (Evans, 1981; Evans and Green, 2003). Mineralogically they consist of forty to seventy percent hornblende, twenty to fifty percent plagioclase, five to forty percent biotite, and trace amounts of quartz (Evans and Green, 2003). Evans (1981) interprets these rocks as originally subophitic diabase based on the percentages of relic pyroxenes, primary hornblende, and plagioclase. Using U-Th-Pb and Rb-Sr dating techniques, Evans (1981) acquired ages of 1371 ± 6 Ma and 1167 ± 63 Ma, respectively. However, the Rb-Sr data is not reliable due to metamorphism and an assumption that the intrusions originated in the mantle. Doughty and Chamberlain (1996) used U-Pb mass spectrometry dating techniques on

zircons from these intrusions to obtain an age of 1379 ± 1 Ma for the diabase, which is similar to the 1371 ± 7 Ma date obtained for the associated granites (Evans and Zartman, 1990). This set of sills contains a large layered mafic intrusion exposed along the Salmon River and is associated with subsidence that was initiated by renewed rifting (Evans and Zartman, 1990; Doughty and Chamberlain, 1996). This suggests that the main rift axis of the Belt-Purcell basin propagated to the south (Burtis et al., 2003a, 2003b).

Neoproterozoic Sills and Dikes (Windermere Intrusive Group)

The fourth and most recent intrusive episode is the subject of this study. Projects focusing on the sills and dikes of this system have been sporadic and no work has been done to correlate the individual sill and dike exposures throughout the basin. This intrusive episode occurred during Neoproterozoic time after sedimentation ceased in the Belt-Purcell basin and is probably not related to the development of the basin. It is more probable that these sills and dikes are associated with early phases of Neoproterozoic Windermere rifting. Therefore, this study identifies the fourth intrusive episode as the Windermere sill and dike system or Windermere intrusive group.

Previous Work – Windermere Intrusive Group

The few previous investigations focusing on the Windermere intrusive group were limited, for the most part, to reconnaissance investigations. Correlation of the sills and dikes in this region only used K-Ar and Ar-Ar dating and general descriptions of mineralogy. Harlan et al. (1997) studied the ages and geochemistry of associated dike swarms in northern Wyoming (Figure 6). This data is compared to the data provided by

this study in an attempt to establish the regional extent of the Montana sills. This information will be very useful for analysis of Precambrian plate positions as well as tectonic events that initiated the break-up of the Proterozoic supercontinent, Rodinia; namely the Windermere rifting event.

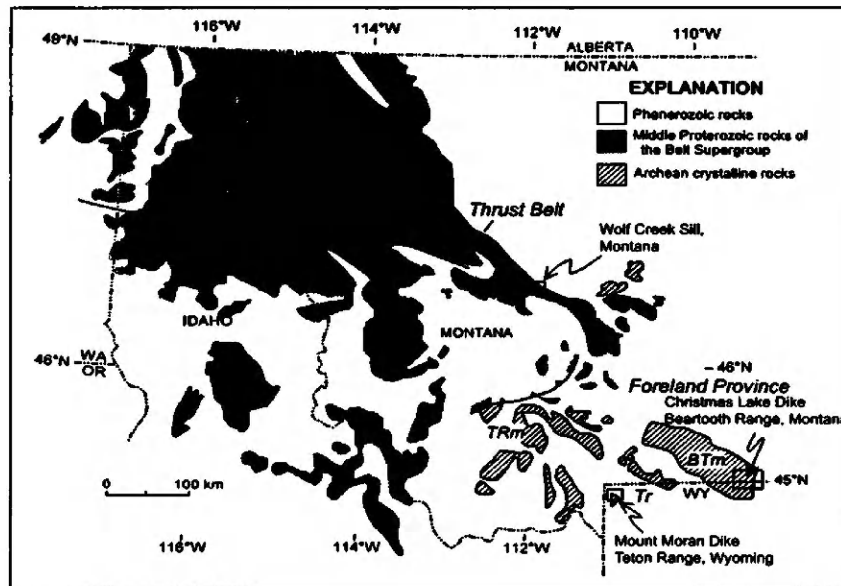


Figure 6. Mount Moran and Christmas Lake dikes and Wolf Creek sill sampled by Harlan et al., (1997) (after Harlan et al., 1997).

Northwestern Montana

Work on these sills in northwestern Montana was previously limited almost exclusively to reconnaissance projects sponsored by the U. S. Geological Survey and Montana Bureau of Mines and Geology. Ross et al. (1955) located some of the larger sills on their geologic map of Montana, but researchers did not attempt detailed studies until Eisenbeis (1958) conducted a study of a sill near Milltown, approximately 10 km east of Missoula. A cliff face exposes this sill on the southern side of the Milltown dam, at the confluence of the Blackfoot and Clark Fork Rivers (Figure 7). Eisenbeis analyzed, in detail, the petrology and mineralogy of this sill and established it

as a normal tholeiite with diabase texture. This study also analyzed the geochemical composition of the sill (Appendix II, Table 5). Based on similarities in mineralogy, Eisenbeis suggested a relationship between the Milltown dam sill and several other diabase outcrops within a 20 km radius of Missoula, including a sill near Bonner (Figure 8). Nelson and Dobell (1961) described a granophyre found at some sill outcrops that appeared to be related to the intrusive bodies in the Milltown area.

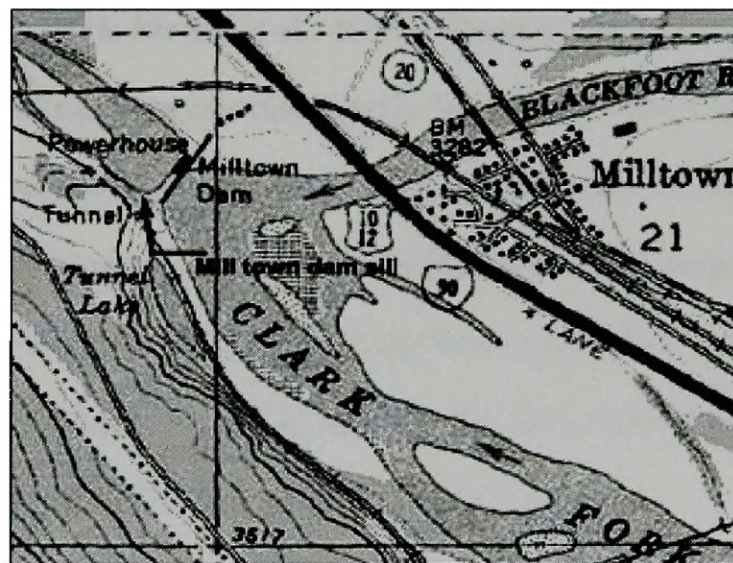


Figure 7. Location of Milltown dam sill.

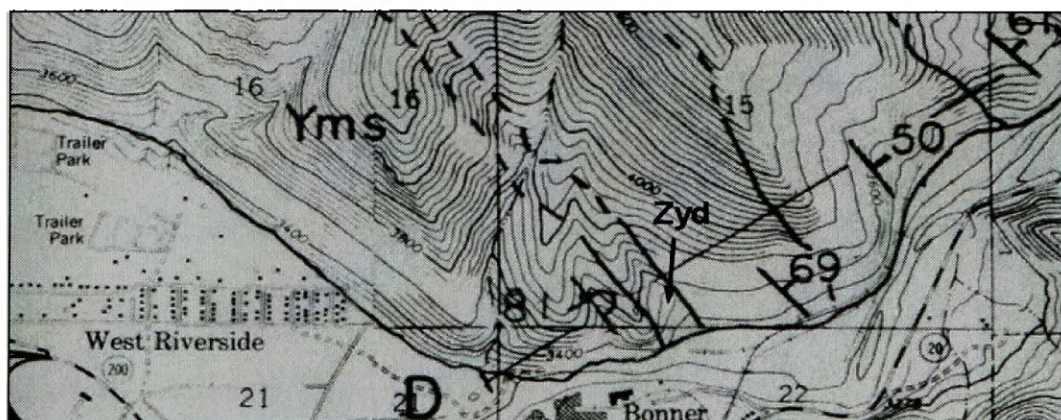


Figure 8. Location of Bonner sill "Zyd"(Watson, 1984).

Nelson and Dobell (1961) described the sills in the Milltown/Bonner area while mapping for the U. S. Geological Survey. After analyzing thin sections obtained “sporadically” during fieldwork, Nelson and Dobell suggested that the sills were related to other sills in northwestern Montana. In the attempt to correlate these sills with other diabase intrusions in Montana, Nelson and Dobell compared the mineralogy with descriptions provided by other workers (Daly, 1912; Calkins and Emmons, 1915; Fenton and Fenton, 1937; Deiss, 1943; Mertie et al., 1951). Researchers have since shown that some of these sills, including those associated with the Purcell/Nichol Creek lavas (Daly, 1912; Fenton and Fenton, 1937), are separate formations. Because of their lack of age data for any of the sills in Montana, Nelson and Dobell proposed several possible ages for these rocks, specifically intrusion during Belt-Purcell time, post Belt-Purcell sedimentation but pre-deformation of Belt-Purcell rocks, Laramide or post-Laramide orogenic events, and possibly intruding during Mesozoic time.

Based on a poor exposure of a dike apparently connecting with a lava flow, Mejstrick (1975) suggested that consanguinity existed between the sill and dike set in Glacier National Park and the Purcell/Nichol Creek lavas. McGimsey (1985) found the dike is not geochemically compatible with the Purcell lava, but is very similar to the sill described by Mejstrick. In addition, McGimsey describes an exposure where this dike cuts the Purcell lava and concludes that the dike and sill are younger than the flows. Hunt (1962) dated the sill at 1075-1110 Ma using K-Ar methods on associated hornfels in the country rock because direct dating of the sill and dike is difficult due to the high degree of alteration. Harlan et al. (2003) K-Ar dated a similar sill that intruded the Siyeh

Formation in Canada at 797-796 Ma. It is possible that these sills are part of the fourth intrusive episode.

According to Mejstrick (1975), the thickest section of the Glacier Park sill lies near Siyeh Pass. With minor exceptions, the Siyeh limestone confines the sill and both the upper and lower contacts are sharp and show no deformation due to sill intrusion (Mejstrick, 1975). Associated feeder dikes to the sill however, have deformed the surrounding rock in some locations, such as at the Cracker Lake and Otokomi dikes (Mejstrick, 1975).

The mineralogy of the Glacier Park sill is unusual. Plagioclase and pyroxene compose seventy percent of the sill with the remaining thirty percent comprised mostly of alkali feldspar, quartz, hornblende, and opaque minerals (Mejstrick, 1975). The sill has incorporated abundant xenoliths, comprised mostly of an albite-alkali feldspar variety and a dolomite ± calcite-epidote variety. Based on the abundance of diffusion bands around the xenoliths, Mejstrick (1975) attributes the unusual mineralogical composition to the assimilation of the xenoliths during intrusion, creating percentages of plagioclase and alkali feldspar-quartz that are higher than typical diabase.

This sill also has granophyre present in some exposures. However, unlike the granophyre near Milltown, the granophyre associated with this complex may not be a product of differentiation of the diabase. Observations made by Mejstrick (1975) indicate that the granophyre is an aggregate of xenoliths and diabase and is the result of the assimilation of the xenoliths. Alkali feldspar and quartz, found mostly in graphic intergrowths and altered plagioclase, dominate the mineralogy of the granophyre. With

the exception of a few local anomalies the granophyre associated with the sill becomes less abundant where the sill thins (Mejstrick, 1975).

Determination of the age of the Milltown and associated sills began in the early 1960's when Obradovich and Peterman (1968) used K-Ar methods to date a sill, possibly related to the Milltown intrusion, at 760 Ma in the Alberton area. Mudge (1972) and Harrison (1972) used this and the date published by Hunt (1962) during their studies to constrain the timing of Belt-Purcell deposition. Neither author used the dates in conjunction with geochemical analysis to correlate sills across the Belt-Purcell basin. When mapping the geology of Montana, federal and state workers continued to use these dates and general mineralogy when both describing the sills and distinguishing between three recognized intrusive events. But they did not attempt to correlate individual sills on the map itself and all Precambrian sills were mapped as "Zd" or "ZYd" (Nelson and Dobell, 1961; Wells, 1974; Mudge et al., 1982; Harrison et al., 1986; Whipple et al., 1987; Harrison et al., 1992; Lewis, 1998). This resulted in local maps that show a general group of sills and dikes and make it very difficult to distinguish between separate intrusive events.

In Wood Canyon, approximately 35 km west of Augusta, a U. S. Geological Survey reconnaissance investigation noted a "diorite/gabbro" sill (Mudge et al., 1968). They proposed that this sill was the same age as those found in Alberton and Milltown, but their completed geochemical analysis never was used to correlate the sills due to a lack of data for the other sills (Mudge et al, 1968). Schmidt (1978) analyzed the gabbro sill near Wolf Creek (Figure 9) and suggested that, based on mineralogy, this sill closely resembled that of the Milltown and Alberton sills and was the same age. This study also

analyzed the geochemistry of the Wolf Creek sill (Appendix II, Table 6), unfortunately, as in 1968, there was little data available for comparison.

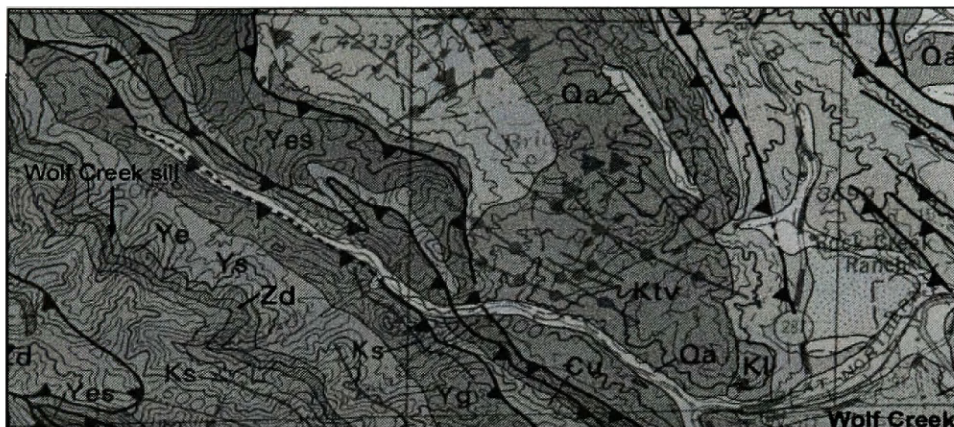


Figure 9. Wolf Creek sill “Zd” sampled by Schmidt (1978) in Wood Canyon. (map by Mudge et al., 1982).

Northern Wyoming

Research conducted in southern Montana and northern Wyoming coincided with the early work in northwestern Montana. The work focused specifically on a tholeiitic dike swarm that intruded Archean basement rocks in the Beartooth Mountain range (Prinz, 1964; Mueller 1971, et al., 1973; Harlan et al., 1997). When analyzing the petrography and field relations of the mafic intrusions, Prinz (1964) recognized four intrusive events of varying ages with unique TiO_2 contents for each event. Condie et al. (1969) proposed ages of 2500 Ma, 1900 to 2200 Ma, 1400 to 1800 Ma, and 700 to 1000 Ma as potential periods of intrusion. Mueller (1971) examined these dikes in terms of their geochemistry (Appendix II, Table 7) and geochronology (Figure 6). He verified that each age group was chemically unique, but also that each group had similarities. All of the groups showed depletion of Sr, a low average Al_2O_3 content, low K/Rb ratio, high

Rb/Sr ratio and non-overlapping TiO₂ amounts (Mueller, 1971). The youngest group of dikes produced a K-Ar age of 700 Ma, which falls in the youngest age range inferred by Condie et al. (1969). In 1973, there was an additional study, which used x-ray fluorescence to analyze the geochemical composition of the Beartooth mafic rocks. This study divided the dikes, based on TiO₂ content, into groups I, II, III, and then sub-divided group III into groups III and IIIA based on SiO₂, MgO, and Sr values (Mueller and Rogers, 1973). Groups III and IIIA still had unique TiO₂ ranges after being subdivided (Mueller and Rogers, 1973). Samples taken from the chilled or very fine-grained portions of the Christmas Lake dike provided a K-Ar date of 740 ±32 Ma for group IIIA. This date is close, within error, to the 700 Ma date obtained by Mueller (1971) for the same sill, and corresponds to the K-Ar date of 780 Ma obtained by Hanson and Gast (1967) from another dike in the group (Baadsgaard and Mueller, 1973).

In 1997, Harlan et al. conducted a study to correlate the youngest sills and dikes in Montana with a dike swarm in northwestern Wyoming and south-central Montana. This study examined the ⁴⁰Ar-³⁹Ar age and paleomagnetic data from a dike in the Beartooth Range, a dike in the Teton Range, and one sill located near Wolf Creek, Montana (Figure 9). Geochronologic results from this study produced a ⁴⁰Ar-³⁹Ar age of 769 ±5 Ma for the Mount Moran dike (Teton Range), 774 ±4 Ma for the Christmas Lake dike (Beartooth Range), and 776 ±5 Ma for the sill near Wolf Creek (Harlan et al., 1997). An additional study by Harlan et al. (2003), dated the Christmas Lake dike at 779 ±3.0 Ma using Pb ratios in baddeleyite, and recalculated the Mount Moran and Wolf Creek sill ages of Harlan (1997) using a revised international hornblende standard (MMhb-1) at 772 Ma and 779 ±5 Ma, respectively.

The paleomagnetic data from the Mount Moran and Christmas Lake dikes yielded similar virtual geomagnetic poles (VGP) for each dike, which also corresponds to the VGP from dikes in the southern Tobacco Root Mountains, Montana, and dikes located in the Mackenzie Mountains, northwestern Canada (Harlan et al., 1997). U-Pb dates from the Tobacco Root dikes range from 776 ± 4.6 Ma to 781.7 ± 3.8 Ma (Harlan et al., 2003), while LeCheminant and Heaman (1994) U-Pb dated the Mackenzie dikes at 779 Ma. Late Cretaceous-Early Tertiary tectonic interference with the paleomagnetic record prevented sampling the Wolf Creek sill for paleomagnetic analysis. Based on their analysis, Harlan et al. (1997, 2003) concluded that these late Proterozoic dikes and sills were part of a 780 Ma regional magmatic event.

It is within this context that the present study examines the Neoproterozoic sills and dikes to determine their extent in northwestern Montana, their possible relationship with Windermere rifting and regional magmatism within Laurentia, and possible use as a piercing point for Precambrian continental plate reconstruction.

Sample Locations

This study examined seven sites and used previously published data for four other locations to analyze the structure, geochemistry, and geochronology of sills and dikes comprising the Windermere intrusive group, the youngest mafic system in the Belt-Purcell basin of northwest Montana. The primary sampling sites in Montana, located at Alberton, Milltown, Turah, Rogers Pass, McDonald Reservoir, Holland Lake, and the Kootenai National Forest (Figure 10) can be located on several U. S. Geological Survey and Montana Bureau of Mines and Geology $1^\circ \times 2^\circ$ geologic quadrangle maps (Mudge et

al., 1982; Harrison et al., 1986; Harrison et al., 1992; Lewis, 1998). Hand samples and structural data were collected from Milltown, but geochemical data from this site came from Eisenbeis (1958). Wolf Creek data was obtained from Schmidt (1978), and data for the Beartooth dikes came from Mueller, 1971). Together, these sites create an east-west section across the trend of exposures of the Windermere intrusive group and a northwest-southeast section along the trend (Figure 11). Samples for U-Pb zircon dating were collected at Rogers Pass, Turah, and Holland Lake because these sites expose a significant amount of granophyre. All sites provided structural and geochemical data. GPS coordinates for each sample site are listed in the appendices.

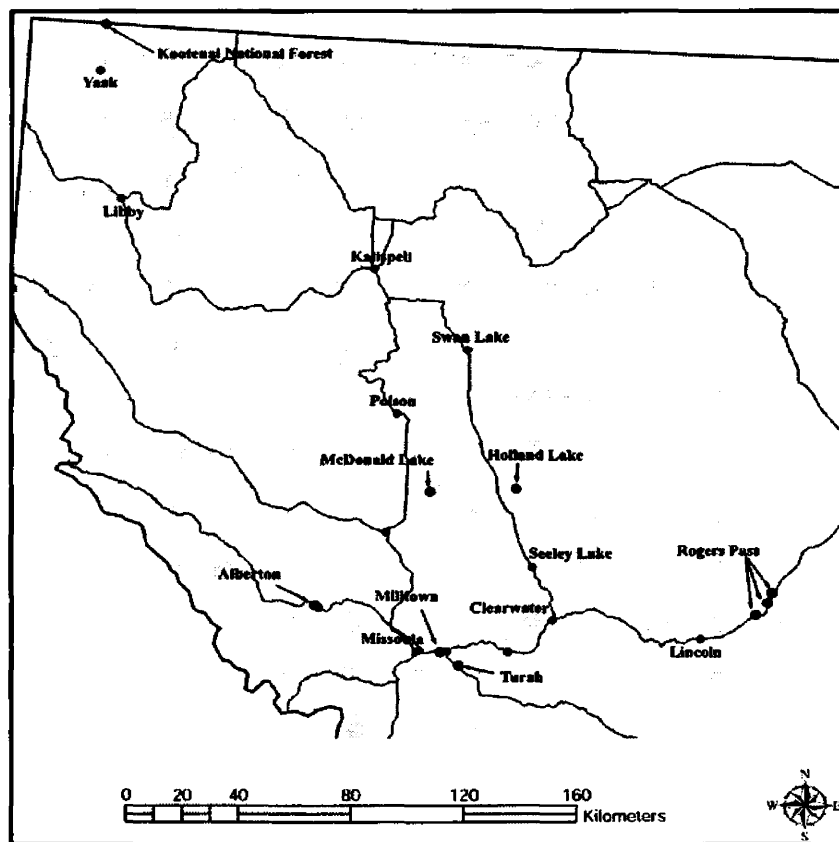


Figure 10. Sample sites for this study. All sites located on this map with GPS coordinates using ArcGIS.

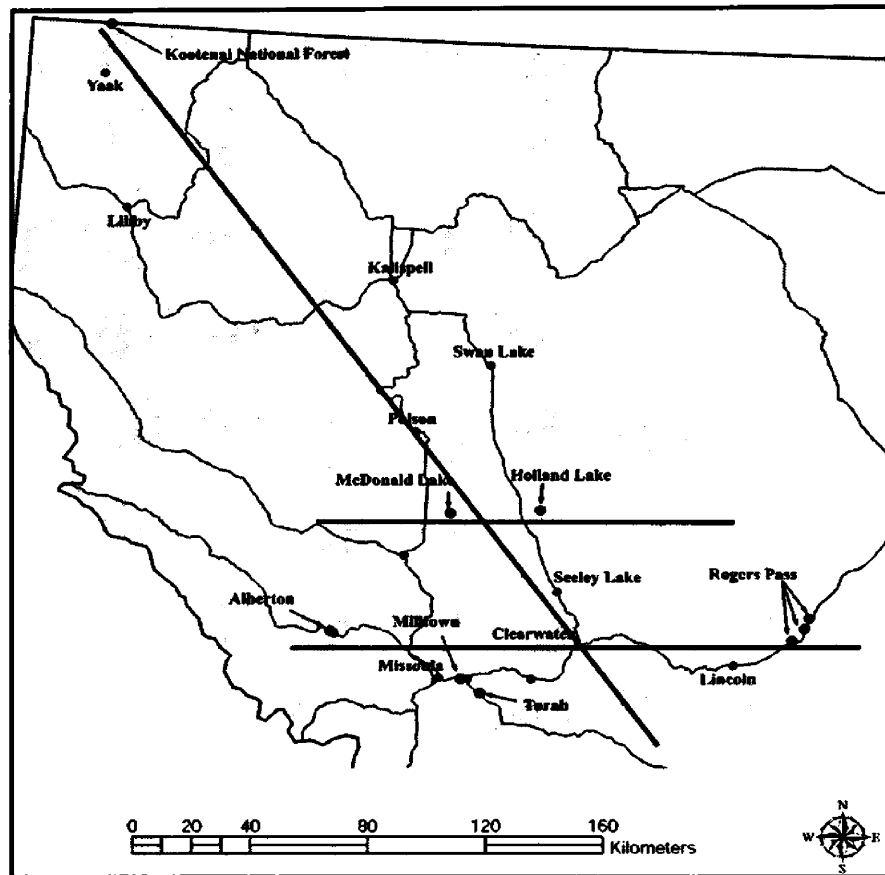


Figure 11. The sample sites are located on east-west and northwest-southeast sections across the trend of sill and dike exposures.

In Montana, most of the intrusions of this system are sills, except in the Ninemile area where a dike swarm intruded the Belt-Purcell Supergroup. Most sites have a single sill that occupies a single horizon, although sills may jump formations between sites. According to previous work (see above section) they may represent exposures of a single sill now segmented by faulting and erosion. The Windermere intrusive group, in general, consists of diabase, dominated by sub-equal amounts of pyroxene and plagioclase. Accessory minerals include hornblende, biotite, apatite, quartz, and several alteration minerals. Chilled margins are generally very fine-grained and extend several centimeters into the sill. These zones grade into fine-grained zones that are several meters wide, which in turn abut medium-grained zones that are typically only three to four meters

wide. The zones of medium-grain size then grade into coarse-grained zones, which compose the interior of the sills. As the grain size increases, the percentage of pyroxene declines, and plagioclase increases, along with the accessories. Hornblende and biotite are mostly absent in the very fine and fine-grained areas of the sill. However, because they increase in both size and abundance with grain size towards the centers of the sills, they most likely formed during late-stage cooling and/or low-grade metamorphism. Only large exposures of thick sills contain all zones. Each exposure, however, contains a fine-grained zone.

Rogers Pass-Wolf Creek Area

Two thrust plates expose sections of a Neoproterozoic sill in the Rogers Pass-Wolf Creek area (Figure 12). A cliff exposes the westernmost sill (MT-CC) on the north side of Highway 200, near the junction with Mike Horse Creek Road (N 47° 02' 36.0", W 112° 24' 89.3"). At this location, the sill intruded the Spokane Formation. Thickness could not be determined directly for this site, but a thickness of 125 m was inferred from a cross-section drawn farther to the north (Mudge et al., 1982). Located in the hanging wall of the Hoadley thrust, the outcrop consists of fractured, dark grey, coarse-grained diabase. Some iron staining is present around grains. No major veins occur at this location. Large plagioclase, pyroxene, and amphibole grains are present on fresh surfaces. Alteration was limited, although some chlorite and epidote are present.



Figure 12. Sill locations “Zd” near Rogers Pass. Sample site indicated by arrows. (map after Mudge et. al, 1982).

The second exposure (MT-RPM) lies to the north of Hwy 200 approximately 2.5 km to the east of Rogers Pass (N 47° 05' 13.6", W 112° 22' 14.6") in the hanging wall of the Hoadley thrust as mapped by Winston (1986) (Figure 13). This sill intrudes the Spokane Formation and is faulted several times. The lower contact is exposed twice within a 15 m section (Figure 14a and b). Another feature of this outcrop is an Eocene dike that cuts through the sill (Figure 13). Because of the faults, thickness cannot be determined for this site. However, a thickness of 150 m was interpolated from the same cross-section used at MT-CC.



Figure 13. Sample site RPM, 2.5 km east of Rogers Pass (dark rock). The large light grey rock in the middle of the photo is an Eocene dike that has intruded this sill. Another, smaller Eocene intrusion can be seen above the truck.



Figure 14a. The two lower contacts (arrows) exposed at sample site RPM north of hwy 200, near Roger Pass. Note truck for scale.



Figure 14b. Two lower contacts (black lines) exposed at sample site RPM, near Rogers Pass.

The sill is very fractured and is dark grey to black. Actinolite and epidote are present on fracture surfaces and malachite is present near the Eocene dike. The sill is very fine-grained a few centimeters from the lower contact. Grain size increases to fine and medium away from the contact and, approximately 20 m from the contact, the sill becomes coarse-grained. In hand specimen, greyish-black fresh surfaces contain grains of plagioclase and pyroxene, and iron staining occurs along fractures.

Thin sections from the fine-grained section show low-grade metamorphism, with minor amounts of epidote, chlorite, and hornblende. Sub-equal amounts of equigranular plagioclase and pyroxene are present; the pyroxene consists of both augite and pigeonite grains. Pigeonite lamellae are present in many augite grains (Figure 15). Some plagioclase is saussuritized and some pyroxene is uralitized. Other minerals include magnetite/ilmenite intergrowths (some with limonite rims), quartz, and apatite. Plagioclase dominates the groundmass, which is rich in alteration minerals, such as epidote and chlorite. Fractures lined with limonite occur in sample MT-RPM-01.

Although alteration occurs throughout the specimens, bands of total alteration occur that do not appear to be related to fractures. Samples MT-RPM-01 and MT-RPM-02 are from the fine-grained section of the sill near the lower contact (Figure 16) (Appendices A and B).

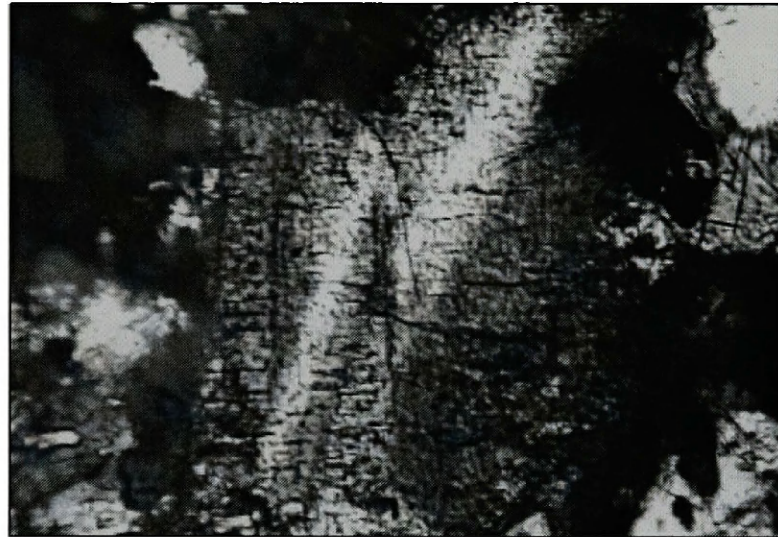


Figure 15. Pigeonite lamellae (light bands) in Augite grain from a Rogers Pass sample. Augite grain is 1.25 mm across.



Figure 16. Collection points for samples MT-RPM-01 and MT-RPM-02.

The eastern most exposure (RPE) lies in the hanging wall of the Steinbach thrust on the north side of Hwy 200 (N 47° 07' 22.4", W 112° 21' 03.3"), and can be traced on the Choteau 1° x 2° geologic quadrangle map southeast to an area near Wolf Creek (Figure 17) (Mudge et al., 1982). Schmidt (1978) studied the sill near Wolf Creek and the present study uses his geochemical data (Appendix II, Table 6). The sill intrudes the Empire Formation at this location. Near the poorly exposed contacts, the sill is fractured to the point that only pebble-size pieces could be collected, and is rusty and dark grey. No large veins are present. Actinolite and epidote are absent from fracture surfaces.



Figure 17. The trace of a sill "Zd" from sample site RPE (north arrow) to the Wolf Creek site (south arrow). (Map by Mudge et al., 1982).

In hand sample, these rocks are slightly iron-stained, and fresh surfaces are a lighter grey than the weathered surfaces. Equigranular plagioclase and pyroxene (augite and pigeonite) are present in sub-equal amounts in thin section. Minor hornblende, biotite, quartz, magnetite/ilmenite intergrowths, epidote, and chlorite are present, mostly in the matrix. With the exception of magnetite/ilmenite, these minerals are most likely

alteration products or formed during late-stage cooling. Sericitization has affected most of the plagioclase while most of the pyroxene has heavily-uralitized cores. Some of the magnetite/ilmenite intergrowths have limonite rims. Micrographic textures are rare but present in sample MT-RPE-22. Samples MT-RPE-04 and MT-RPE-22 were collected from the fine-grained portion of this section (Figure 18) (Appendix I and II).



Figure 18. Sample locations at site RPE north of hwy 200. Samples were taken approximately 15 m apart.

This exposure contains granophyre throughout the outcrop (Figure 19). The granophyre is whitish-grey to pinkish-grey and is coarse-grained. It is not as fractured as the diabase and is fairly competent when struck with an eight-pound sledgehammer. The granophyre is not as coarse-grained as the granophyre at Turah and lacks epidote and actinolite veins. Plagioclase is almost 100 percent altered and only faint grain boundaries remain, with, in rare cases, original twin extinction preserved. Granophyre sample RP-03-01 contained a 1x2 mm dark, rounded xenolith, most likely of the diabase, with sharp boundaries with the granophyre. Over 45 kg were sampled for zircon dating (RP-KRC-02-2; Appendix I).



Figure 19. Granophyre (below black line where arrows point) at sample site RPE. Black line represents approximate contact of diabase and granophyre.

Milltown-Bonner-Turah

The exposures at Milltown, Bonner, and Turah, Montana appear to be a single sill cut by various faults associated with the Blackfoot thrust and Clark Fork-Ninemile fault (Figure 8). Therefore, they are described together in this section. This sill intrudes the Mount Shields Formation of the Missoula Group. Contacts, exposed at Bonner and Milltown dam, are sharp and distinct, indicating intrusion into lithified sedimentary rock.

The best exposure is located adjacent to the Milltown dam at the confluence of the Blackfoot and Clark Fork rivers (N 46° 52' 6.27", W 113° 54' 10.14"). Approximately 30 m thick, the sill crops out in a cliff on the south side of the Clark Fork River (Figure 20). Highly fractured and severely weathered, the sill strikes northwest and dips southeast (Eisenbeis, 1958). Hand samples are dark grey to black and have been heavily iron-

stained brown. Millimeter-scale actinolite and chlorite veins are associated with many of the fractures, although large-scale veins are not present. The sill is fine-grained near the contacts and medium-grained in the interior. Obtaining a large fresh surface was extremely difficult due to the fractured nature of the sill, but small fresh surfaces were dark grey and heavily veined with iron stains. Crystals of plagioclase and pyroxene occur on fresh surfaces. No samples were taken from this exposure for thin sectioning or geochemical analysis. Instead, this study uses Eisenbeis' (1958) geochemical data since it was this exposure that he examined (Appendix II, Table 5).

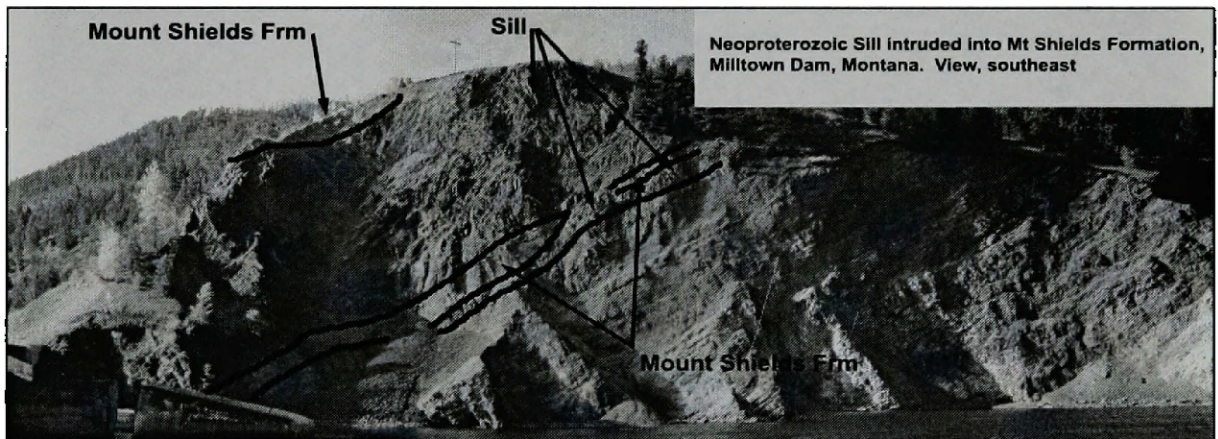


Figure 20. Sill exposure near the Milltown dam on the southern bank of the Clark Fork River. Cliff is about 60 m high.

A cliff west of the Blackfoot River and just north of Bonner, behind the Stimson Lumber yard exposes a sill near Bonner ($N 46^{\circ} 54' 33.47''$, $W 113^{\circ} 52' 12.12''$). Striking northwest, the sill is tilted vertically and only the lower contact is exposed (Figure 21). The thickness of the sill is approximately 140 m as determined from cross-sections by Nelson and Dobell (1961) and Watson (1984). Hand samples from this site are identical to the specimens obtained at the Milltown dam, although not as fractured. The sill can be traced across the river to a cliff on the east side of Highway 200 (Figure 8). The

Blackfoot fault cuts the sill at Hwy 200 and has highly deformed and metamorphosed the diabase to a greenschist (Sears and Clements, 2000). Large quartz veins cut the deformed sill and actinolite-chlorite-epidote formed on many fracture surfaces. Because this sill is related to the Milltown sill, analysis relies on the data from Eisenbeis (1958).

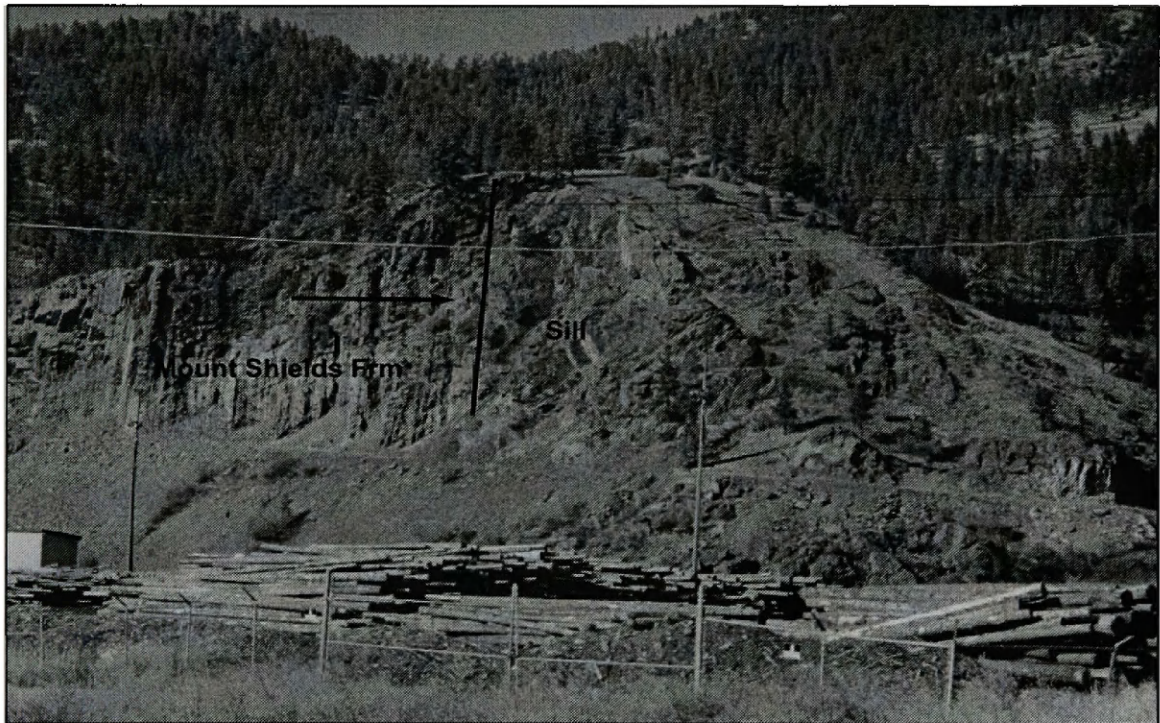


Figure 21. A sill at Bonner. The Mount Shields Fm is almost vertical at this location. Up section is in the direction of the arrow. Black line represents sill contact.

A cliff north of Highway 210 exposes a sill near Turah (N 46° 49' 39.13", W 113° 48' 20.32") (Figure 22). No strike, dip, or thickness measurements were possible due to the lack of exposed contacts. Like the sites at Bonner and Milltown, the medium-grained tholeiitic diabase is fractured, with multiple veins of actinolite on fracture surfaces. Iron staining is present and crystals of plagioclase and pyroxene are visible on fresh surfaces.

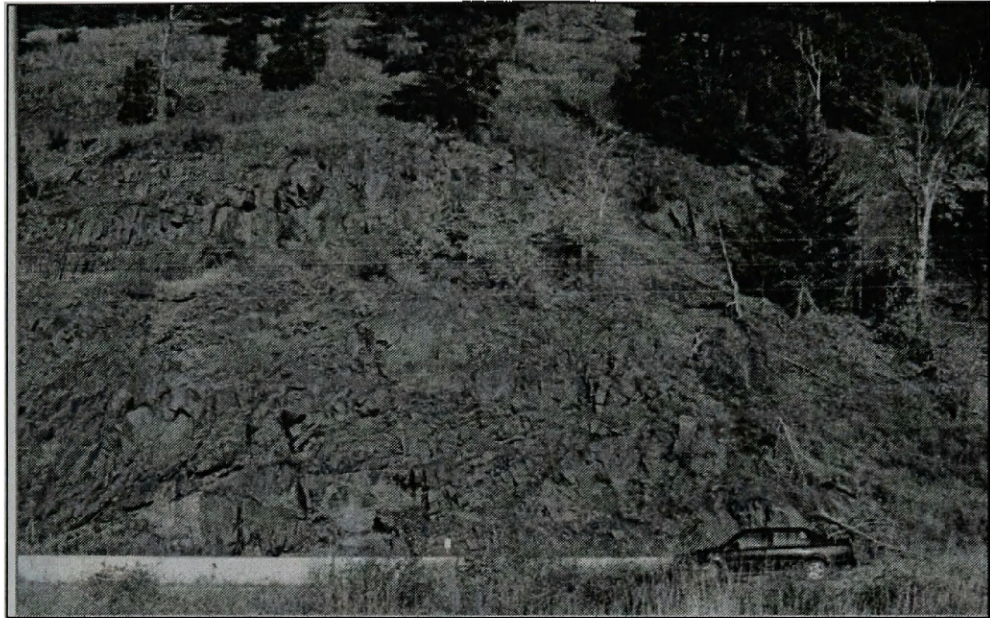


Figure 22. Sill location at Turah. No contacts are exposed in this photo. View is to the North.

The Turah location is unique in that it contains granophyre, which in some areas appears to commingle with the diabase, throughout the exposure (Figure 23). The lack of sill/country rock interaction, including wall rock xenoliths in the sills, indicates that the granophyre presumably was derived from the magma. Veins of epidote and actinolite 1-2 cm wide cut through the granophyre on fracture surfaces, although it is fractured less than the diabase. The granophyre is light grey to pinkish-white and in hand sample has large grains of plagioclase, some amphibole, quartz, and minor amounts of chlorite and epidote. In thin section, the plagioclase is altered almost entirely to clay minerals. Graphic intergrowths of quartz and feldspars and relic myrmekitic intergrowths of plagioclase and quartz are very common (Figure 24). The hornblende and epidote appear to be secondary alteration products. A few rare remnants of pyroxene are also present, but it is difficult to distinguish their type. Over 45 kg of granophyre (MT-TU-01) were collected for analysis of zircons (Appendix I).



Figure 23. Granophyre at Turah. Black line represents contact between diabase and granophyre. Note telephone pole at right for scale.

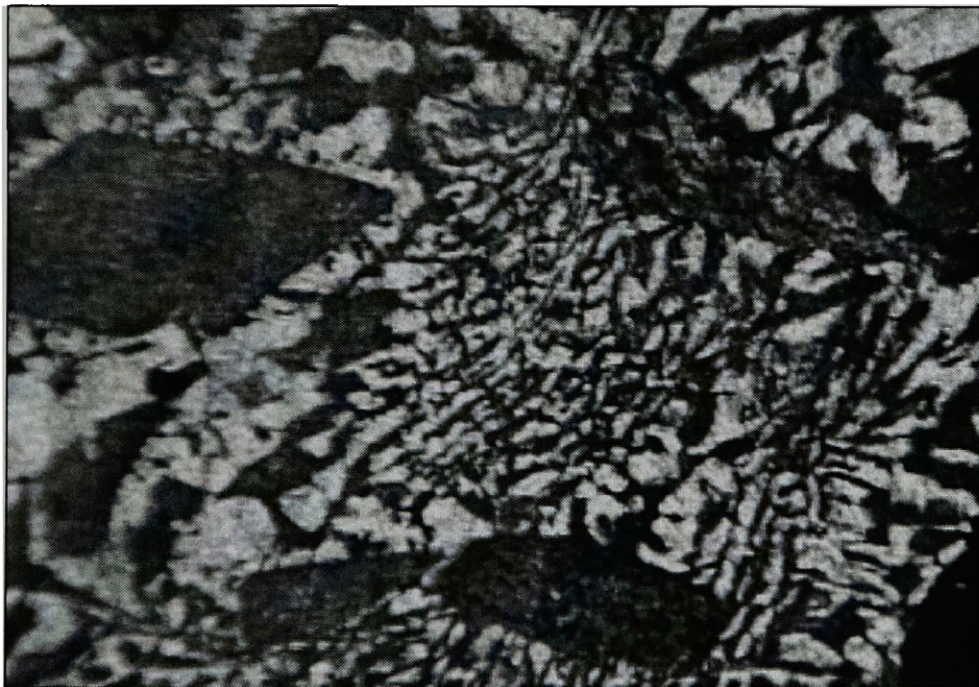


Figure 24. Graphic and micrographic textures from a Turah sample. View is 1.5 mm across.

Holland Lake

A sill lies in the footwall of the Swan Fault at the west end of Holland lake in the Swan Mountain Range (N 47° 24' 0.0", W 113° 34' 54") (Figure 25). The sill intruded the Helena Formation at this location but no contacts are exposed. At this location, the Helena Formation strikes north-northwest and dips east. The outcrop is not as well exposed in this glaciated terrain as at the previous sites because the area is forested heavily and there are no roadcuts. A spot where the Forest Service blasted a trail through the sill and a small cliff 70 m up from the trail are the best exposures, although Holland Creek cuts through the sill farther east down the trail. The sill at this location appears to be fractured less than at other sites.

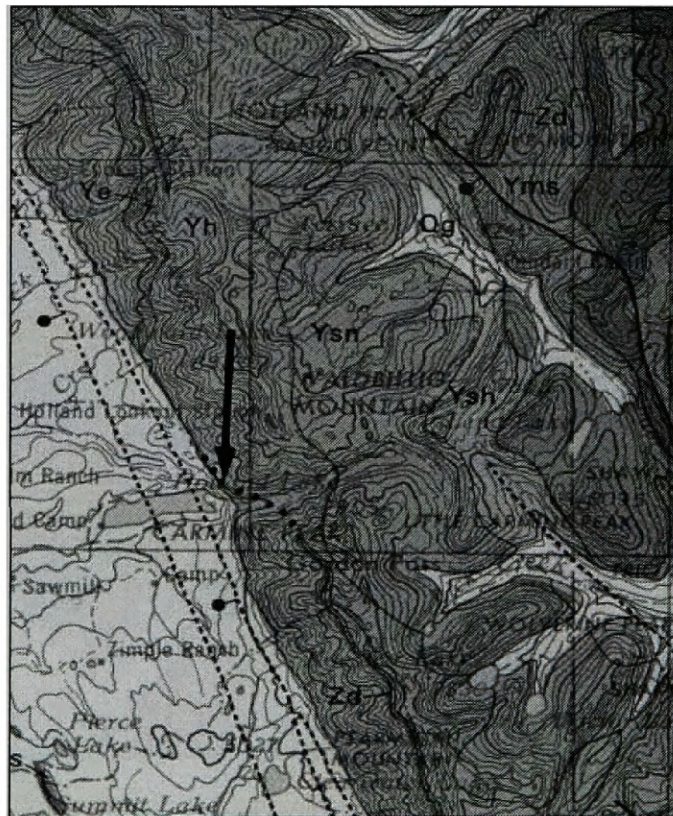


Figure 25. Sill location at Holland Lake. Sill exposure is dotted where it was not mapped. Arrow points to sample site. (map after Mudge et al., 1982).

The outcrop is very coarse-grained, and whitish to light grey in color. Hand samples show very little iron staining and no veins. Fresh surfaces are the same color as the outcrop and plagioclase is the most abundant mineral. Some float rocks are pinkish in color due to the presence of potassium feldspar. Thin sections show plagioclase grains with almost 100 percent alteration, quartz, fairly altered microcline grains, graphic and myrmekitic textures and perthitic intergrowths of alkali feldspar (Figure 26 and 27). Because the thin sections are very similar in appearance, mineralogy, and alteration to granophyre found at Rogers Pass and Turah, this site is presumably a large exposure of granophyre.

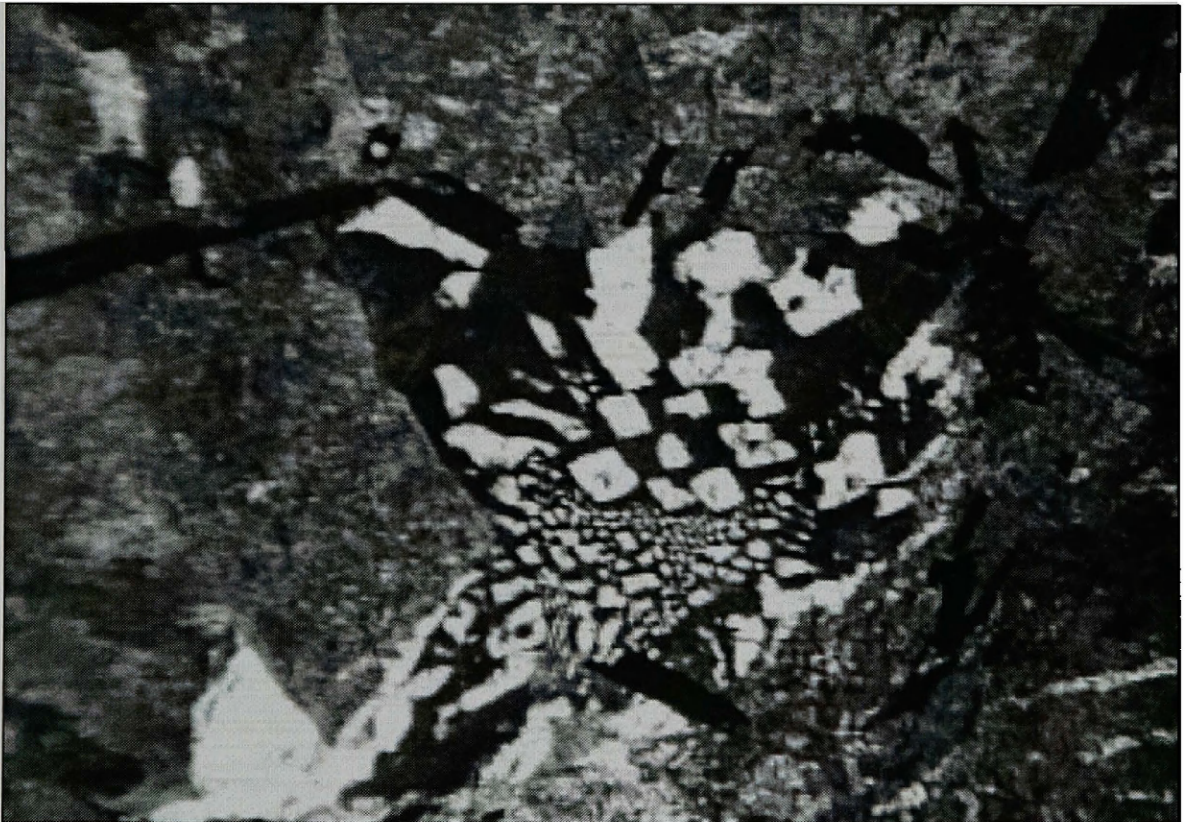


Figure 26. Graphic texture from a Holland Lake sample. View is 3 mm across.

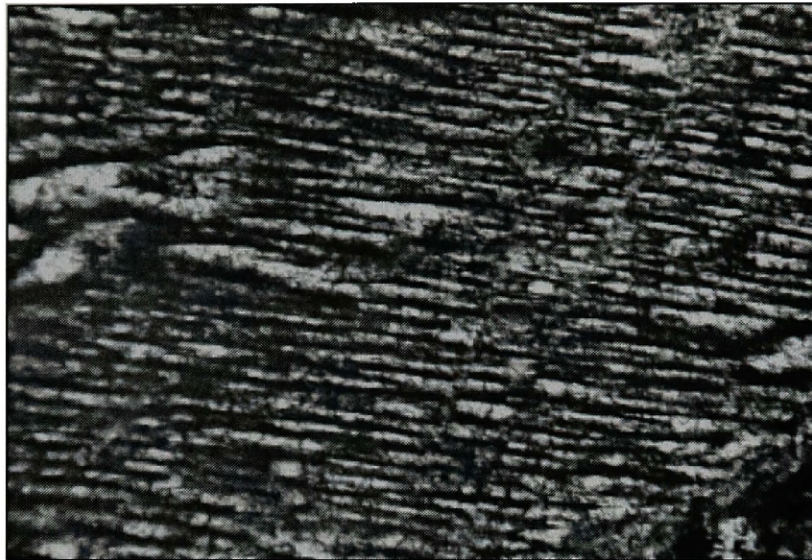


Figure 27. Perthitic texture in alkali feldspar found in a sample from Holland Lake. View is 0.75 mm across.

The cliff above the trail contains many xenoliths of Belt-Purcell rocks (Figure 28). These inclusions are mostly elongated and range in size from a centimeter to about 15 cm long and up to 5 cm wide (Figure 29). They are not recrystallized and still contain their original bedding (Figure 30). Their edges are sub-rounded, but their boundaries with the granophyre are sharp with minor rims of epidote occurring on some inclusions. One of the whitish-grey hand specimens collected at this location contained a large (11x5 cm) very well-rounded xenolith, a discovery apparent only on closer examination (Figure 31a, b). No recrystallization occurred within a zone one centimeter from the top of the inclusion. Below that zone total recrystallization occurred. Mineralogy consists of quartz with chlorite and amphibole, indicating that it is most likely a Belt-Purcell quartzite. Although the boundary at the top of the inclusion is sharp, the bottom contact is not; this along with the rounded shape and recrystallization, indicates some chemical interaction between the magma and xenoliths. Samples of the pinkish-grey rocks showed no signs of inclusions and 45 kg (MT-HL-13) were collected for dating (Appendix I).



Figure 28. Cliff exposure north of trail at Holland Lake. This outcrop contains many xenoliths of Belt-Purcell rock.

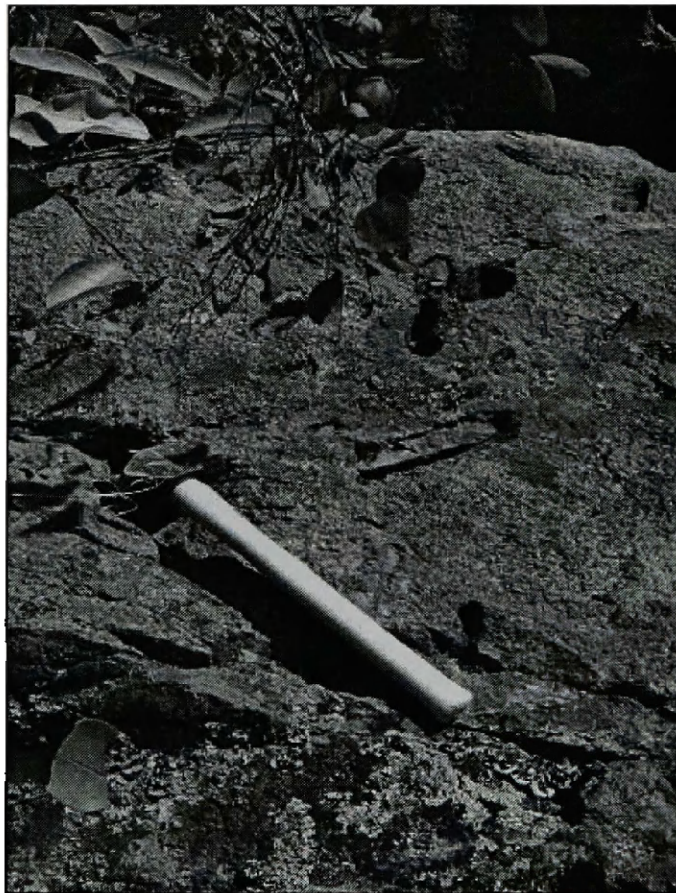


Figure 29. Xenoliths in the a cliff at Holland Lake.



Figure 30. The xenoliths at Holland Lake still retain their original bedding.

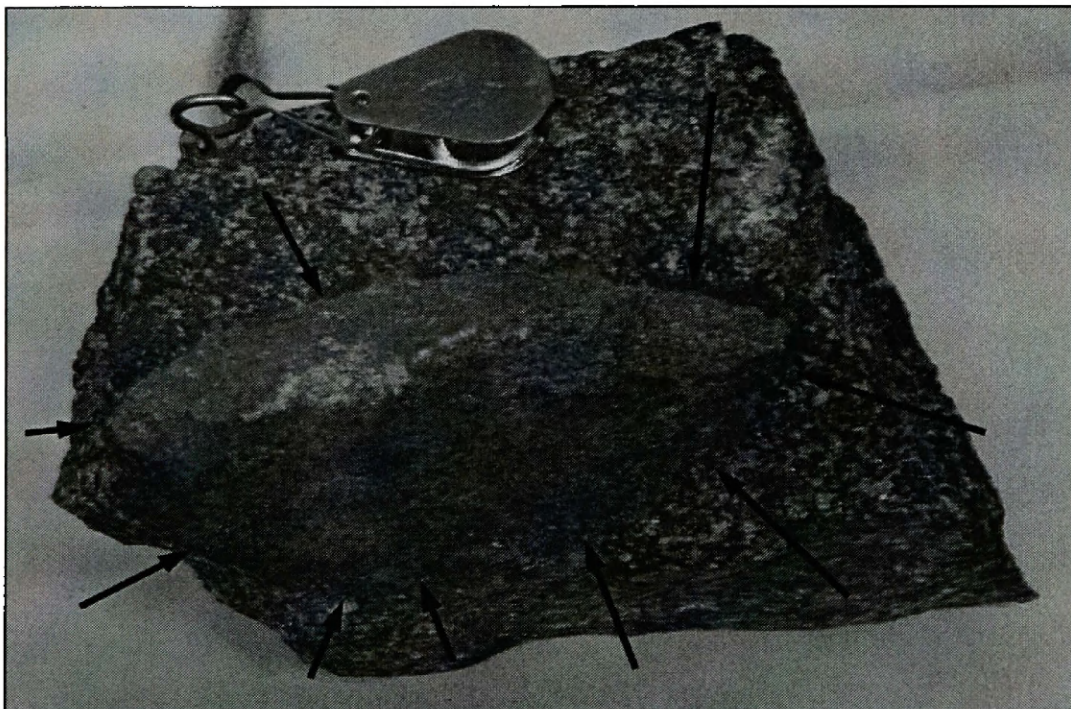


Figure 31a. Xenolith in Holland Lake sample. The top cm is not recrystallized and the boundary with the granophyre is sharp.

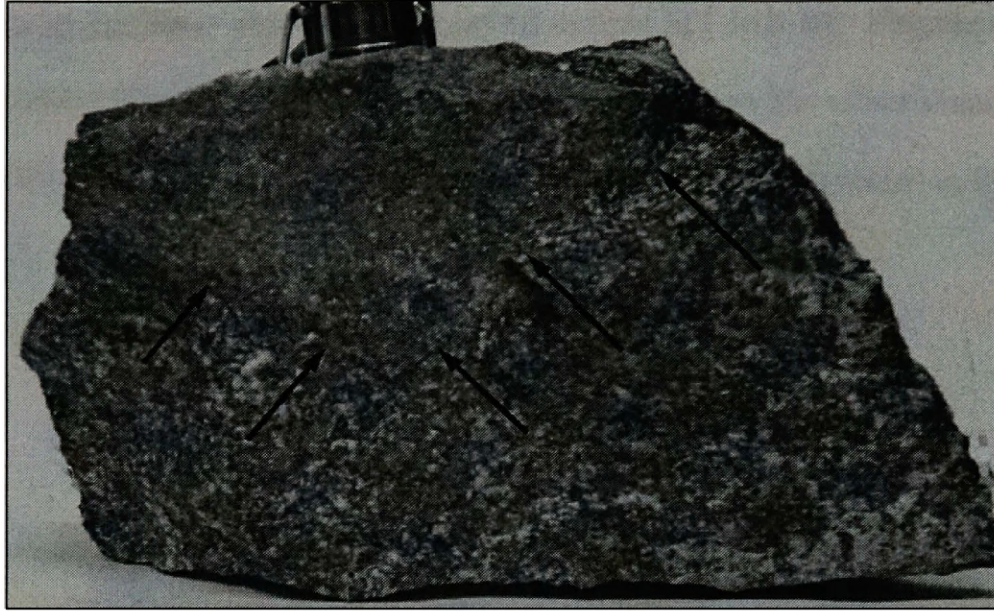


Figure 31b. Same sample as above with a closer view of the recrystallized lower portion of the xenolith. The lower boundary is not as well defined as the top.

McDonald Reservoir

North of McDonald Reservoir, in the Mission Mountains, a sill crops out in a cliff face (N 47° 25' 35.8", W 113° 59' 04.1") (Figure 32). This sill extends horizontally along the full length of the cliff for approximately 3 km and the contacts with the surrounding Empire Formation are sharp. The sill is about 60 m thick, strikes northwest, dips northeast, and is dark grey to black in color (Figure 33). Fractures are very common and iron staining is present along fracture surfaces.

Hand specimens show a range of grain size. Fine-grained samples are dark grey to black with brown iron stains on the surface. Actinolite and epidote on fracture surfaces are present, but are not as commonly or as well developed as in previous sites. Fresh surfaces are grey with plagioclase and pyroxene present, and have veins of brown iron stains. Thin sections contain sub-equal amounts of plagioclase and pyroxene (augite

and pigeonite), as well as magnetite/ilmenite intergrowths, and quartz. Most plagioclase and pyroxene grains show signs of alteration in sample MT-MR-01. Plagioclase grains in sample MT-MR-02 have very little alteration, while alteration has affect almost all of the pyroxene grains. Graphic textures of feldspar and quartz are also present in these samples.



Figure 32. Sill location at McDonald Reservoir. Arrows point to sill mapped in the area. The largest arrow points to the sample site used in this study. (Map after Mudge et al., 1982).



Figure 33. Sill location at McDonald Reservoir. The sill is exposed along a 3 km stretch of the cliff face. Arrow shows location of MT-MR-01 and MT-MR-02.

Coarse-grained samples are lighter in color, more grey than black. Iron staining is still present but not as widespread as in the fine-grained samples. The color is the same on a fresh surface, and plagioclase and pyroxene are the most abundant minerals. Iron

staining tends to occur around grains instead of veins. The coarser-grained samples are more competent than their fine-grained counterparts.

A very coarse-grained sample found in float might represent granophyre associated with the sill at this location. The hand samples are whitish grey to light grey and have very little iron staining (Figure 34). They are extremely competent and fresh surfaces are whitish grey. Plagioclase is the dominant mineral, but some pyroxene, amphibole, and quartz are present. Small xenoliths of Belt-Purcell rock are present in the sample and are recrystallized, but have sharp boundaries with the granophyre. Two of the larger xenoliths found in hand specimens measure 2x3.5 cm and 1.4x2.3 cm (Figure 35). No outcrop of granophyre was found, but when viewed from the south side of the reservoir, a light grey zone is seen near the upper contact in one portion of the sill (Figure 36). Unfortunately, this area is inaccessible without scaling the cliff prohibiting sample collection. Because granophyre was not verified in the outcrop, this sill was not dated. Samples MT-MR-01 and MT-MR-02 were collected from the fine-grained section of the sill (Figure 33) (Appendix I and II).

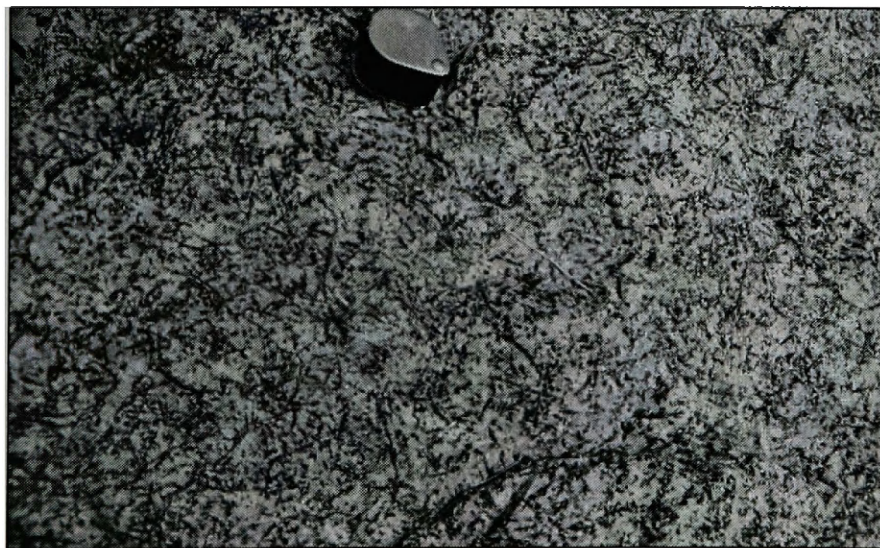


Figure 34. Granophyre boulder found near McDonald Reservoir.

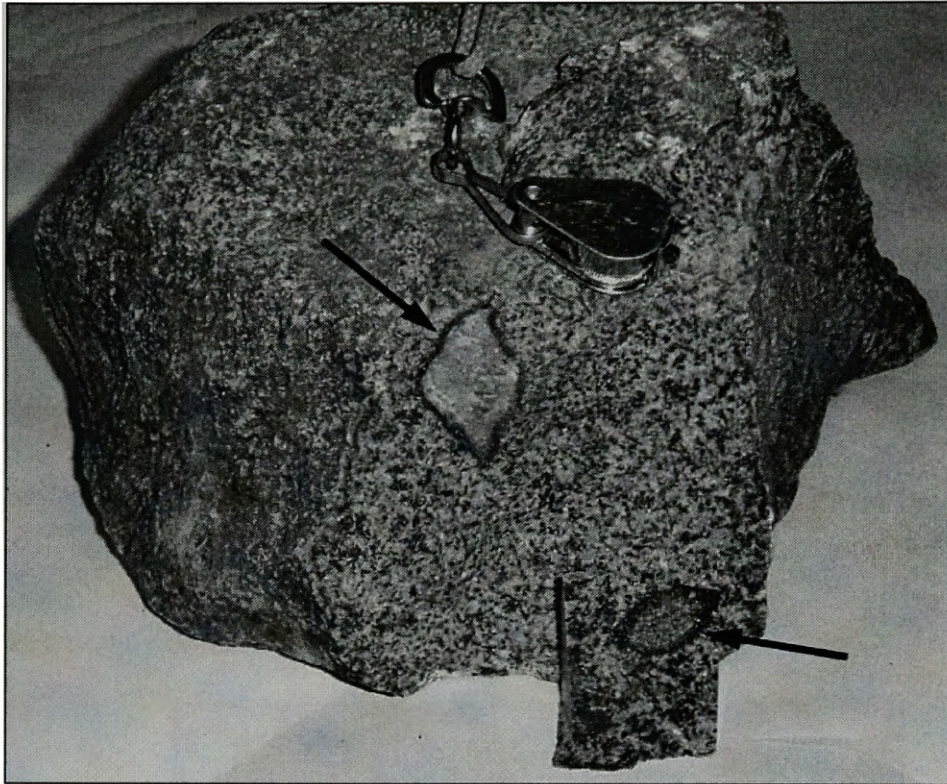


Figure 35. Two Belt-Purcell xenoliths found in granophyre sample from McDonald Reservoir. Comprised of carbonate and quartz they are surrounded by rims of amphibole and possible chlorite.



Figure 36. Location of granophyre at McDonald Reservoir.

Alberton

This sill crops out east of Alberton, Montana, in a road cut along Interstate 90 (N47° 0' 45.6", W 114° 29' 39.12") in the hanging wall of a thrust fault located to the east (Figure 37) (Lonn, 1984). At this location, the sill intrudes the Garnet Range Formation. The sill forms a small hill that is cut by I-90. No contacts are exposed, prohibiting direct strike and dip measurements (Figure 38). However, the Garnet Range Formation at this location strikes northeast and dips northwest.

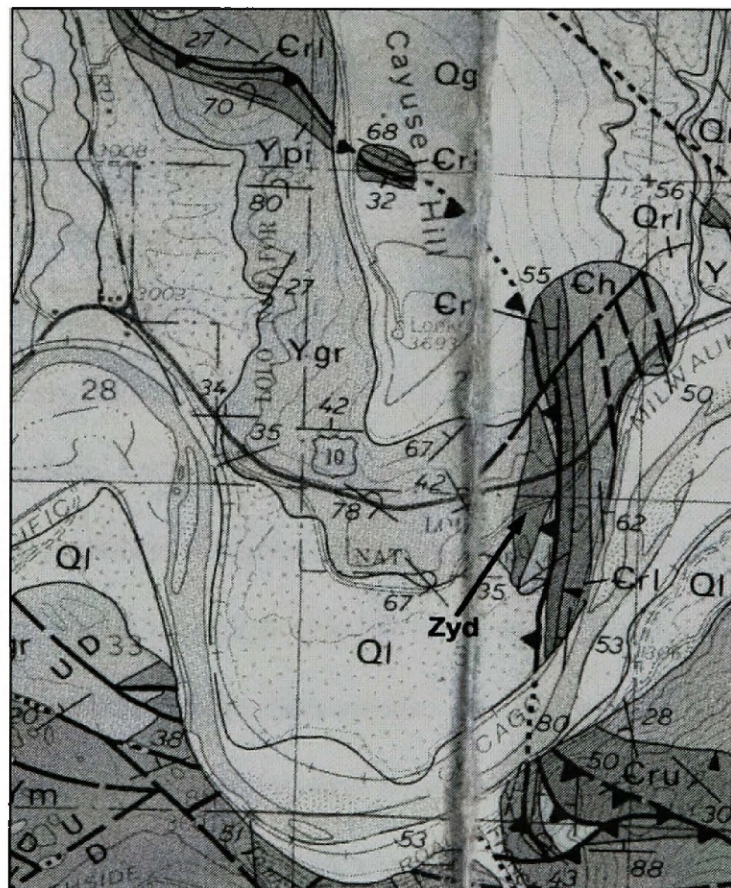


Figure 37. Sill location “ZYd” near Alberton. (map after Wells, 1974).

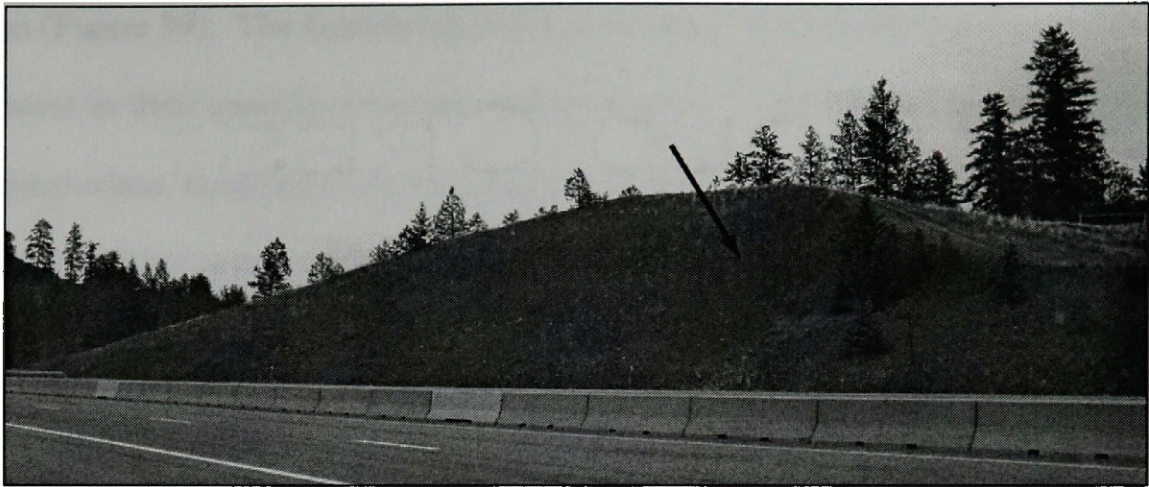


Figure 38. Sill exposure along I-90 at the Ninemile exit. Arrow shows location of sample site for MT-ALE-01.

The sill, approximately 50 m thick, is highly fractured and composed of fine- to medium-grained diabase. In hand specimen, the sill is dark grey with a slight green tinge and with brown iron stains along fractures. Actinolite, epidote, and chlorite are present on some fracture surfaces. No major veins are present in this exposure, although some small quartz veins were found in some float rocks. Fresh surfaces are light grey and also tinted green, with visible crystals of plagioclase and pyroxene. The green tinge and presence of actinolite, epidote, and chlorite indicate greenschist metamorphism of the sill. In thin section, sub-equal amounts of equigranular plagioclase and pyroxene dominate the samples. Two pyroxenes, augite and pigeonite, are present. An exact amount of each pyroxene is difficult to determine due to their similar optical properties. Some hornblende, quartz, chlorite, biotite, apatite, and intergrowths of magnetite and ilmenite are also present. Most of the plagioclase has undergone some sericitization, while the pyroxenes have undergone some uralitization during metamorphism. Most of the alteration seen in thin section is limited to zones, primarily around fractures. Micrographic textures between quartz and feldspar are rare but present in samples from

this location (Figure 39). The hornblende and biotite most likely crystallized late in the cooling process as their quantity increases with grain size. The groundmass consists mostly of plagioclase, magnetite/ilmenite, and minor quartz. Chloritization in the groundmass resulted in a green hue, most likely the source of the green seen in hand-specimen. MT-ALE-01 was collected from the fine-grained section at this location (Figure 38) (Appendix I and II). MT-A1-02 is taken from a small dike 4 km west of the sill (Figure 40) (Appendix I and II). Numerous dikes crop out north of Alberton and appear to feed several sills that may be related to the Windermere intrusive group (Sears et al., 1998).



Figure 39. Micrographic texture found in a sample from Alberton. Notice long apatite grains. View is 1 mm wide.

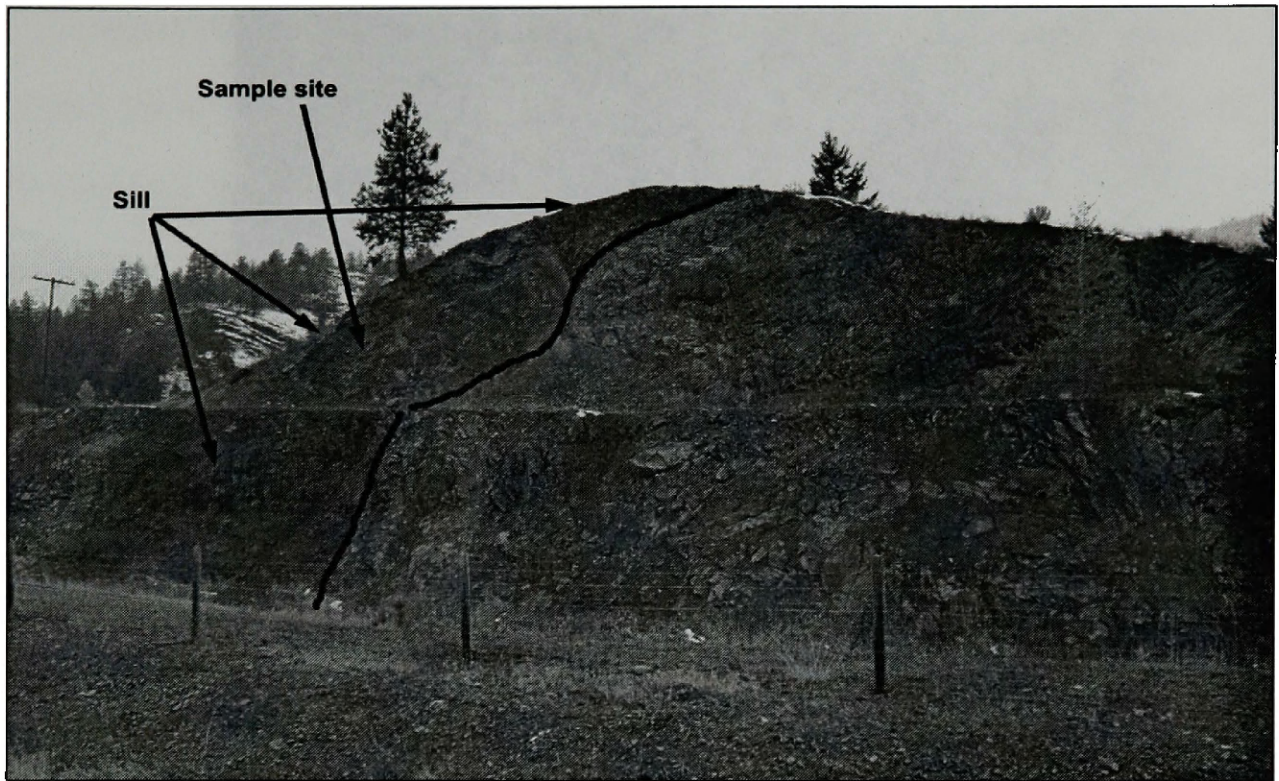


Figure 40. The location of a small dike 4 km west of the sill near Alberton. This figure also shows the sample site of MT-AI-02.

Kootenai National Forest

An extremely poor exposure of a sill is located north of Yaak, near the Canadian border, in the Kootenai National Forest (N 49° 0' 13.17", W 115° 41' 57.1") (Figure 41). This location is forested heavily and soil covers the sill except for a small outcrop on the southern side of a forest road (Figure 42). Contacts with the surrounding middle member of the Wallace Formation are not exposed; however, the Wallace rocks strike almost due north and dip west.

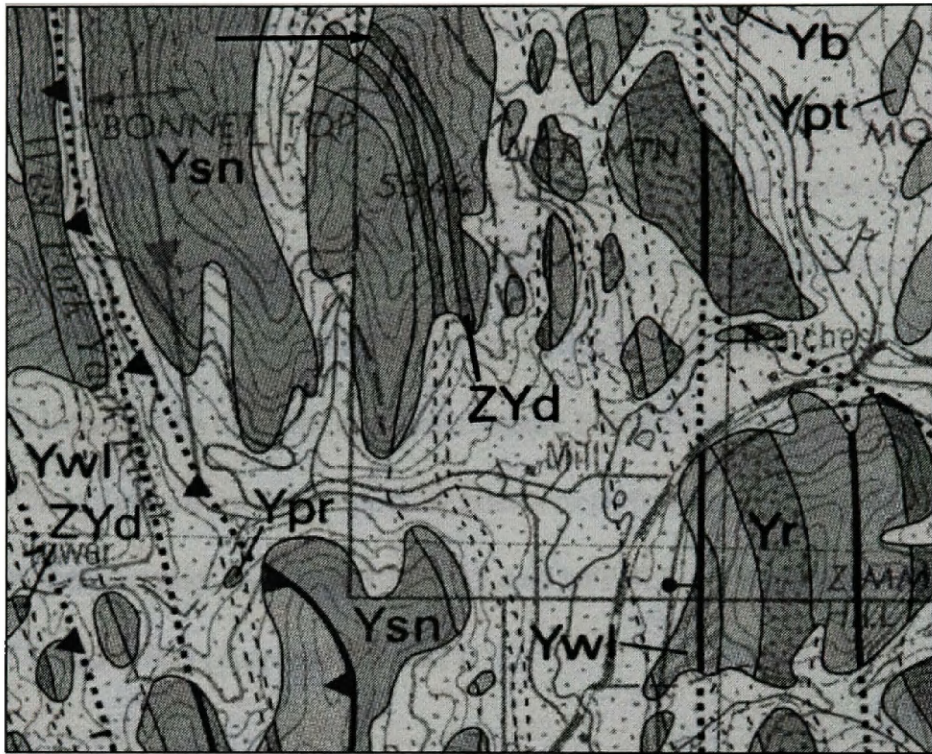


Figure 41. Sill location in the Kootenai National Forest, near the Montana-Canada Border. Arrow shows sample location. (map after Harrison et al., 1992).



Figure 42. Exposure of a sill in the Kootenai National Forest. This sill is in a heavily forested area and is mostly covered by soil. Arrow shows sample location for MT-KF-01.

About 20-m thick, the sill is extremely weathered and is brown at this location. It is highly fractured and crumbles to brown dust when hit with a rock hammer. The rock debris near the road yielded several fairly competent samples. Fresh surfaces of these samples were greenish-grey with heavy iron staining in veins and around grains. These samples are fine-grained with visible plagioclase, pyroxene, and chlorite. In thin section, at least 40 percent alteration to chlorite and hornblende has affected all plagioclase and pyroxene grains. Complete alteration occurs in zones near fractures. Sample MT-KF-01 was collected from this outcrop, while MT-KF-02 and MT-KF-03 were collected from float near the road (Figure 42) (Appendix I and II).

Structure

The sills and dikes of this study intrude middle Proterozoic formations of the Belt-Purcell Supergroup in Montana and may relate to 750-780 Ma mafic dikes to the southeast in Wyoming (Harlan et al., 1997, 2003) that correlate with the early phase of Neoproterozoic Windermere rifting. The dikes in the Beartooth and Teton ranges of Wyoming intrude mostly Archean basement rock (Harlan et al., 1997). All sill contacts observed in this study are sharp with no disruption of the country rock, indicating that the sills intruded after lithification of Belt-Purcell sediments. A dike swarm intrudes the younger part of the supergroup (Garnet Range Formation) in the Alberton area, but not the Cambrian Flathead Sandstone, which unconformably overlies Belt-Purcell rocks (Wells, 1974; Kruger, 1988). A sill in Glacier Park, originally correlated with part of the Purcell complex by Meistrick (1975), has an apparent cross-cutting relationship with the Purcell lava (McGimsey, 1985). The apparent intrusion into already lithified sediments,

the 796-797 K-Ar date of Harlan et al. (2003), and the facts that the sill cross-cuts the Purcell Lavas (as observed by McGimsey (1985)) and is cut by the sub-Cambrian unconformity, demonstrate that they are younger than the Purcell lava and older than the Flathead Sandstone.

Palinspastic maps provide views of the Windermere sill and dike system as it existed at the time of emplacement. The present study obtained thickness and depth data from field data collected during this project, Eisenbeis (1958), Mejstrick (1975), Mudge et al. (1968,1982), Watson (1984), and restored cross-sections (Price and Sears, 2000; Sears, unpublished data). Figure 43 shows the reconstructed thickness of the Windermere intrusive group on a palinspastic map, which removes the effects of Jurassic through Paleocene thrusting and Cenozoic extension. Parallel to the northwest-trending basin axis, the deepest segments of the sills intruded the lower parts of the Belt-Purcell Supergroup. The dike swarms in northern Wyoming (Harlan, 1997) and near Alberton, Montana are also aligned with the basin axis. At the eastern margin of the basin, the Cambrian Flathead Sandstone unconformably overlies the sills. Although the sill and dike in Glacier Park are too altered for geochemical comparison, they do correlate well structurally with the Windermere intrusive group in Montana in Figure 43. Figure 44 shows the depth from the Cambrian unconformity (base of the Flathead Sandstone) to the top of the sills. From the basin axis, the sills rise systematically outward to both the northeast and southwest across the width of the basin, defining a bowl-shape. While the sills thin and rise towards the basin margins, they do not necessarily propagate into younger strata of the Belt-Purcell Supergroup. This is because the stratigraphic units conform to the basin shape and fill accommodation space. Younger sedimentary units do

not reach the original basin margin, which allowed the sills to intrude older units at shallow depths (Figure 45). The thickness and shape of the Windermere sills shown in Figures 43 and 44 and position of the dike swarms may indicate a feeder conduit along the central axis of the basin.

The dike swarms intruding Archean basement rocks in the Teton and Beartooth ranges and the Proterozoic Belt-Purcell rocks near Alberton area fall in line with the inferred feeder conduit on the palinspastic map (Figure 43). These dike swarms may represent early intrusion and magma conduits that fed the sills. As the magma rose, it encountered the horizontal strata of the Belt-Purcell basin. The strata facilitated sill formation within the basin, following the easily-parted bedding planes instead of creating new fractures through the very competent Belt-Purcell rocks. As the magma progressed laterally through the basin, it encountered existing fractures. At these junctions, the sill followed the fractures to shallower depths and moved vertically through stratigraphic units.

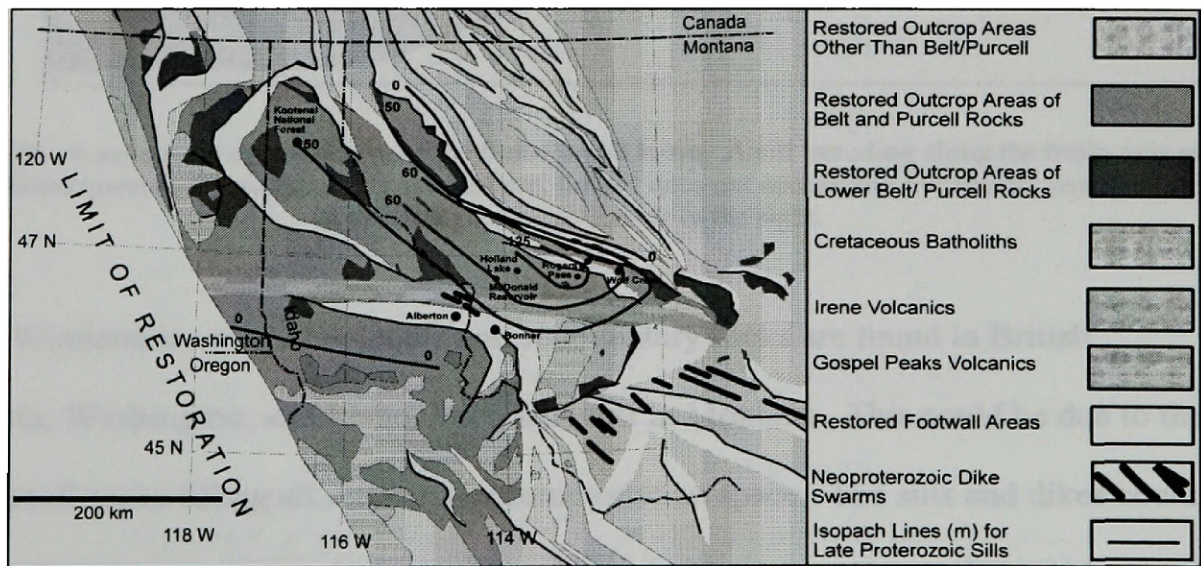


Figure 43. The minimum total thickness of the Windermere sills and dikes on a palinspastic map (Map after Price and Sears, 2000).

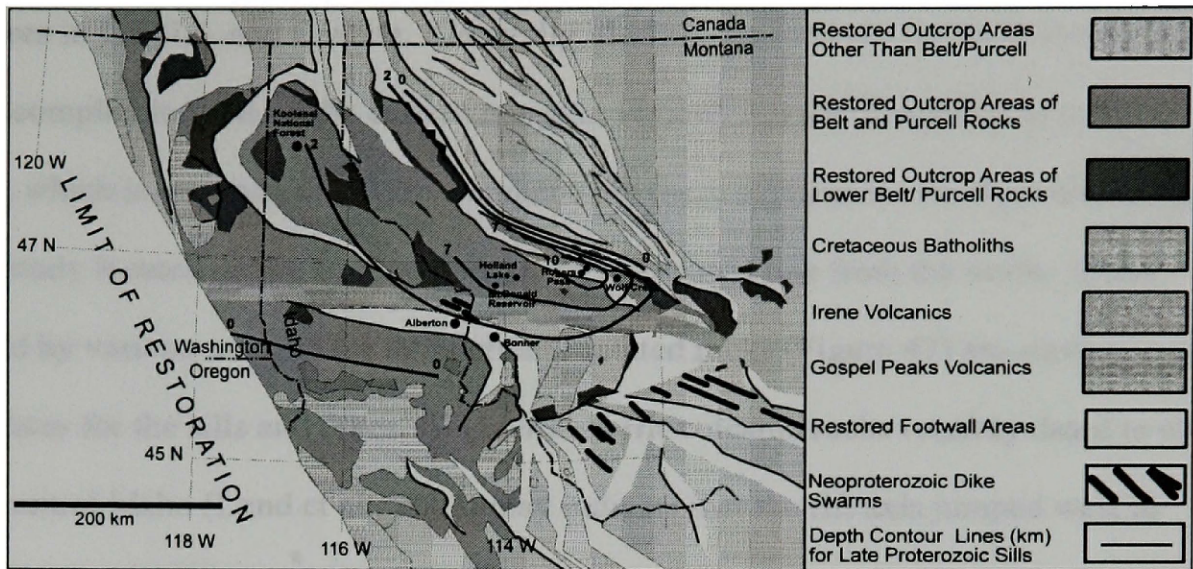


Figure 44. The minimum depth to the top of the Late Proterozoic sill from the base of the Cambrian Flathead Formation on a palinspastic map. (Map after Price and Sears, 2000).

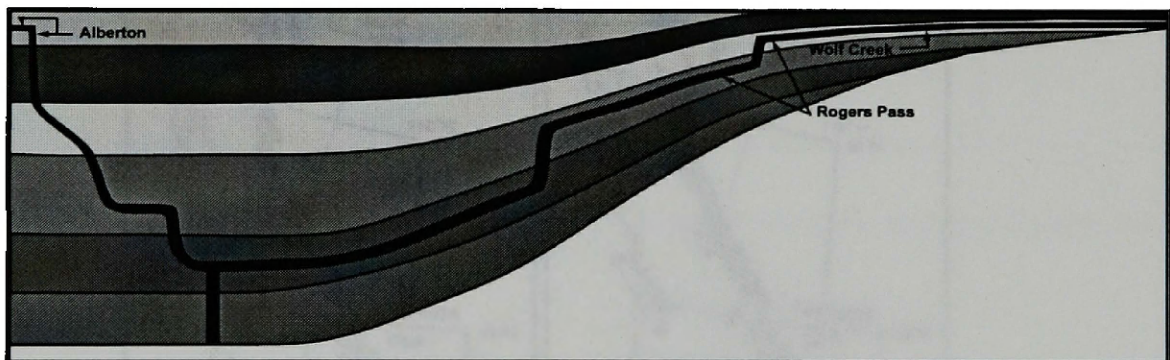


Figure 45. A schematic cross-section of the Belt-Purcell basin. A sill intruding along the basin axis and rises outward towards the margins. As shown here, the sill does not necessarily intrude the youngest strata at the basin margins. East is to the right.

Windermere-related volcanic and sedimentary rocks are found in British Columbia, Washington, and Idaho, but are absent in Montana. This could be due to the Belt-Purcell rocks filling all sediment accommodation space. The sills and dikes could be the only representatives of Windermere rifting in Montana. Comparison with Windermere volcanic rocks indicates that the sills and volcanic rocks are coeval. Figure 46 shows the location of the intrusive system of this study with respect to Windermere

exposures in the U.S. and Canada. Generally, these rocks follow a northern trend with the sill complex located on the eastern margin. Figures 46a and b show an en echelon pattern, which is common in rift environments, in these exposures with the sills and dikes of this study located on the southeastern tip of the second line from the north. Dates obtained by various workers for Windermere-related rocks (Figure 47) are similar to the argon dates for the sills and dikes. Windermere rift volcanic rocks recently dated to 685 Ma in central Idaho (Lund et al., 2003) may indicate that the rift axis jumped west to establish the eventual margin of Laurentia. This is compatible with the proposed coeval relationship between the sills and dikes, and the Windermere event.

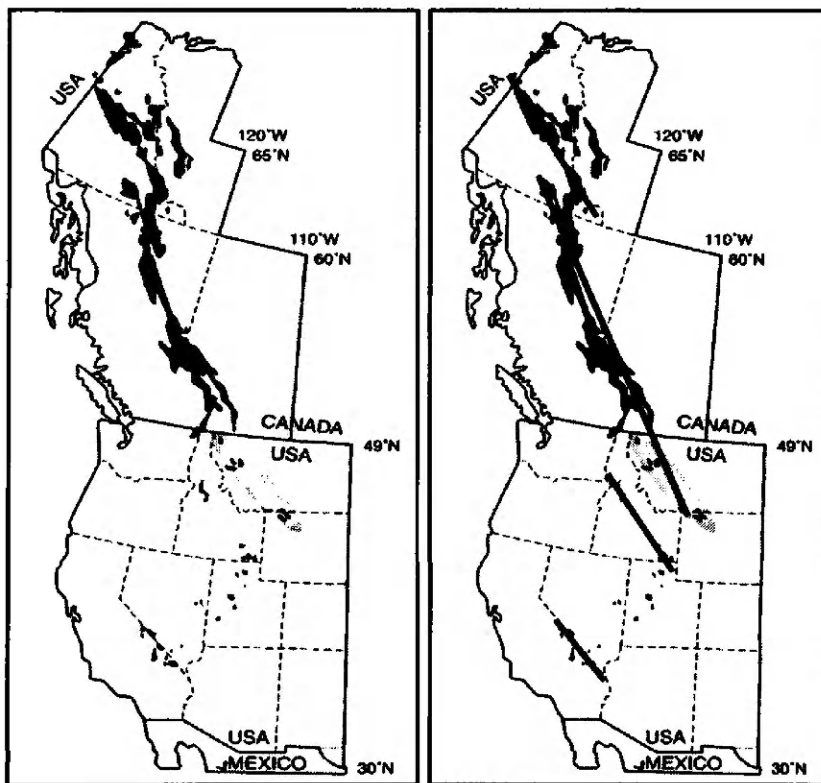


Figure 46.

Figure 47.

Figure 46a and 46b. Maps of Windermere-related volcanic and sedimentary rocks. The sills and dikes of this study are circled. An en echelon pattern in the Windermere rift. The sills and dikes of this study (circled) lie at the southeastern end of the second northern line. (after Ross et al., 1995).

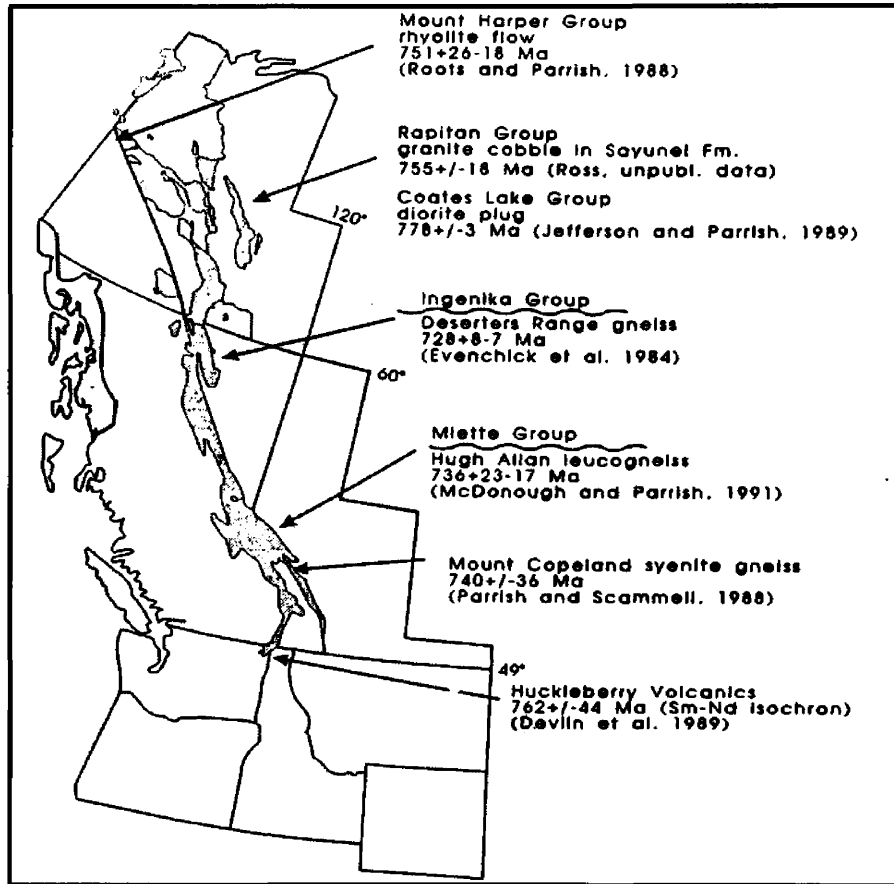


Figure 47. Location and ages of Windermere-related rocks in northwestern America and Canada. (after Ross et al., 1995).

U-Pb Dates

As technology has improved, isotopic dating has become an important tool for correlating geologic formations and processes. Researchers have used Ar-Ar and K-Ar dating methods to establish an age for the Windermere sills and dikes at various locations, but those techniques may contain a larger degree of error as subsequent geologic events, such as reheating, can easily reset the argon system. U-Pb dating of suitable minerals can be more reliable, as techniques have advanced in recent years. Furthermore, U-Pb ratios in zircon require much higher temperatures to reset the isotopic

system once the system is closed. However, secondary lead contamination occurring during subsequent tectonic events may cause problems when using this method. Careful analysis of the data is required to minimize these effects. This study obtained zircon U-Pb dates for three sites in an attempt to verify the age of the Neoproterozoic sills in northwestern Montana and used this data to correlate the sill exposures and establish a possible correlation with Windermere rifting.

Methods

Samples collected for U-Pb analysis of zircons came from the granophyric portion of the sills, since the mafic rocks typically lack sufficient quantities of zircon for dating. Rogers Pass, Turah and Holland Lake (Figure 10) had large bodies of exposed granophyre. The collection of more than 45 kg of sample per site maximized the potential for recovery of zircon grains. Prior to shipment, the samples were broken into smaller pieces using a sledgehammer and examined for xenoliths. Only samples with no visible inclusions were sent for analysis. Dr. K. R. Chamberlain performed the U-Pb analysis using thermal ionization mass spectrometry (TIMS) at the University of Wyoming. Isolation of zircon grains followed standard separation techniques involving crushing, Wilfley table, and heavy liquid and magnetic separation. Analysis of handpicked magmatic zircon grains followed methods modified from Krogh (1973, 1982a, b) and Parrish et al. (1987).

Results

At the time of this writing, preliminary U-Pb analysis has been completed only for the granophyre sample from Rogers Pass (RP-KRC-02-2). It yielded a crystallization age of 763 ± 12 Ma (Figure 48). This date corresponds well within error of the K-Ar date of 760 ± 25 Ma (Obradovich and Peterman, 1968) for the sill near Alberton, and the ^{40}Ar - ^{39}Ar dates of 776 ± 5 Ma (Wolf Creek sill), 769 ± 5 Ma (Mount Moran dike), and 774 ± 4 Ma (Christmas Lake dike) reported by Harlan et al. (1997). Concordia intercepts were also at 950 Ma and 51 ± 20 Ma. Most likely, the 950 Ma intercept is related to lead contamination from the incorporation of the Belt-Purcell xenoliths found in the granophyre. This can be a significant problem with U-Pb dating. The intercept at 51 Ma presumably is related to Eocene intrusive events. Eocene time represents a period of magmatic activity in northwestern Montana and numerous basalt dikes are mapped throughout the region. At sample site RPM, (Figure 12) located approximately 6 km to the west of the granophyre sample site, an Eocene basalt dike intrudes the Windermere sill (Figure 13). Other dikes invade this section 2-3 km east of the sample site. These intrusions could have produced hydrothermal activity that could have contaminated the Windermere sill. Preliminary results from the Turah samples also indicate high lead contamination levels, which may negatively affect the analysis.

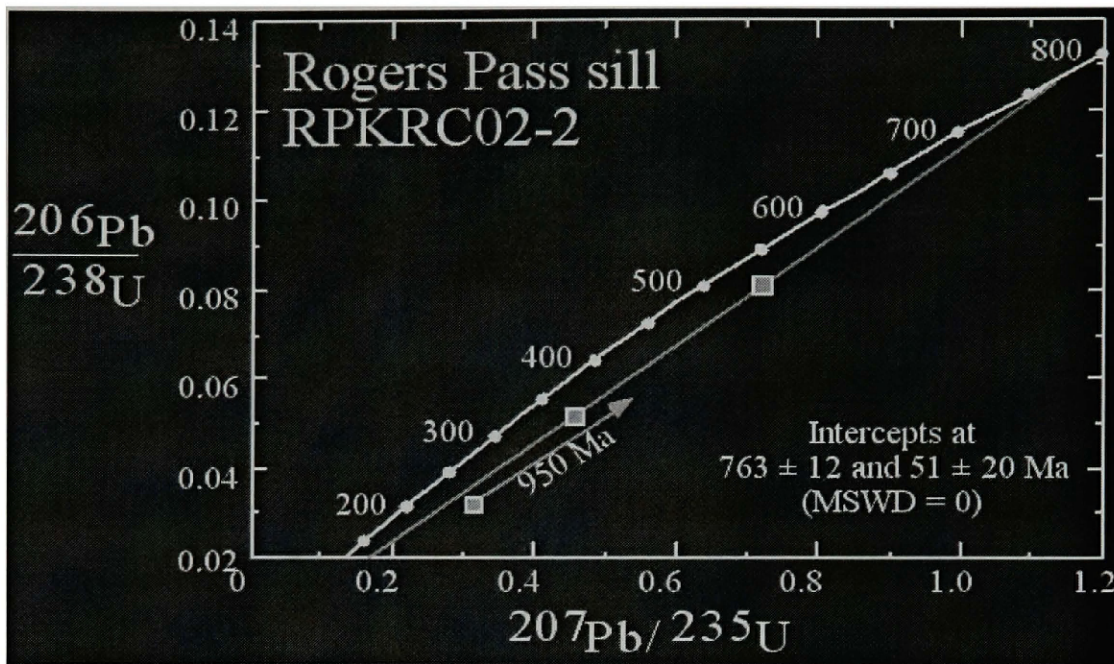


Figure 48. Geochronology results from the U-Pb analysis on zircons during this study.

Geochemical Analysis

Methods

Sampling methods at each site followed standards designed to minimize the effects of grain-size and metamorphism during geochemical analysis. Exposed chill zones at some sample sites are typically a few centimeters thick, followed by a 1 m thick zone consisting of fine-grained diabase. The grain-size typically coarsens towards the interior of these sills. Samples taken from the chill zones at each sampling site maximize the potential of analyzing primary magma composition, as coarser grains reflect longer cooling times, which allow for greater magmatic differentiation and contamination from fluids from the country rock. However, since most sites lack exposed chill zones this was not possible. Most sample sites exhibit fine-grained zones and samples ultimately were taken from these sections for the same reasons one would normally sample from the chilled zone. Due to the lack of upper-contact exposures at most locations, the majority

of samples collected came from areas near the lower contact of the sills. The similarity of each sample location minimized any effects of chemical differences between the different zones within the sill.

The samples were sawn and examined for veins and zones of high alteration, particularly around cracks. This was especially important due to the general highly fractured state of the sills, which allowed for veins of epidote, actinolite, and zones of alteration. Many samples were found to contain high percentages of weathering products, and only samples with minimal alteration were sent for thin sectioning. Samples were sent to Quality Thin Sections in Tucson, Arizona for processing.

Each thin section was examined for any signs of microscopic veins and chemical alteration. To further minimize any effects of impurities and late-stage alteration, samples with any veins or those which had over fifty percent of their mineral grains affected by alteration were discarded from geochemical analysis. Chips were created from the best samples in a steel crusher. Since contamination from the rock crusher tends to concentrate in the dust after crushing, the rock chips selectively were hand picked, washed, blown dry with compressed air, and sealed in a plastic bag. The chips were ground to a powder less than 70 microns coarse in a steel puck and ring grinder. Most of the samples were ground for two minutes, while a few required longer grind times (Appendix I). In order to account for any contamination from the saw, chipper, and grinder, a pure coarse-grained quartz (QTZ-01) sample was processed along with the rock samples and its analytical data is included in the appendices. The powder was weighed immediately, placed in plastic vials, and shipped to the GeoAnalytical Lab at Washington State University located in Pullman, Washington. Two plastic vials, one

containing 3.5 g and the other 2.0 g of ground powder, per sample were analyzed by X-ray fluorescence (XRF) and inductively coupled plasma mass spectrometer (ICP-MS), respectively, for whole-rock analysis. Johnson et al. (1999) and Knaack et al. (1994) describe the XRF and ICP-MS procedures, respectively, used in this study. This study included two exceptions to the procedures stated above. Samples MT-KF-01 and MT-KF-02 were analyzed despite their high degree of alteration because their thin sections were not available when all the samples were required to be at the laboratory. These samples, however, provided useful information when interpreting the effects of alteration on these rocks and comparing other workers' data with results from this study. Contamination from the preparation of samples, based on the quartz blank, was very low. The analytical data are provided in Appendix II.

For each sample sent for XRF and ICP-MS analysis, a polished thin section was created for electron microprobe analysis. Microprobe analysis focused on pyroxene and plagioclase grains because they represent early magma composition. Because of the difficulty in determining the exact timing of crystallization of the hornblende and biotite grains, these minerals are unreliable for geochemical comparison of the magma from which the sills crystallized. Each thin section was mapped, and selected pyroxene and plagioclase grains that did not contain sericitization or urialization were circled for easy recognition under the electron microprobe. The polished sections received a coating of carbon to enhance electrical conductivity and analyzed (for number, type of grains analyzed per section and resulting data see Appendix II).

Geochemical Results

The Windermere sills are basaltic in composition. Specifically, the average content of SiO₂, MnO, CaO, MgO, K₂O, and Na₂O falls within the continental tholeiite range. They have a high concentration of TiO₂ (average 2.7%) that is more typical of alkalic basalts. The TiO₂ content is unique to this group of intrusions and is a possible identifying characteristic for the Windermere sills and dikes because it is significantly higher than typical tholeiites.

The sills follow a typical mafic-tholeiite trend in Figure 49, with the exception of the highly altered MT-KF samples that plot closer to a typical mafic-alkaline trend. This is due to an increase in the more mobile elements in the weathered samples. The immobile element compositions of the weathered samples, however, are similar to the less-weathered samples. MT-AL-02 shows lower concentrations of the immobile elements, which also could be due to slight metamorphism during Mesozoic tectonic events. Trends on a Large Ion Lithophile (LIL) and High Field Strength (HFS) diagram (Figure 50) show a similar pattern, with the more-altered samples concentrating the more-mobile elements. Elevated peaks in the more-mobile elements are most likely the result of alteration, which has affected all samples to some degree. Graphs plotting mobile versus immobile or immobile against immobile elements (Figures 51-53) show, like most of the other graphs, a close grouping of the less-weathered samples. However, this data does not establish that the sills are part of a continuous sill within the Belt-Purcell basin. However, it does imply that the individual outcrops are similar in composition and a product of one magma type, i.e. basalt.

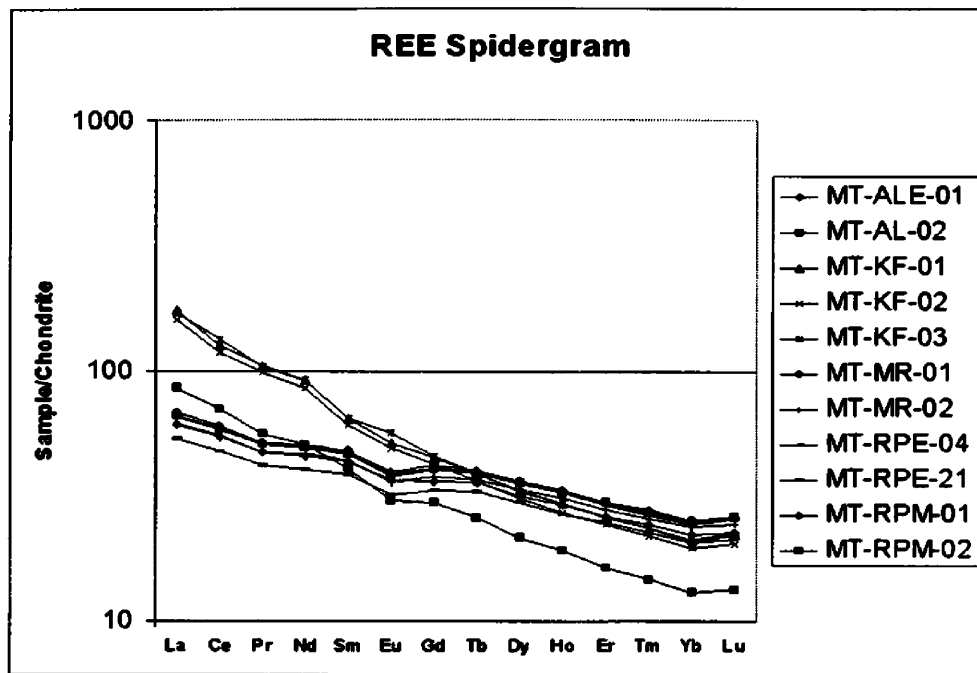


Figure 49. The sills follow a similar trend in the REE spidergram. MT-KF-01; 02; 03 have increased amounts of the more-mobile elements because they are significantly weathered. Their concentration of immobile elements is similar to those of the less weathered.

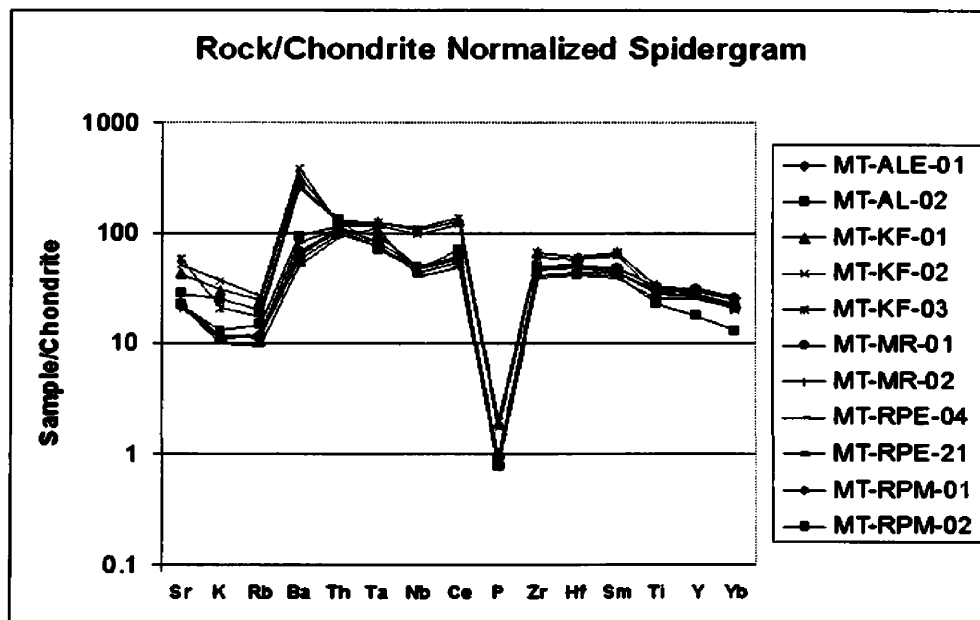


Figure 50. The sills follow a similar trend in the rock/chondrite spidergram. MT-KF-01; 02; 03 and MT-AL-02 have increased amounts of the more-mobile elements due to weathering and metamorphism. (chondrite data from Sun and McDonough, 1989 and Anders 1989 and Anders and Grevesse, 1989).

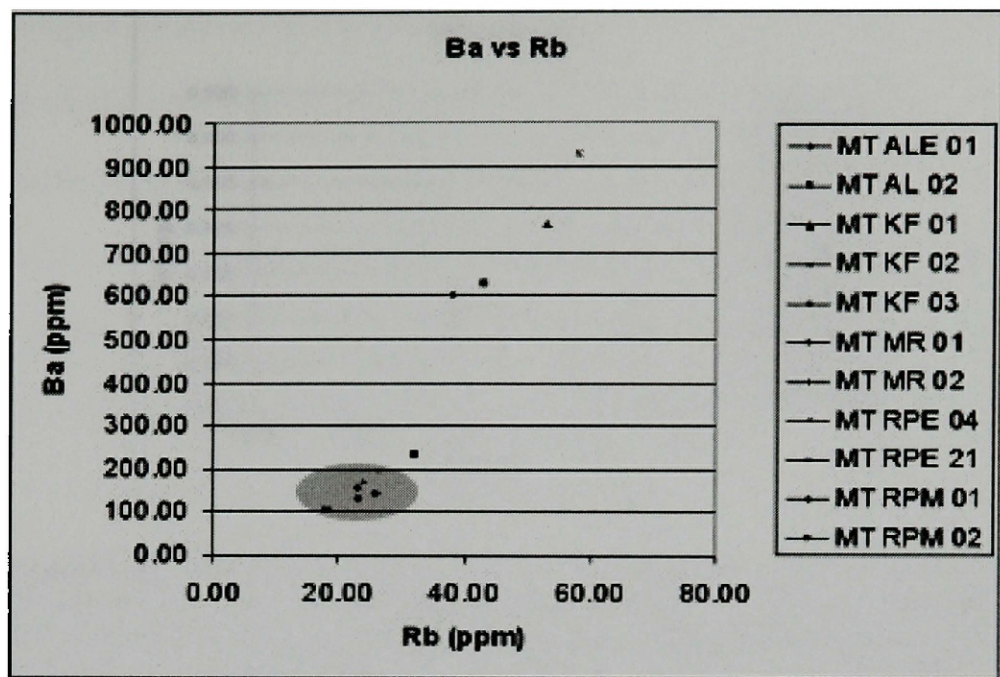


Figure 51. With the exception of the more altered samples, the sills plot in a close group (shaded). Ba and Rb are very mobile during alteration.

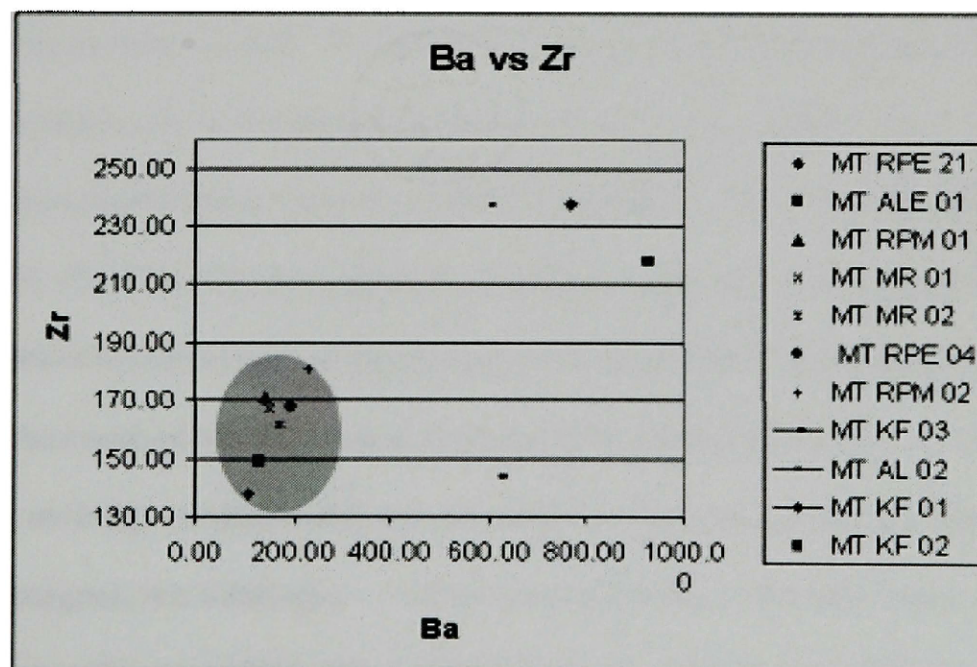


Figure 52. The close grouping of the sills in this graph indicates a similar composition between the sills. While Ba is very mobile, Zr is not. This indicates that the Zr content of the sills, even in the weathered samples, has not been affected by alteration.

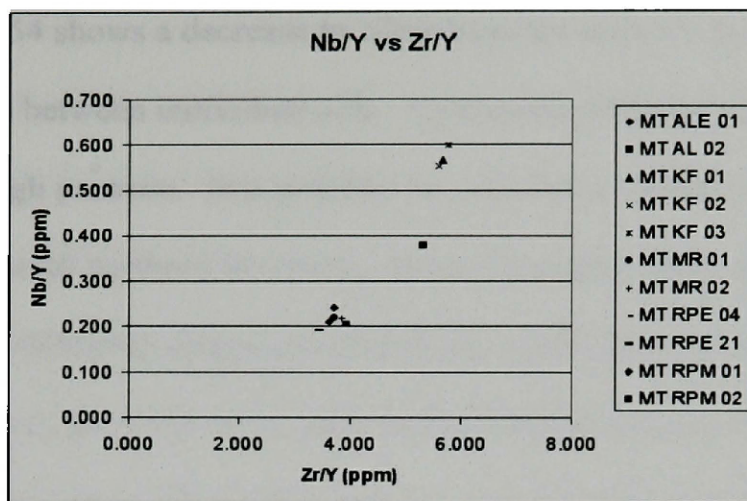


Figure 53. This graphs the mobile element Nb divided by immobile Y against Zr divided by Y, two immobiles. The sills plot in a very close group in this graph and like the previous graphs the more weathered samples plot away from the group. These two groups plot along a line that passes through MT-AL-02 may appears to represent a trend in alteration. If alteration could be removed from these samples it appears all samples would plot in the same group.

Figure 54, which plots the total alkalis against total silica, shows samples from the sills and dikes plot in two groups within the tholeiite field of the graph, but close to the alkalic-tholeiite discrimination line. The dikes in Wyoming sampled by Mueller (1971) plot further to the right from the discrimination line than do the Montana sills. There is no apparent relationship between the two groups in this figure. The subalkalic trend of this group of sills, which is not uncommon in rift zones, could be due to several factors, including an alkali-enriched source in the mantle, contamination of the magma as it moved through the crust, partial melting at high pressure within the mantle, or a small degree of partial melting. A high-alkali source within the mantle would most likely produce alkalic magma, not subalkalic. Crustal contamination of the sills in the study area does not seem to be a possible explanation for the elevated alkali content in the samples. One would expect a greater degree of variation of the alkalis and an increase in silica between the individual sills and dikes depending on amount of crustal

contamination. Figure 54 shows a decrease in silica from the dikes to the sills and very little variation in alkalis between individual sills. A plausible explanation might be partial melting under high pressure. It is possible the pressure conditions in the mantle were not equivalent beneath northern Wyoming and northwestern Montana, which may have resulted in slightly different magma compositions in each area. A small degree of partial melting as rifting began might also explain the differences between the two groups. The initiation of rifting would cause the lithosphere to thin and a small degree of adiabatic partial melting of the mantle could produce magma with an elevated alkaline content. This magma may have intruded through the lithosphere ultimately forming the sills. As this rifting progressed, adiabatic melting continued at a greater degree, producing a less-alkalic magma. This less-alkalic magma followed the original magma and cooled as dikes in Wyoming and Alberton. While this study verified neither theory, both represent possible explanations for the differences in alkalinity between the two groups in Figure 54.

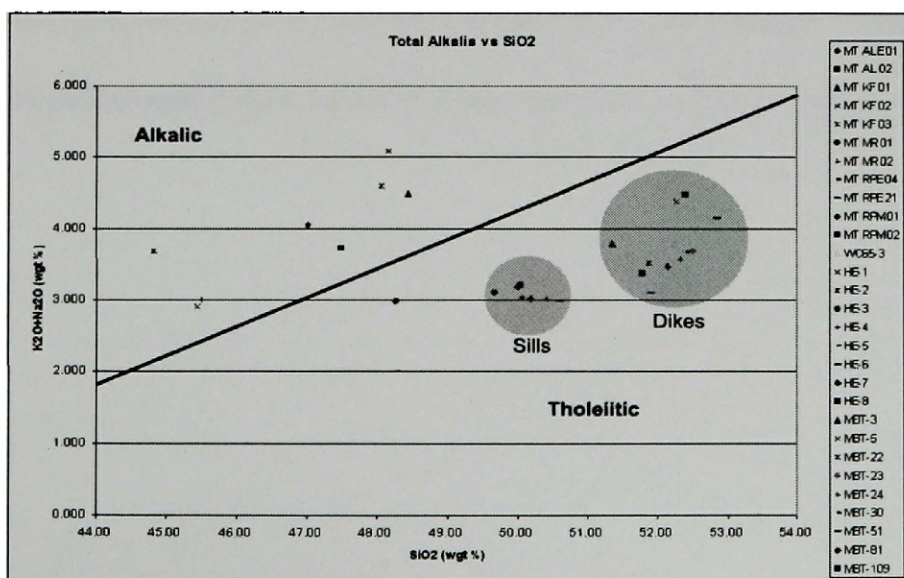


Figure 54. Total alkalis vs. silica. The dikes and sills plot in two separate groups in the tholeiite field with weathered samples scattered to the left in the alkalic field. (WC65-3 from Schmidt (1978); HE samples from Eisenbeis (1958).

In Figures 55 and 56 sample data from the Wyoming dike group IIIA (Mueller, 1971) were included with the data from the Montana sills to try and determine a relationship between the sills and dikes. These figures plot various major oxides against total silica. The least altered samples (MT-ALE-01; MT-MR-01, 02; MT-RPE-04, 21; MT-RPM-01, 02; WC65-3; HE-5; and MBT-3, 5, 22, 23, 24, 30, 51, 81, 109) generally plot in two groups, a sill group and dike group. The extremely weathered samples scatter to the left of these two groups. Generally, trends (from right to left) starting from the Wyoming dikes show a decrease in silica concentrations. The alkalis and CaO slightly increase (from right to left) between the two groups. The increasing trend of alkalis and CaO is consistent with possible crustal contamination from the argillite and carbonates of the Belt-Purcell Supergroup. However, the decreasing trend in silica in these graphs is not consistent with contamination by silica-rich Belt-Purcell rocks. This decrease is in fact the opposite of what one would expect since the rocks of the Belt-Purcell basin are silica-rich and should increase silica contents as contamination occurred. These trends are compatible with partial melting at variable pressures and varying degrees of partial melting.

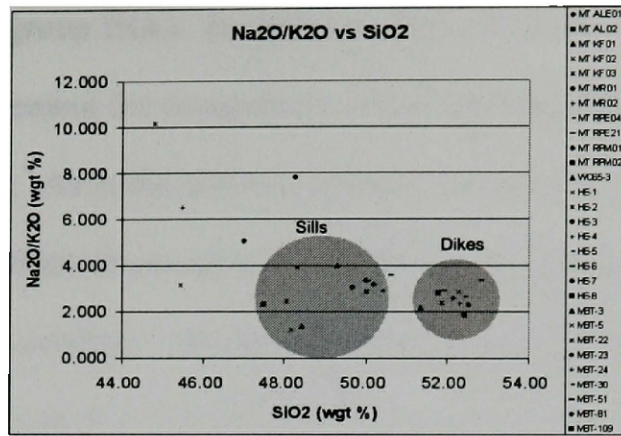


Figure 55. Sills and dikes plot in two different groups in this graph. The alkalis increase slightly from dikes to sills. (WC65-3 from Schmidt (1978); HE samples from Eisenbeis (1958)).

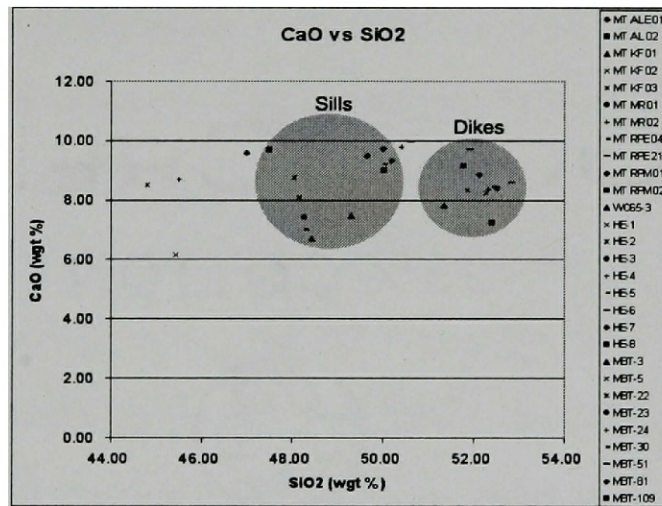


Figure 56. In this graph sills and dikes plot in two different groups. CaO increases slightly from dikes to sills. (WC65-3 from Schmidt (1978); HE samples from Eisenbeis (1958)).

Because no apparent relationship between the two groups is evident in the previous figures, this study analyzed the one element whose content in both the sills and dikes is unique. The TiO_2 content of the sills and dikes is higher than typical tholeiites, and, as stated above, could be used as an identifier for these sills and dikes. Based on Mueller (1971) and Mueller and Rogers (1973) grouping of the Wyoming dikes based on TiO_2 content, it is reasonable to suggest that the sills in Montana might also be grouped

with the youngest dike set (group IIIA). In addition, titanium is not a very mobile element making it a good element for comparison of the sills and dikes. In Figure 57, TiO_2 is plotted against silica. As in the previous graphs the samples plot in two groups, a sill group and dike group. Silica decreases (from right to left) between these groups, and the amount of TiO_2 remains constant. Weathered samples in the following figures are typically scattered and inconsistent. Therefore, they will not be discussed further. Again, no apparent relationship is visible in this figure.

Figure 58 plots TiO_2 against aluminum and Figure 59 plots TiO_2 against MgO . In these figures, both the sills and dikes plot in one group indicating similar magma composition. It is important to note that MgO can be considered an early crystallizing constituent and is not very mobile during alteration. This is significant when considering that both the sills and dikes have similar MgO and TiO_2 contents. To further investigate this similarity, other major oxides were plotted against MgO (Figures 60-63). With the exception of Figure 63, the sills and dikes again plot in one group. This is noteworthy because the oxides plotted can be very mobile during any type of alteration process that may have affected the rocks. In Figure 63, silica content decreases from the top between the dikes and sills while MgO remains uniform between all the samples. The similar MgO , Al_2O_3 , CaO , and TiO_2 contents between the sills and dikes suggest a single parent magma.

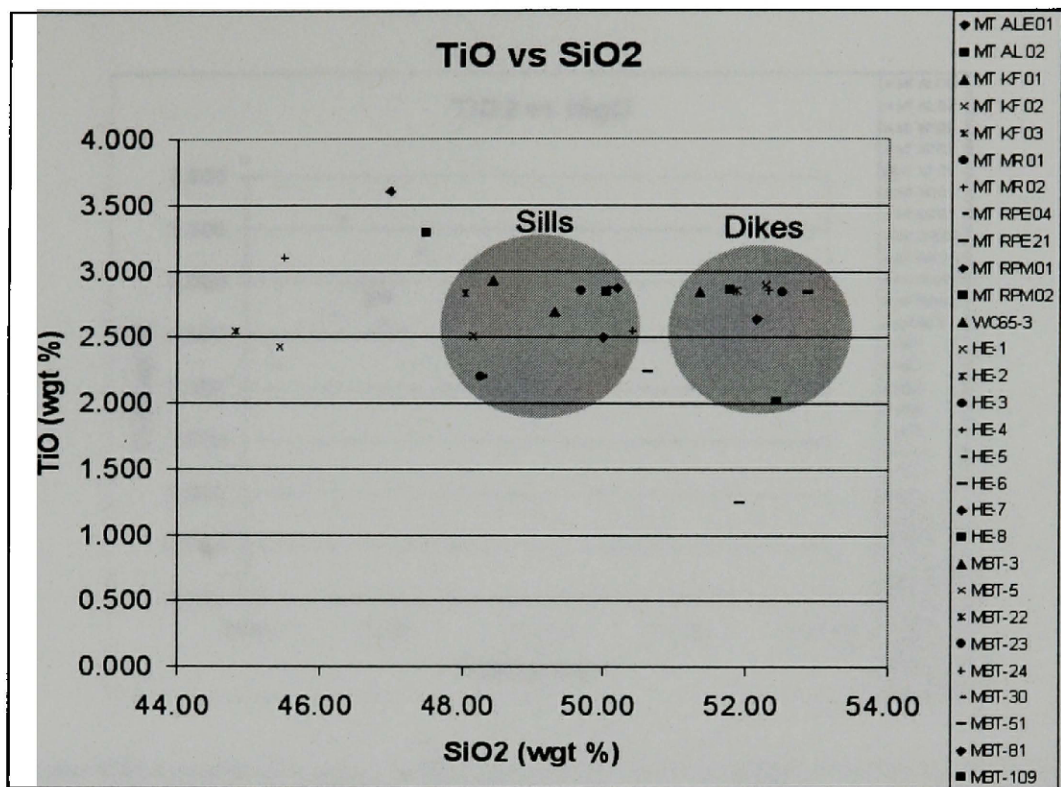


Figure 57. TiO₂ vs. silica graph. Sills and dikes plot in separate groups that show a decrease in SiO₂ from dikes to sills. TiO₂ contents remain constant. (WC65-3 from Schmidt (1978); HE samples from Eisenbeis (1958)).

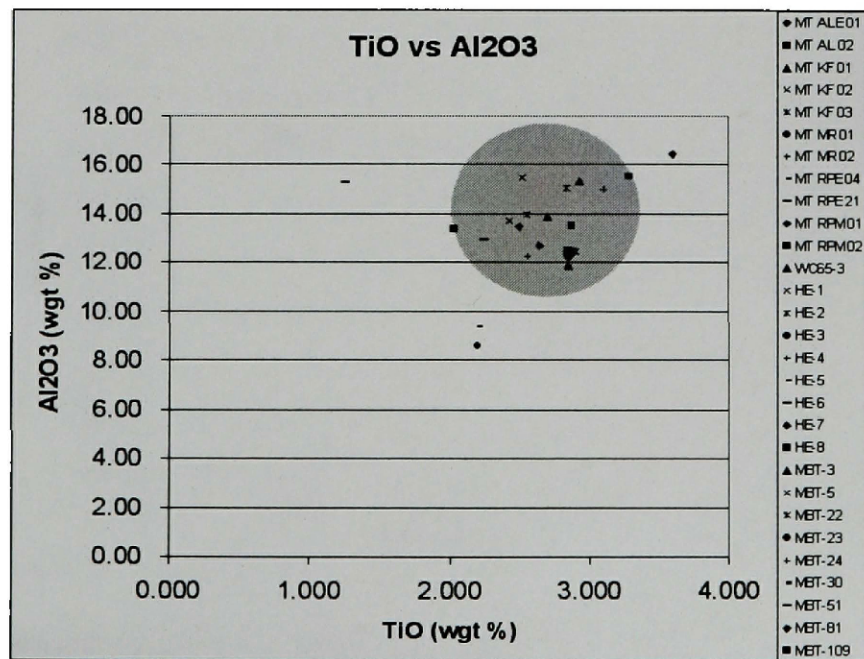


Figure 58. Sills and dikes plot in one group indicating similar TiO₂ and Al₂O₃ amounts. (WC65-3 from Schmidt (1978); HE samples from Eisenbeis (1958)).

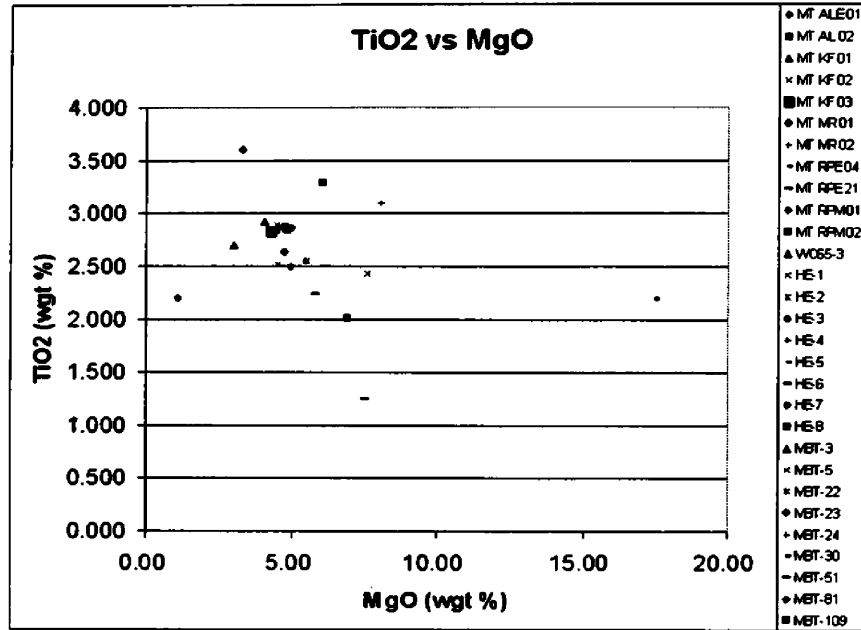


Figure 59. Sills and dikes plot in one group indicating similar TiO₂ and MgO amounts. (WC65-3 from Schmidt (1978); HE samples from Eisenbeis (1958)).

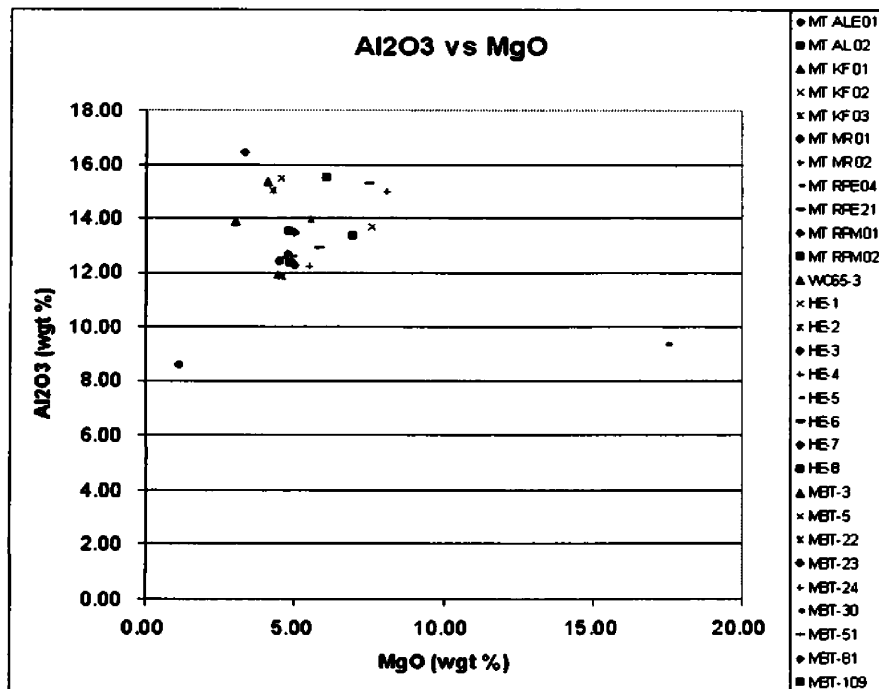


Figure 60. Sills and dikes plot in one group indicating similar Al₂O₃ and MgO amounts. (WC65-3 from Schmidt (1978); HE samples from Eisenbeis (1958)).

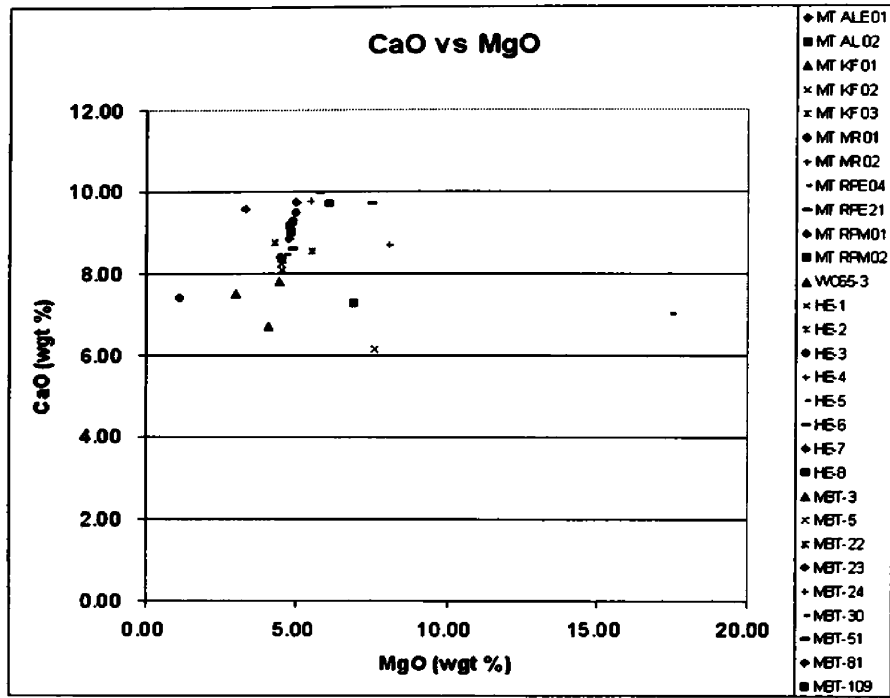


Figure 61. Sills and dikes plot in one group indicating similar MgO and CaO amounts. (WC65-3 from Schmidt (1978); HE samples from Eisenbeis (1958)).

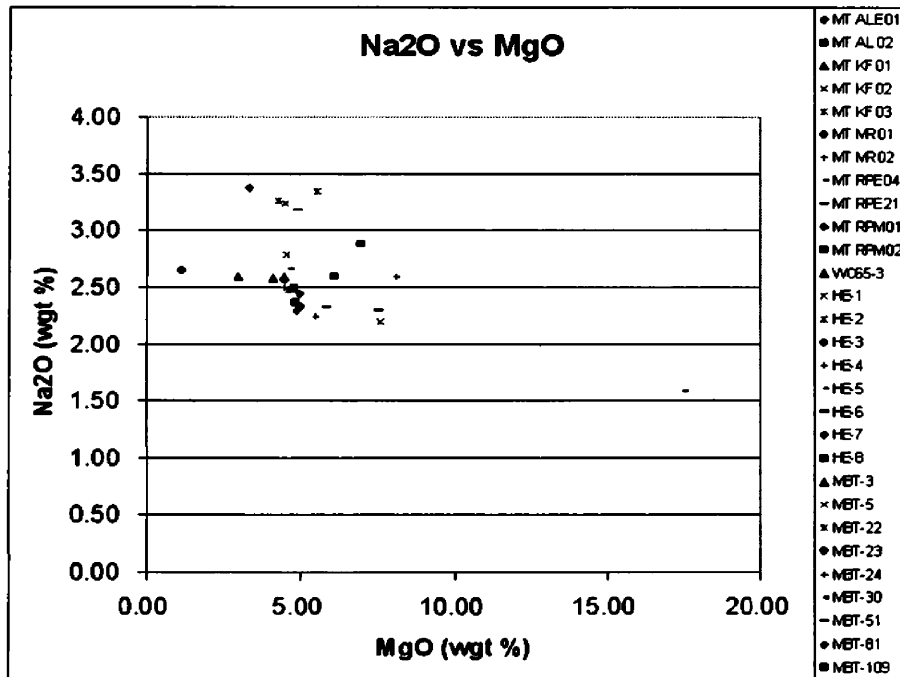


Figure 62. Sills and dikes plot in one group indicating similar Na₂O and MgO amounts. (WC65-3 from Schmidt (1978); HE samples from Eisenbeis (1958)).

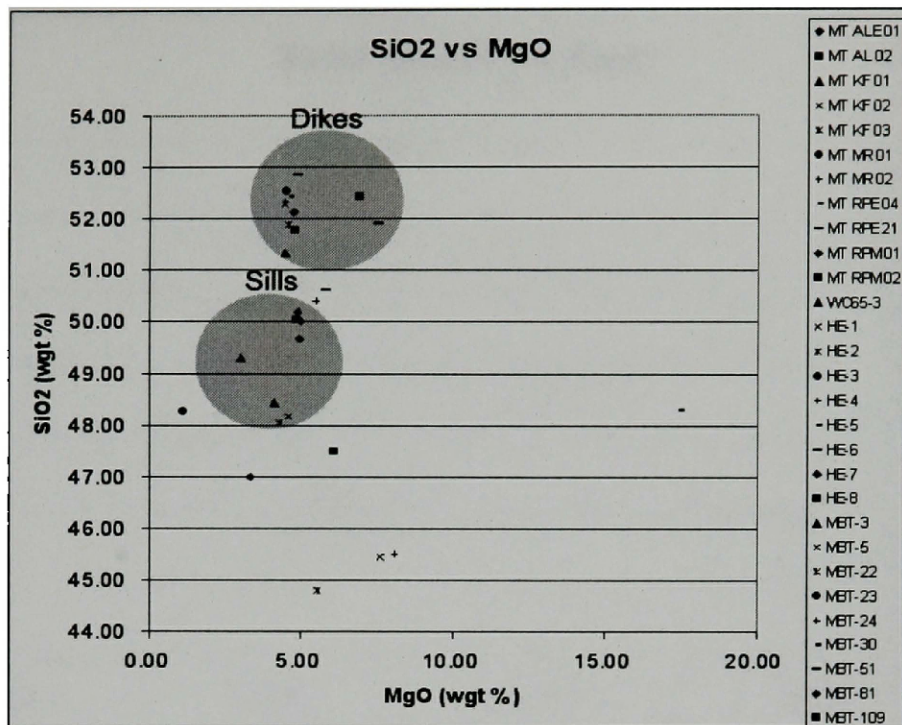


Figure 63. In this graph, the sills and dikes plot in two separate groups that show a decrease in SiO₂ from dikes to sills. MgO content remains constant. (WC65-3 from Schmidt (1978); HE samples from Eisenbeis (1958)).

In an effort to minimize the affects of alteration in analysis, microprobe studies were conducted on mineral grains in seven rock samples that showed very little alteration (Appendix II). The results plot very close together (Figures 64-66d). There is no variation in silica in Figures 64-65b, while the oxides vary between minerals. It is interesting to note that the variation in oxides occurs on a within samples, i.e. data from two grains in one sample plot in different areas on the graph. Although the groups in Figures 66a-d are not as close, the same variation patterns are seen. The microprobe analysis does not add any significant data that would help sill correlation to the XRF/ICP-MS data.

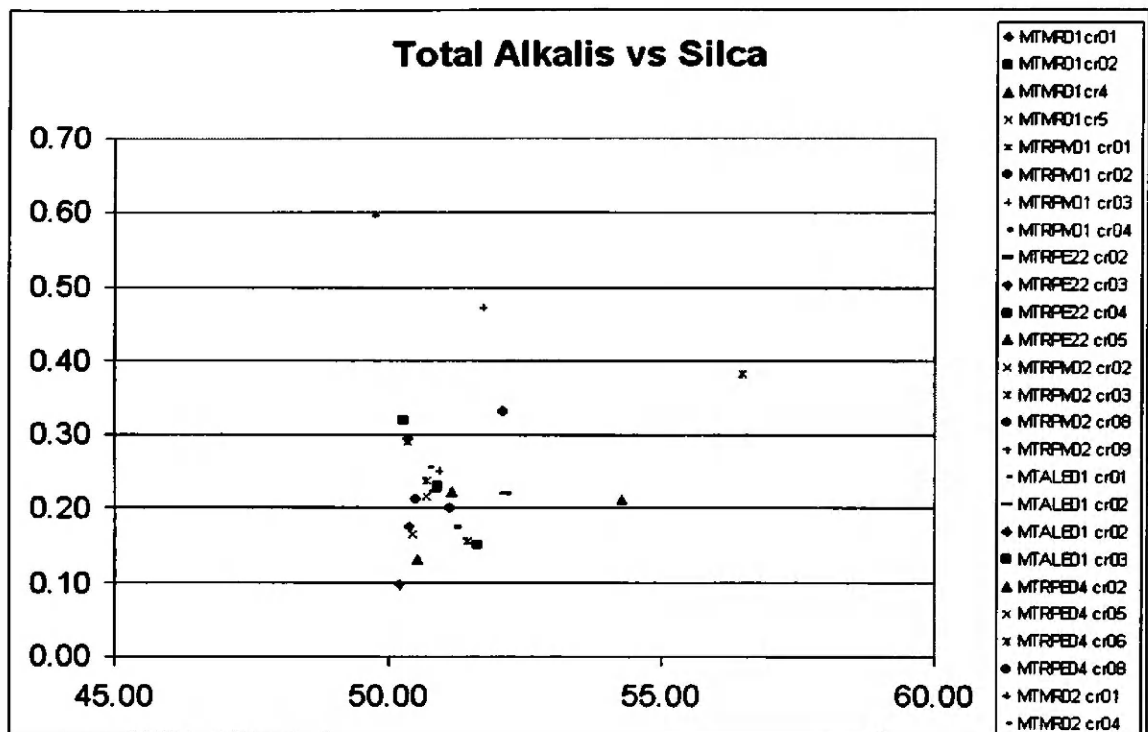


Figure 64. This graphs plots electron microprobe data from individual pyroxene grains. Silica remains constant in this graph, while the total alkalis decreases from the top. There is no consistent pattern between samples as minerals from the same sample may plot either near the top of the group or bottom. The trend represents differences between the minerals, not the rocks.

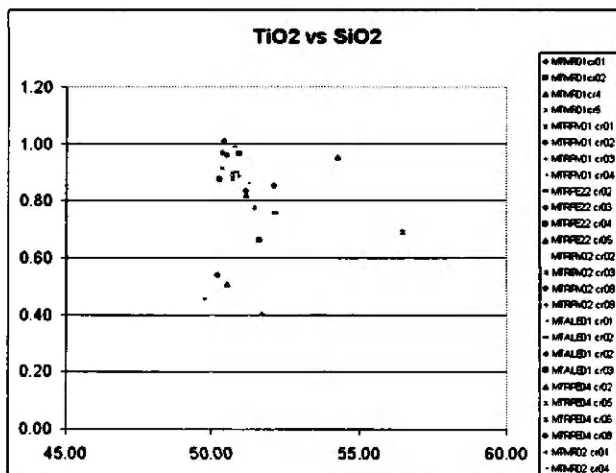


Figure 65a

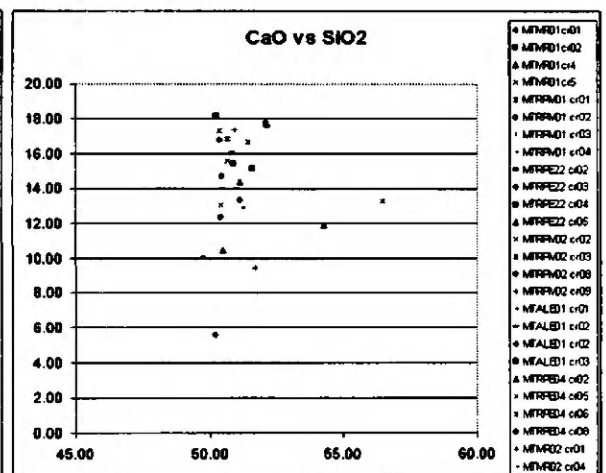


Figure 65b

Figure 65a and b. As in the previous figures the silica in Figures 65a and b remains constant while TiO2 and CaO content decreases from the top. This trend is most likely due to differences in the pyroxene grains and not the rock.

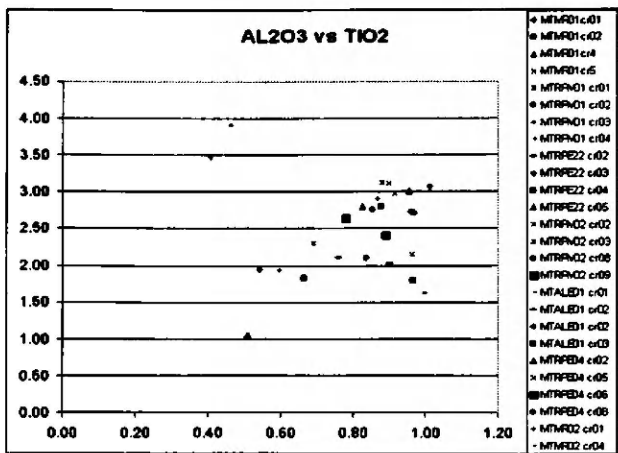


Figure 66a.

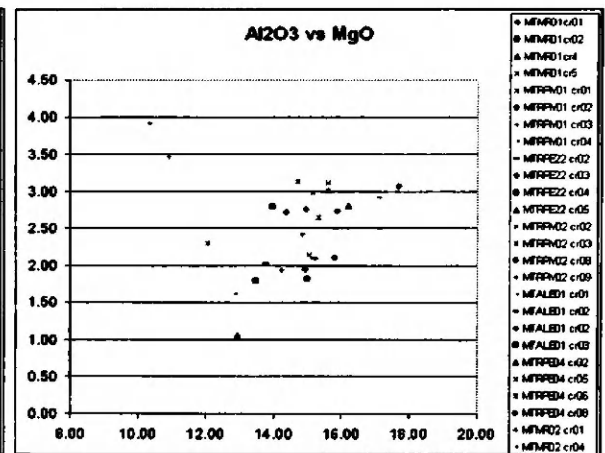


Figure 66b.

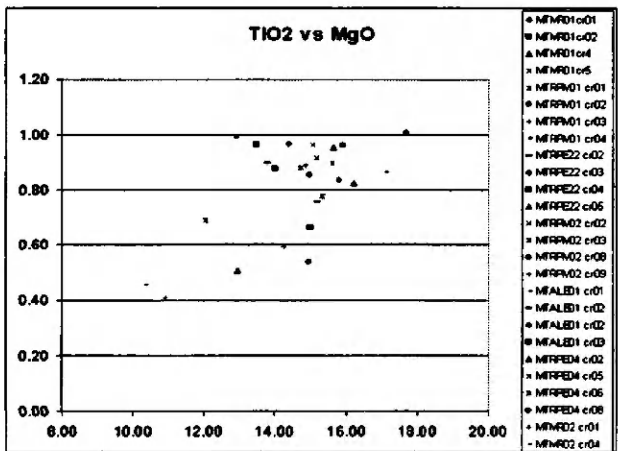


Figure 66c.

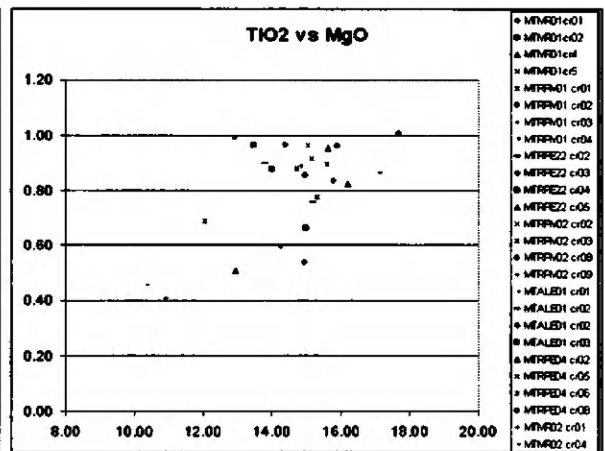


Figure 66d.

Figures 66a-d. Both silica and oxide content are similar in most of the pyroxene grains. Like the previous graphs, data from different pyroxene grains in the same rock plot in various areas of the groups. This intermingling implies a similar composition between grains of all the samples, but does not show any genetic link between sills. (WC65-3 from Schmidt (1978); HE samples from Eisenbeis (1958)).

Plots of other tholeiitic basalt sills found in the literature follow very similar patterns to the graphs presented in this work. To further examine these trends, several samples from the much older Paradise sill (Poage, 1997) were plotted with the Windermere sills (Figure 67a and 67b). While the LIL/HFS and Rock/Chondrite diagrams do show major variations, the variations occur in the more-mobile elements and they almost certainly are related to alteration. The comparisons between the two sills

show no variations that are statistically significant as the overall patterns are similar. The similarity of composition between the older and younger sills implies that the trends are related to the magma type rather than the genetic evolution of the magma. It is significant that, in Figure 68, the Paradise sill plots in a separate group below the sills and dikes of this study. The Paradise sill has a lower overall alkali content that distinguishes this sill from those of this study. Since TiO_2 content is such a unique component of the Windermere intrusions, this oxide was plotted for both the Paradise sill and the younger sills and dikes in Figures 69a-b. These graphs clearly show that the Paradise sill plots in a separate group from the Windermere sills and dikes. Not only does this difference imply that the Windermere intrusions are unique, but it supports the use of the TiO_2 as an identifying characteristic.

Emplacement of individual sills and dikes occurs in relatively short geologic time spans and none of the sills are extraordinarily thick or show signs of multiple intrusions. They may have intruded and cooled fast enough to prevent significant fractionation, and, since they lack multiple intrusions, changes in magma composition that might indicate a common source are not present. The linear characteristic of in the trend of weathering indicates that the most-weathered samples could presumably have had an original composition close to the less-weathered samples. The close grouping of less-altered samples in both the whole-rock and microprobe mineral composition graphs also indicates that all the samples came from one type of igneous rock, in this case diabase. The differences in alkali content, TiO_2 , and MgO in Figures 68-69b between the Windermere intrusions and the Paradise sill suggest that the Windermere intrusions are unique diabase intrusions in the Belt-Purcell basin. The high TiO_2 content (2.69%) of the

sills and dikes is uncommon for subalkaline tholeiites and is compatible with the hypothesis that the Windermere sills and dikes represent a single and distinct intrusive event.

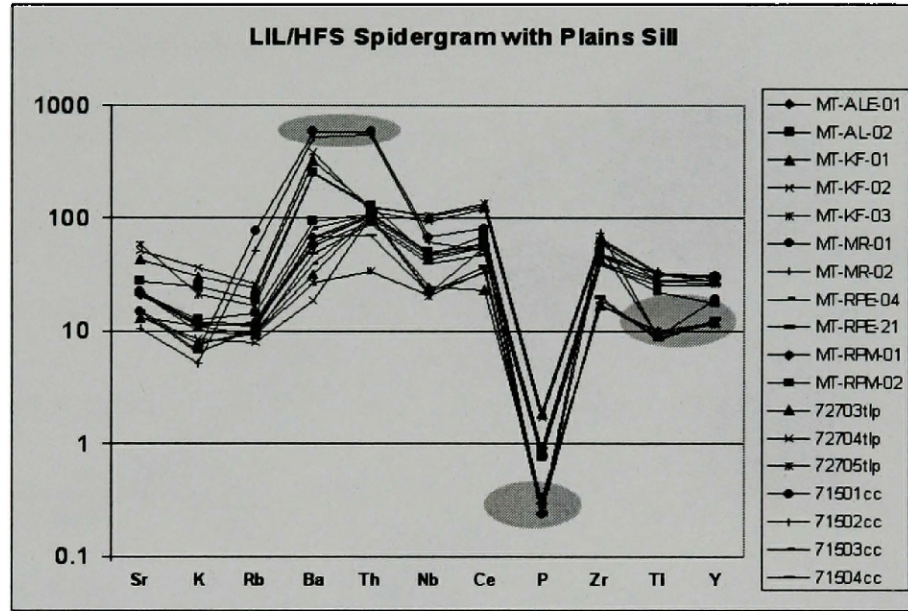


Figure 67a.

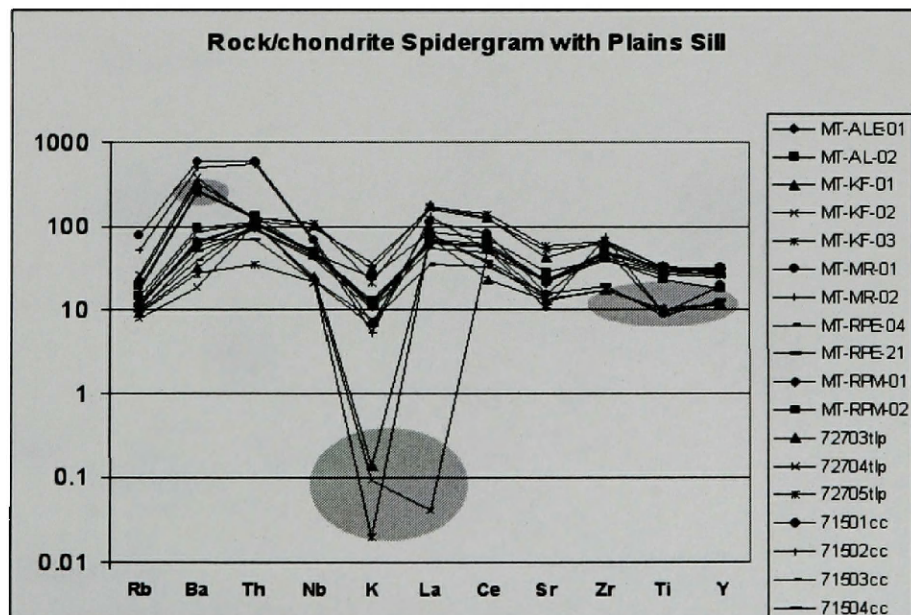


Figure 67a and b. Data from the Plains sill (Poage, 1997) is plotted with those of this study. The patterns are very similar. Major variations occur at the mobile elements (shaded). Minor variations occur at the immobile elements (shaded). The trends are compatible with a single magma type and do not distinguish between intrusions. (chondrite data in Figure 72b from Sun and McDonough, 1989 and Anders and Grevesse, 1989). (WC65-3 from Schmidt (1978); HE samples from Eisenbeis (1958); samples tlp and cc from Poage (1997)).

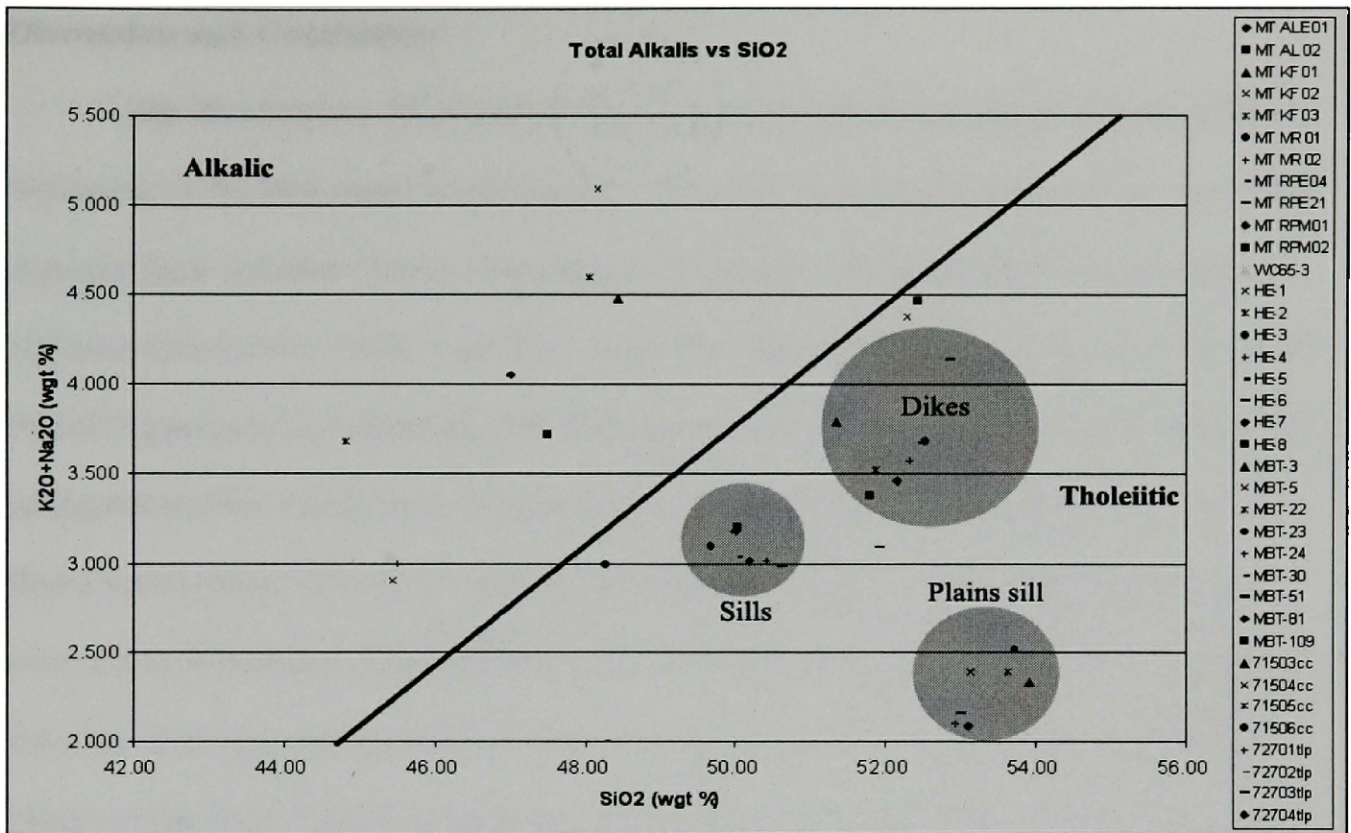


Figure 68. Total alkalis vs. silica graph with Plains sill included. Plains sill plots in a separate group from both dikes and sills. (WC65-3 from Schmidt (1978); HE samples from Eisenbeis (1958); samples tlp and cc from Poage (1997)).

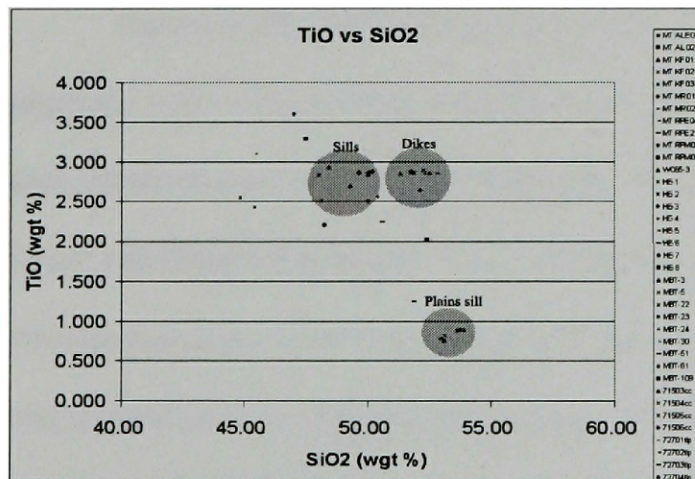


Figure 69a.

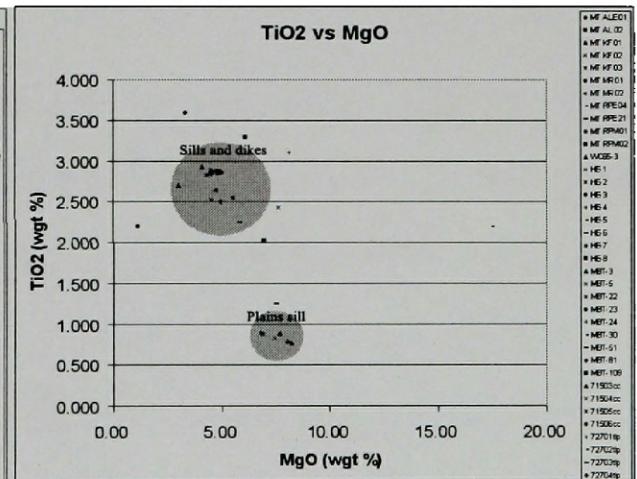


Figure 69b.

Figure 69a and b. The Plains sill plots in a separate group from the dike group and sill group. The TiO_2 content of the Plains sill is clearly not as high as in the Windermere intrusions. (WC65-3 from Schmidt (1978); HE samples from Eisenbeis (1958); samples tlp and cc from Poage (1997)).

Discussion and Conclusions

The Windermere dikes and sills are regionally extensive, ranging from northern Wyoming to the Montana-Canada border. Mesozoic and Cenozoic tectonic events have exposed these intrusive bodies throughout this region. Structurally the dikes intruded Archean basement rocks in Wyoming, while the sills intrude the formations of the Belt-Purcell Supergroup in Montana after lithification of those sediments. When plotted on a palinspastic map, the thickest and deepest segments of the sills follow the axis of the Belt-Purcell basin, which is co-linear with the dike swarms in the Alberton, Montana, area and in Wyoming. This indicates the dike swarms may be part of a conduit that fed the sills. The sills would develop when the magma followed the horizontal bedding planes of the Belt-Purcell Supergroup. The sills rise and thin from the inferred conduit towards the basin margins, creating a regional bowl-shape that conforms to the overall structure of the basin.

Zircon U-Pb dates determined from the granophyre associated with these sills correlate well, within error, with the argon dates determined by previous workers for sills near Alberton and Wolf Creek, Montana, as well as with dates determined for dikes in the Teton and Beartooth ranges. This correlation also suggests the sills never exceeded the reset temperature of the argon system and indicates shallow intrusion. Harlan (1997, 2003) associates the dikes in Wyoming with the Wolf Creek sill using age data. The Wolf Creek sill can be traced on the Choteau 1° x 2° geologic map (Mudge et al., 1992) northwest to the same outcrop analyzed and dated in this study. Combined with the correlation of argon ages, it is probable that the dikes and sills are coeval.

The Windermere intrusive rocks are tholeiitic diabase basalt in composition, dominated by plagioclase, augite, and pigeonite. Tectonic events have fractured and metamorphosed the intrusive rocks to low-grade greenschist facies locally, while weathering has affected some exposures. Geochemical data incorporating data from Milltown (Eisenbeis, 1958), the Wyoming dike swarm (Mueller, 1971), and Wolf Creek (Schmidt, 1978) show possible alteration effects. Removal of alteration from these rocks appears to move the data points closer to the less-altered samples, indicating a single parent magma. The dike swarms appear to be at or near the origin of intrusion because the dikes are in line with an apparent conduit system found on the palinspastic map (Figures 43 and 44) and with the trend in maximum thickness of the sills. Furthermore, the dike swarms intrude Archean basement rocks in Wyoming. As the magma production continued, it became less alkalic, most likely due to either change in pressure or degree of partial melting, resulting in less alkalic dikes in the Teton and Beartooth ranges. Although an older sill shows similar geochemical trends, the Windermere magma intruded the youngest of Belt-Purcell rocks after their lithification, appears to cut the Purcell lava, and is truncated at the Cambrian unconformity, clearly demonstrating that it is younger than the earlier intrusions. In addition, the high average TiO_2 content makes the Windermere intrusions unique features within the Belt-Purcell basin

Windermere-related sedimentary rocks occur in British Columbia, Washington, and Idaho, but are absent in Montana. This could be due to the Belt rocks filling all sediment accommodation space and the termination of basin growth. A map locating Windermere-related rocks throughout northwestern America reveals an en echelon pattern, which is typical of rift zones. The dikes and sills are located on the eastern

margin of this pattern. In addition to their structural relationship, there is a strong correlation in ages between the Windermere sedimentary rocks and the sills and dikes of this study (Figure 47). The sills and dikes may represent the earliest Windermere rift activity and may comprise the only related rocks in Montana.

The timing of initial Windermere rift activity associated with the break-up of the supercontinent Rodinia is complex and not fully understood. Dates inferred for initial rift activity and deposition of Windermere rocks vary in age but concentrate around 760 Ma to 650 Ma. This range is most likely due to progression of rift activity along the rift axis. Devlin et al. (1988) obtained a Sm-Nd date of 762 ± 44 Ma for Windermere volcanic Huckleberry Formation in northeastern Washington. This age correlates well with the ages determined on the dikes and sills of this study. Furthermore, the Huckleberry Formation is en echelon with the sills and dikes of this study (Figure 47), suggesting they are coeval. Recent studies dated Windermere rift volcanic rocks as 685 Ma in central Idaho (Lund et al., 2003) and 667-717 Ma in southern Idaho (Fanning and Link, 2003), indicating that the rift axis may have jumped west to establish the eventual margin of Laurentia. Several researchers have proposed that actual continental separation occurred around 570 Ma to 555 Ma (Bond and Kominz, 1984; Bond et al., 1984; Colpron et al., 2002). The western margin of the Laurentian craton truncated both the Windermere intrusive group rocks and the three previous intrusive episode rocks (Höy, 2000). This truncation is significant when reconstructing Precambrian plate margins, as the intrusions are also likely to be found on the opposing plate.

Ernst and Buchan (2000) identified the Wolf Creek sill of Schmidt (1978) as being related to the 780 Ma Mackenzie dikes in northwestern Canada and part of a type A

large igneous province. Harlan et al. (2003) also correlate the sills and dikes in Montana and northern Wyoming with intrusions in northwestern Canada and suggest they are part of a ca. 780 Ma magmatic event (Gunbarrel magmatic event) that may be related to the commencement of early Windermere mafic volcanism, i.e. the Huckleberry Formation in northeastern Washington state. Both of these studies base the association of regional intrusions only on age data and geographical relationships with the margins of Laurentia. The correlation of intrusions over such an extended area (greater than 2400 km) strictly based on age and geography can be misleading. A clear relationship between these intrusions, based on a more thorough investigation such as with geochemistry, has not been established.

Although the Windermere intrusive group alone may not be voluminous enough to qualify as a large igneous province by the definition of Coffin and Eldholm (1992, 1994), the term igneous province could be applied, as they are regionally extensive and a very significant feature of the Belt-Purcell basin. If the Windermere intrusive group is associated with the Gunbarrel magmatic event, which remains to be determined in detail, the term large igneous province is valid if applied to all associated intrusions. If the Windermere intrusive group is a segment of an igneous province or LIP (specifically the Gunbarrel magmatic event) that extended beyond Laurentia into the now detached opposing craton a significant piercing point could be established in conjunction with the three previous intrusive events. Hansen et al. (1999) advocate that correlative LIPs on separate cratons establish possible constraints on the comparative arrangement of cratons within supercontinental assemblies. The use of geochronology enables the distinction between such split LIPs (Ernst et al., 1999). Because the likelihood of igneous provinces

with identical ages and compositions in more than one geographic location is statistically low, finding similar igneous provinces on different cratons would suggest that the two cratons were attached prior Rodinia breakup. This relationship would help determine which craton split off from the western margins of Laurentia by comparing similar igneous provinces on the Antarctic, Australian, or Siberian cratons. In addition, finding all four intrusive events would provide much stronger correlation evidence.

The combined data of this study strongly suggests that the Neoproterozoic sills and dikes in western Montana and northern Wyoming are related to a single and distinctive intrusive event associated with Windermere rifting. Other intrusions of similar age have also been recognized in North America, namely the Mackenzie dike swarm and Hottah sheets ca. 780 in northwestern Canada (LeCheminant and Heaman, 1994; Park et al., 1995, Harlan et al., 2003). These intrusions are not necessarily genetically related to the sills and dikes of this study. Increased magmatism occurred around 780-750 Ma on several cratons (Ernst and Buchan, 2000) most likely associated with the break-up of Rodinia. Wingate et al. (1998) used U-Pb and paleomagnetic data to conclude that a dike swarm in central-south Australia ca. 827 was not related to the Mackenzie and Hottah intrusives. Recently Sklyarov et al. (2003) dated a sill in the southern part of the Siberian craton at 758 Ma. Data similar to that gathered in this study is critical when evaluating the timing and relationship of these intrusive events, but the previous studies did not use geochemical or other significant data to establish a genetic association between the intrusions located on the various cratons. Certainly magmatic events can take place over a large interval, whether due to rates of intrusion or episodic pulses and age data alone may provide a clear relationship.

The spatial relationship of the sills and dikes, similar ages, alignment of the bowl shape of the sills (defined by the sill structure) with the northwest trend of the dike swarms, and the high (for tholeiites) average (2.69%) TiO_2 content all argue for a single intrusive event. In addition, the geographic locations, structural position within the en echelon pattern of Windermere-related rock exposures, and age of the sills and dikes support a relationship with early Windermere rift activity.

References

- Alt, D., Sears, J. W., and Hyndman, D. W., 1988, Terrestrial Maria: The origins of large basalt plateaus, hotspot tracks and spreading ridges: *The Journal of Geology*, vol. 96. no. 6. p. 647-662.
- Anders, E. and Grevesse, N., 1989, Abundances of the elements: Meteoric and solar: *Geochimica et Cosmochimica Acta*, vol. 53. p. 197-214.
- Anderson, H. E. and Parrish, R. R., 2000, U-Pb geochronological evidence for the geological history of the Belt-Purcell Supergroup, southeastern British Columbia: *in* Lydon, John W., Trygve, Höy, Slack, John F., and Knapp Marcia E., eds., *The Geological Environment of the Sullivan Deposit, British Columbia: Geological Association of Canada, St. John's, Newfoundland* p. 113-126.
- Baadsgaard, H. and Mueller, P. A., 1973, K-Ar and Rb-Sr ages of intrusive Precambrian mafic rocks, southern Beartooth Mountains, Montana and Wyoming: *Geological Society of America Bulletin*, vol. 84. p. 3635-3644.
- Bishop, D. T., 1973, Petrology and geochemistry of the Purcell Sills in Boundary County, Idaho: *in* Belt Symposium I. Idaho Bureau of Mines and Geology, Special Publication, p. 15-66.
- Bond, G. C. and Kominz, M. A., 1984, Construction of tectonic subsidence curves for the early Paleozoic miogeocline, southern Canadian Rocky Mountains: Implications for subsidence mechanisms, age of breakup, and crustal thinning: *Geological Society of America Bulletin*, vol. 95. p. 155-173.
- Bond, G. C., Nickeson, P. A., and Kominz, M. A., 1984, Breakup of a supercontinent between 625 Ma and 555 Ma: new evidence and implications for continental histories: *Earth and Planetary Science Letters*, vol. 70. p. 325-345.
- Bott, M. H. P., The stress regime associated with continental break-up: *in* *Magmatism and the Causes of Continental Break-up*, Storey, B. C., Alabaster, T., Pankhurst, R. J., eds. *The Geological Society Special Publication No. 68.* p. 125-136.
- Buckley S. N. and Sears, J. W., 1993, Shallow emplacement of sills into wet Belt Supergroup sediment at Perma, western Montana: *in* Belt Symposium III, Berg, Richard B. ed., *Montana Bureau of Mines and Geology, Special Publication 112.* p. 32-43.
- Burtis, E. W., Sears, J. W., and Chamberlain, K. R., 2003a, Geometry of mafic sills in the Mesoproterozoic Belt-Purcell Basin, northern Rocky Mountains: *Geological Society of America, Abstracts with Programs*, vol. 35. no. 5. p. 41.

- Burtis, E. W., Sears, J. W., and Chamberlain, K. R., 2003b, Windermere sill and dike complex in northwestern Montana: Implications for the Belt-Purcell Basin: Northwest Geology, Tobacco Root Geological Society/Montana State University, vol. 32. p. 186-189.
- Cadman, A. C., Heaman, L., Tarney, J., Wardle, R., and Krogh, T. E., 1993, U-Pb geochronology and geochemical variation within two Proterozoic mafic swarms, Labrador: Canadian Journal of Earth Sciences, vol. 30. p. 1490-1504.
- Calkins, F. C., and Emmons, W. H., 1915, Description of the Phillipsburg Quadrangle, Montana: US Geological Survey Atlas, Folio 196.
- Chamberlain, K. R., Sears, J. W., and Doughty, P. T., 2003, The Case for Episodic rifting, subsidence, and deposition in the Belt-Purcell Basin, 1470 1370: Northwest Geology, Tobacco Root Geological Society/Montana State University, vol. 32. p. 190-191.
- Coffin, M. F, and Eldholm, O., 1992, Volcanism and continental break-up: A global compilation of large igneous provinces: *in* Magmatism and the Causes of Continental Break-up, Storey, B. C., Alabaster, T., Pankhurst, R. J., eds. The Geological Society Special Publication No. 68. p. 17-30.
- Coffin, M. F., and Eldholm, O., 1994, Large igneous provinces: Crustal structure, dimensions, and external consequences: Reviews of Geophysics, vol. 32. p. 1-36.
- Colpron, M., Logan, J. M., and Mortensen, J. K., 2002, U-Pb zircon age constraint for late Neoproterozoic rifting and initiation of the lower Paleozoic passive margin of western Laurentia: Canadian Journal of Earth Sciences, vol. 39. p. 133-143.
- Condie, K. C., Barsky, C. K., and Mueller, P.A., 1969, Geochemistry of Precambrian diabase dikes from Wyoming: Geochimica et Cosmochimica Acta, vol. 33. p. 1371-1388.
- Cook, F. A. and Van der Velden, A. J., 1995, Three-dimensional crustal structure of the Purcell Anticlinorium in the Cordillera of southwestern Canada, Geological Society of America Bulletin, vol. 107. no. 6. p. 6642-664.
- Courtney, R. C. and White, R. S., 1986, Anomalous heat flow and geoid across the Cape Verde Rise: Evidence for dynamic support from a thermal plume in the mantle, Geophysical Journal of the Royal Astronomy Society, vol. 87. p. 815-867.
- Cressman, E. R., 1985, The Prichard Formation of the lower part of the Belt Supergroup (Middle Proterozoic) near Plains, Sanders County, Montana: U. S. Geological Survey Bulletin I-553, 64p.

- Cressman, E. R., 1989, Reconnaissance stratigraphy of the Prichard Formation (Middle Proterozoic) and the early development of the Belt basin, Washington, Idaho, and Montana: U. S. Geological Survey Professional Paper 1490, 80p.
- Daly, R. A., 1912, Geology of the North American Cordillera at the forty-ninth parallel: Canadian Geological Survey Mem. 38. p. 799.
- Dalziel, I. W. D., 1991, Pacific margins of Laurentia and East Antarctica-Australia as a conjugate rift pair: evidence and implications for an Eocambrian supercontinent: *Geology*, vol. 19. p. 598-601.
- Dalziel, I. W. D., Lawyer, L. A., Murphy, J. B., 2000, Plumes, orogenesis, and supercontinental fragmentation: *Earth and Planetary Science Letters*, vol. 178. p. 1-11.
- Deiss, C.F., 1943, Stratigraphy and structure of the southwest Saypo Quadrangle, Montana: *Geological Society of America Bulletin*, vol. 54. p. 205-262.
- Devlin, W., Brueckner, H. K., and Bond G. C., 1988, New isotopic data and preliminary age for volcanics near the base of the Windermere Supergroup, northeastern Washington, U. S. A.: *Canadian Journal Of Earth Sciences*, vol. 25. p. 1906-1910.
- Doughty, P. T., and Chamberlain, K. R., 1996, Salmon River Arch revisited: New evidence for 1370 Ma rifting near the end of deposition in the middle Proterozoic Belt-Purcell Basin: *Canadian Journal of Earth Sciences*, vol. 33. p. 1037-1052.
- Eisenbeis, H.R., 1958, The Petrogenesis of the Milltown Dam Sill, Missoula County, Montana: M. S. Thesis, Montana State University 37p.
- Ernst, R. E., 1999, Mantle plume events during the assembly and breakup of Rodinia: The record from short-duration large igneous provinces: *GSA Abstracts with Programs*, vol. 31. no. 7. p. 316.
- Ernst, R. E. and Buchan, K. L., 2000, Large mafic magmatic events through time and links to mantle-plume heads, *in* *Mantle Plumes: Their Identification through Time*, Buchan, Kenneth L. and Ernst, Richard E., *eds.* Geological Society of America Special Paper 352. p. 1-4.
- Evans, K., 1981, Geology and geochronology of the eastern Salmon River Mountains, Idaho, and implications for regional Precambrian Tectonics, Ph.D. Thesis, The Pennsylvania State University, 222 p.

- Evans, K. V, Aleinikoff, J. N., Obradovich, J. D., and Fanning, M. C., 2000, SHRIMP U-Pb geochronology of volcanic rocks, Belt Supergroup, western Montana: evidence for rapid deposition of sedimentary strata: *Canadian Journal of Earth Sciences*, vol. 37. p. 1287-1300.
- Evans, K. V. and Green, G. N., 2003, Geologic map of the Salmon National Forest and vicinity, East-Central Idaho: USGS Geologic Investigation Series I-2765.
- Evans, K. V., and Zartman, R. E., 1990, U-Th-Pb geochronology of middle Proterozoic granite and augen gneiss, Salmon River Mountains, east-central Idaho: *Geological Society of America Bulletin*, vol. 102. p. 63-73.
- Fanning, M. C. and Link, P. K., 2003, 700 Ma U-Pb SHRIMP age for Sturtian (!) diamictites of the Pocatello Formation, southeastern Idaho: *Geological Society of America, 2003 Annual Meeting, Abstracts with Programs*, vol. 35. no. 6. p. 389.
- Fenton, C. L., and Fenton, M. A., 1937, Belt Series of the North; Stratigraphy, sedimentation, paleontology: *Geological Society of America Bulletin*, vol. 48. p. 1873-1969.
- Frost, C. D. and Winston, D., 1987, Nd isotope systematics of coarse- and fine-grained sediments: Examples from the middle Proterozoic Belt-Purcell Supergroup: *Journal of Geology*, vol. 95. p. 309-327.
- Hansen, R. E., Bowring, S. A., and Dalziel, I. W., 1999, Emplacement of Large Igneous Provinces in the Kalahari and Laurentian Cratons at 1.1 Ga: Implications for Rodinia assembly: *GSA Abstracts with Programs*, vol. 31. no. 7. p. 430
- Hanson, G. N. and Gast, P. W., 1967, Kinetic studies in contact metamorphic zones: *Geochimica et Cosmochimica Acta*, vol. 31. p. 1119-1153.
- Harlan, S., S., Heaman, L., LeCheminant, A. N., and Premo, W. R., 2003, Gunbarrel mafic magmatic event: A key 780 Ma time marker for Rodinia plate reconstructions: *Geology*, vol. 31. no. 12. p. 1053-1056.
- Harlan, S., S., Geissman, J. W., and Snee, L. W., 1997, Paleomagnetic and ^{40}Ar - ^{39}Ar geochronologic data from late Proterozoic mafic dikes and sills, Montana and Wyoming: *U. S. Geological Survey Professional Paper 1580*, 16 p.
- Harrison, J. E., 1972, Precambrian Belt Basin of the Northwestern United States: Its geometry, sedimentation, and copper occurrences: *Geological Society of America Bulletin*, vol. 83. p. 1215-1240.
- Harrison, J. E., Cressman, E. R., and Whipple, J. W., 1992, Geologic and structure maps of the Kalispell 1° x 2° Quadrangle, Montana and Alberta British Columbia: *US Geological Survey Map I-2267*, scale: 250,000.

- Harrison, J. E., Griggs, A. B., and Wells, J. D., 1986, Geologic and structure maps of the Wallace 1° x 2° Quadrangle, Montana and Idaho: US Geological Survey Map I 1509-A, scale 1: 250,000.
- Hoffman, P. F., 1991, Did the breakout of Laurentia turn Gondwanaland inside-out?: *Science*, vol. 252. p. 1409-1412.
- Höy, T., 1989, The age, chemistry, and tectonic setting of the middle Proterozoic Moyie Sills, Purcell Supergroup, southeastern British Columbia: *Canadian Journal of Earth Sciences*, vol. 26. p. 2305-2317.
- Höy, T., Anderson, D., Turner, R. J. W., and Leitch, C. H. B., 2000, Tectonic, Magmatic and Metallogenic History of the Early Synrift Phase of the Purcell Basin, Southeastern British Columbia: *in* Lydon, John W., Trygve, Höy, Slack, John F., and Knapp Marcia E., eds., *The Geological Environment of the Sullivan Deposit, British Columbia: Geological Association of Canada, St John's, Newfoundland* p. 32-60.
- Hunt, G, 1962, Time of Purcell eruption in southeastern British Columbia and southwestern Alberta: *Journal of the Alberta Society of Petroleum Geology*, vol. 10. p. 438-442.
- Jefferson, C. W., 1978, Correlation of Middle and Upper Proterozoic strata between north-western Canada and south and central Australia: *Geological Society of America Programs with Abstracts*, vol. 7. p. 429.
- Johnson, D. M., Hooper, P. R., and Conrey, R. M., 1999, XRF analysis of rocks and minerals for major and trace elements on a single low dilution Li-tetraborate fused bead: Department of Geology, Washington State University, GeoAnalytical Laboratory website:
http://www.wsu.edu:8080/%7Egeology/Pages/Services/DJ_Paper/DJPaper.html
- Karlstrom, K. E., Åhäll, K., Harlan, S. S., Williams, M. L., McLelland, J., and Geissman, J. W., 2001, Long-lived (1.8-1.0 Ga) convergent orogen in southern Laurentia, its extensions to Australia and Baltic, and implications for refining Rodinia: *Precambrian Research*, vol. 111. p. 5-30.
- Keen, C. E., 1987, Some important consequences of lithospheric extension: *in* *Continental Extensional Tectonics*, Coward, M. P., Dewey, J. F., and Hancock, P. L., eds. Geological Society Special Publication No 28. p. 67-73.
- Knaack, C., Cornelius, S., and Hooper, P., 1994, Trace element analysis of rocks and minerals by ICP-MS: Department of Geology, Washington State University, GeoAnalytical Laboratory website:
<http://www.wsu.edu:8080/%7Egeology/Pages/Services/ICP.html>

- Krogh, T. E., 1973, A low-contamination method for hydrothermal decomposition of zircon and extraction of U and Pb for isotopic age determinations: *Geochimica et Cosmochimica Acta*, vol. 37. p. 485-495.
- Krogh, T. E., 1982a, Improved accuracy of U-Pb zircon ages by the creation of more concordant systems using an air abrasion technique: *Geochimica et Cosmochimica Acta*, vol. 46. p. 637-649.
- Krogh, T. E., 1982b, Improved accuracy of U-Pb zircon dating by selection of more concordant fractions using a high gradient magnetic separation technique: *Geochimica et Cosmochimica Acta*, vol. 46. p. 631-635.
- Kruger, J. M., 1988, Late Proterozoic and early Cambrian structural setting of western Montana and the stratigraphy and depositional environment of the Flathead Sandstone in west-central Montana: University of Montana M. S. Thesis, 109 p.
- LeCheminant, A. N. and Heaman, L. M., 1994, 779-Ma mafic magmatism in the northwestern Canadian shield and northern Cordillera: A new regional time marker: *in* Abstracts of the Eighth International Conference on Geochronology, Cosmochronology, and Isotope Geology, Lanphere, M. A., Dalrymple, G. B., and Turrin, B. D., eds. US Geological Survey Circular 1107.
- Lewis, R. S., 1998, Preliminary geologic map of the Butte 1° x 2° quadrangle, Montana Bureau of Mines and Geology Open File Report 363, 16 p. scale 1:250,000.
- Lonn, J., 1984, Structural geology of the Tarkio area, Mineral County, Montana. MS Thesis, University of Montana. 51p.
- Lund, K., Aleinikoff, J. N., Evans, K. V. C., and Fanning, M., 2003, SHRIMP U-Pb geochronology of Neoproterozoic Windermere Supergroup, Central Idaho: Implications for rifting of western Laurentia and synchronicity of Sturtian glacial deposits: *Geological Society of America Bulletin*: vol. 115. No. 3. p. 349-372.
- Lydon, J. W., 2000, A Synopsis of the current understanding of the geological environment of the Sullivan Deposit: *in* Lydon, John W., Trygve, Höy, Slack, John F., and Knapp Marcia E., eds., *The Geological Environment of the Sullivan Deposit*, British Columbia: Geological Association of Canada, St. John's, Newfoundland p. 12-31.
- Lyons, T. W., Luepke, J. J., Schreiber, M. E., and Zieg, G. A., 2000, Sulfur geochemical constraints on Mesoproterozoic restricted marine deposition: Lower Belt Supergroup, northwestern United States: *Geochimica et Cosmochimica Acta*, vol. 64. no. 3. p. 427-437.
- McGimsey, R. G., 1985, The Purcell Lava: Glacier National Park, Montana: USGS Open-File Report 85-0543, Denver, Colorado, 191 p.

- Mejstrick, P. F., 1975, Petrogenesis of the Purcell Sill: Glacier National Park, Montana: Master's Thesis, University of Montana, 74 p.
- Mertie, J. B. Jr., Fischer, R. P., and Hobbs, S. W., 1951, Geology of the Canyon Ferry Quadrangle, Montana: US Geological Survey Bulletin 972.
- Morgan, W. J., 1981, Hotspot tracks and the opening of the Atlantic and Indian Oceans, *in* Emiliani, C., eds., *The Sea, Volume 7, The Oceanic Lithosphere*. Wiley Interscience, New York, p. 443-487.
- Moore, E. M., 1991, Southwest US-East Antarctic (SWEAT) connection: a hypothesis: *Geology*, vol. 19. p. 425-428.
- Morgan, W. J., 1971, Convection plumes in the lower Mantle: *Nature*, vol. 230. p. 42-43.
- Mudge, M. R., 1972, Pre-Quaternary rocks in the Sun River Canyon Area, northwestern Montana: US Geological Survey Professional Paper 663-A, 142 p.
- Mudge, M. R., Earhart, R. L., Whipple, J. W., and Harrison, J. E., 1982, Geologic and structure map of the Choteau 1° x 2° Quadrangle, Western Montana: US Geological Survey Map I-1300, scale 1:250,000.
- Mudge, M., R., Erickson, R. L., and Kleinkopf, D., 1968, Reconnaissance geology, geophysics, and geochemistry of the southeastern part of the Lewis and Clark Range, Montana: US Geological Survey Bulletin 1252-E, 35 p.
- Mueller, P. A., 1971, Geochemistry and geochronology of the mafic rocks of the Southern Beartooth Mountains, Montana and Wyoming, Ph.D. Thesis, Rice University, 78 p.
- Mueller, P., A., and Rogers, J. J. W., 1973, Secular chemical variation in a series of Precambrian mafic rocks, Beartooth Mountains, Montana, and Wyoming: *Geological Society of America Bulletin*, vol. 84. p. 3645-3652.
- Nelson, W. H., and Dobell, J. P., 1961, Geology of the Bonner Quadrangle, Montana, US Geological Survey Bulletin 1111-F, 234 p.
- Obradovich, J. D. and Peterman, Z. E., 1968, Geochronology of the Belt Series, Montana: *Canadian Journal of Earth Sciences*, vol. 5. p. 737-746.
- Park, J. K., Buchan, K. L., and Harlan, S. S., 1995, A proposed giant radiating dyke swarm fragmented by the separation of Laurentia and Australia based on paleomagnetism of ca. 780 Ma mafic intrusions in western North America: *Earth and Planetary Science Letters*, vol. 132. p. 129-139.

- Parrish, R. R., Roddick, J. C., Loveridge, W. D., and Sullivan, R. D., 1987, Uranium-lead analytical techniques at the Geochronology Laboratory, Geological Survey of Canada. *In* Radiogenic Age and Isotope Studies, Report 1. Geological Survey of Canada, Paper 87-2. p. 3-7.
- Poage, M. A., 1997, Hydration, metamorphism, and diabase-granophyre relations in a thick basaltic sill emplaced into wet sediments, western Montana, M. S. Thesis University of Montana, 132 p.
- Poage, M. A., Hyndman, D. W., and Sears, J. W., 2000, Petrology, geochemistry, and diabase-granophyre relations of a thick basaltic sill emplaced into wet sediments, western Montana: *Canadian Journal of Earth Sciences*, vol. 37. p. 1109-1119.
- Price, R. A., 1964, The Precambrian Purcell System in the Rocky Mountains of southern Alberta and British Columbia: *Bulletin of Canadian Petroleum Geology*, vol. 12. p. 399-426.
- Price, R. A. and Sears, J. W., 2000, A Preliminary palinspastic map of the Mesoproterozoic Belt-Purcell Supergroup, Canada and USA: Implications for the tectonic setting and structural evolution of the Purcell Anticlinorium and the Sullivan Deposit: *in* Lydon, John W., Trygve, Höy, Slack, John F., and Knapp Marcia E., eds., *The Geological Environment of the Sullivan Deposit*, British Columbia: Geological Association of Canada, St. John's, Newfoundland p. 61-81.
- Prinz, M., 1964, Geologic Evolution of the Beartooth Mountains, Montana and Wyoming. Part 5. Mafic Dike Swarms of the Southern Beartooth Mountains: *Geological Society of America Bulletin*, vol. 75. p. 1217-1248.
- Ross, C. P., 1963, The Belt Series in Montana: U. S. Geological Survey Professional Paper 346. 122p.
- Ross, C. P., Andrews, D. A., and Witkind, I. J., 1955, Geologic Map of Montana: Montana Bureau of Mines and Geology.
- Ross, G. M., Bloch, J. D., and Krouse, R. H., 1995, Neoproterozoic strata of the southern Canadian Cordillera and the isotopic evolution of Seawater sulfate: *Precambrian Research*, vol. 73. p. 71-99.
- Ross, G. M., Parrish, R. R., and Winston, D., 1992, Provenance and U-Pb geochronology of the Mesoproterozoic Belt Supergroup (northwestern United States): Implications for age of deposition and pre-Panthalassa Plate Reconstructions: *Earth and Planetary Science Letters*, vol. 113. p. 57-75.

- Ross, G. M. and Villeneuve, M., 2003, Provenance of the Mesoproterozoic (1.45 Ga) Belt Basin (Western North America): Another piece in the pre-Rodinia paleogeographic puzzle: *Geological Society of America Bulletin*, vol. 115. no. 10. p. 1191-1217.
- Schmidt, R. G., 1978, Rocks and mineral resources of the Wolf Creek Area, Lewis and Clark and Cascade Counties, Montana: *US Geological Bulletin* 1441, 91 p.
- Sears, J. W. and Alt, D., 1989, Impact origin of the Belt sedimentary basin: *Geological Society of America, Cordilleran Section, 85th annual meeting, and Rocky Mountain Section, 42nd annual meeting, Abstracts with Programs*. vol. 2. no. 5. p. 142.
- Sears, J. W., Chamberlain, K. R., and Buckley, S. N., 1998, Structural and U-Pb geochronological evidence for 1.47 Ga rifting in the Belt Basin, western Montana: *Canadian Journal of Earth Sciences*, vol. 35. p. 467-475.
- Sears, J. W., and Clements, P. S., 2000, Geometry and kinematics of the Blackfoot thrust fault and Lewis and Clark line, Bonner, Montana: *Geological Field Trips, Western Montana and Adjacent Areas, Roberts, Sheila and Winston, Don, eds. Geological Society of America, Rocky Mountain Section*. p. 123-130.
- Sears, J. W. and Price, R. A., 1978, The Siberian connection: A case for Precambrian separation of the North American and Siberian Cratons: *Geology*, vol. 6. no. 5. p. 267-270.
- Sears, J. W. and Price, R. A., 2003, Tightening the Siberian connection to western Laurentia: *Geological Society of America Bulletin*, vol. 115. no. 8. p. 943-953.
- Sklyarov, E. V., Gladkochub, D. P., Mazukabzov, A. M., Menshagin, Yu. V., Wantanabe, T., and Pisarevsky, S. A., 2003, Neoproterozoic mafic dike swarms of the Sharyzhalgai metamorphic massif, southern Siberian craton: *Precambrian Research*, vol. 122. p. 359-376.
- Sun, S. -S. and McDonough W. F., 1989, Chemical and isotopic systematics of ocean basalts: Implications for mantle compositions and processes: *in Magmatism and in the Ocean Basins, Saunders, A. D. and Norry, M. J., eds. Geological Society of London Special Publication* 42. p. 313-345.
- Walcott, C. D., 1910, Abrupt appearance of the Cambrian fauna on the North American Continent: *in Cambrian Geology and Paleontology II, Smithsonian Miscellaneous Collections*, vol. 57. p. 1-16.
- Walcott, C. D., 1914, Pre-Cambrian Algonkian algal flora: *Cambrian geology and Paleontology III, Smithsonian Miscellaneous Collections*, vol. 64. p. 77-156.

- Walcott, C. D., 1916, Evidences of primitive life: Smithsonian Institution Annual Report (1915), p. 235-255.
- Watson, I. A., 1984, Structure of the Rattlesnake area, west-central Montana: M. S. Thesis, University of Montana. 55p.
- Wells, J. D., 1974, Geologic map of the Alberton Quadrangle, Missoula, Sanders, and Mineral Counties: US Geological Survey Map GQ-1157, scale 1:62,500.
- White, R. S., 1992, Magmatism during and after continental break-up: in *Magmatism and the Causes of Continental Break-up*, Storey, B. C., Alabaster, T., Pankhurst, R. J., eds. The Geological Society Special Publication No. 68. p. 1-16.
- White, R. and McKenzie, D., 1989, Magmatism at Rift Zones: The generation of volcanic continental margins and flood basalts: *Journal of Geophysical Research*, vol. 94. no. B6. p. 7685-7729.
- Whipple, J. W., Mudge, M. R., and Earhart, R. L., 1987, Geologic map of the Rogers Pass Area, Lewis and Clark County, Montana: US Geological Survey Map I-1642, scale 1:48,000.
- Wilson, J. T., 1963, A possible origin of the Hawaiian Islands: *Canadian journal of Physic*, vol. 41. p. 863-870.
- Wingate, T. D., Campbell, Ian H., Compston, William, and Gibson, George M., 1998, Ion microprobe U-Pb ages for Neoproterozoic basaltic magmatism in south-central Australia and implications for the breakup of Rodinia: *Precambrian Research*, vol. 87. p. 135-159.
- Winston, D., 1986, Middle Proterozoic Tectonics of the Belt Basin, western Montana and northern Idaho: *Belt Supergroup, A Guide to Proterozoic Rocks of Western Montana and Adjacent Areas*. Roberts, Sheila, *ed.* Montana Bureau of Mines and Geology, Special Publication 94. p 245-257.
- Winston, D., 1989, Introduction to the Belt: Middle Proterozoic Belt Supergroup, Western Montana, Field Trip Guidebook T334, Winston, D., Horodyski, R. J., and Whipple, J. W., *eds.* 28th International Geological Congress, p. 1-?.
- Winston, D., 1990, Evidence for intracratonic, fluvial and lacustrine settings of middle to late Proterozoic basins of western USA: in *Mid-Proterozoic Laurentia Baltica*, Gower, C. F., Rivers, T., and Ryan, B., eds. Geological Association of Canada Special Paper 38, p. 535-564.

- Winston, D., 1993, Middle Proterozoic rocks of Montana, Idaho and eastern Washington: The Belt Supergroup: *in* Reed, J.C. Jr., Bickford, M. E., Houston, R. S., Link, P. K., Rankin, R. W., Sims, P. K., and Van Schmus, W. R., ed., Precambrian: Conterminous U.S., The Geology of North America, Vol. C-2: Decade of North American Geology, Geological Society of America, p. 487-517.
- Winston, D., 2003, Proposed revision of the Helena and Wallace Formations, mid-Proterozoic Belt Supergroup, Montana and Idaho: Northwest Geology, Tobacco Root Geological Society/Montana State University, vol. 32. p. 172-178.
- Zehnder, C., M., Mutter, J. C., and Buhl, P, 1990, Deep seismic and geochemical constraints on the nature of rift-induced magmatism during breakup of the North Atlantic: Tectonophysics, vol. 173. p. 545-565.

Appendix I
Site Location and Sample Descriptions

Sample Site Location: Alberton

GPS Coordinates: N47° 0' 90.8", W 114° 30' 68.21"

Strike and dip measurements:

(Taken from host rock)

Strike	Dip	Strike	Dip	Strike	Dip
220°	8	216°	16	228°	12

Sample Name: MT-AL-02

50-55% Plagioclase

30-40% Pyroxene – augite/pigeonite

1-3% Magnetite – diamond shaped, metallic in reflected light

1-2% Ilmenite – bladey, elongated

15-20% Epidote, hornblende, biotite, chlorite, apatite

1-3% quartz

Textures

Heavy saussuritization in groundmass and around large grains, plagioclase originally subhedral. Pyroxenes and plagioclase are equigranular and dominate the groundmass.

Grind time for XRF/ICP-MS analysis

5.0 minutes

Sample Site Location: Alberton

GPS Coordinates: N47° 0' 45.6", W 114° 29' 39.12"

Strike and dip measurements:

(Taken from host rock)

Strike	Dip	Strike	Dip	Strike	Dip
210°	35	234°	31	216°	40

Sample Name: MT-ALE-01

50-55% Plagioclase 1 mm

30-40% Pyroxene – augite/pigeonite 1 mm

1-5% Magnetite/ilmenite intergrowths.

15-20% Epidote, hornblende, biotite, chlorite, apatite

Textures

Pigeonite has a 2V of 2-3 degrees and low birefringence. The pyroxenes are slightly altered and there are rare lamellae of pigeonite in Augite. Micrographic textures are common in this sample.

Grind time for XRF/ICP-MS analysis: 4.0 minutes

Sample Site Location: Kootenai National Forest

GPS Coordinates: N 49° 0' 13.17", W 115° 41' 57.1"

Strike and dip measurements:

(Taken from host rock)

Strike	Dip	Strike	Dip	Strike	Dip
345°	31	351°	45	355°	40

Sample Name: MT-KF-01

Fine-grained, 100% altered. Only ghost like outlines remain of plagioclase, no pyroxene remnants remain.

Grind time for XRF/ICP-MS analysis: 2 minutes

Sample Site Location: Kootenai National Forest

GPS Coordinates: N 49° 0' 13.17", W 115° 41' 57.1"

Strike and dip measurements:

(Taken from host rock)

Strike	Dip	Strike	Dip	Strike	Dip
345°	31	351°	45	355°	40

Sample Name: MT-KF-02

35-40% Plagioclase 1.5 –2.5 mm

20-30% Pyroxene 1-2 mm

1-3% Magnetite/ilmenite

20-30% Epidote, hornblende, chlorite, apatite

Textures

All minerals affected by alteration, groundmass is almost 100% altered.

Grind time for XRF/ICP-MS analysis: 3 minutes

Sample Site Location: Kootenai National Forest

GPS Coordinates: N 49° 0' 13.17", W 115° 41' 57.1"

Strike and dip measurements:

(Taken from host rock)

Strike	Dip	Strike	Dip	Strike	Dip
345°	31	351°	45	355°	40

Sample Name: MT-KF-03

35-40% Plagioclase 1.5 –2.5 mm

20-30% Pyroxene 1-2 mm

1-3% Magnetite/ilmenite – altered to limonite

20-30% Epidote, hornblende, chlorite, apatite

Textures

All minerals affected by alteration especially around fractures, groundmass is almost 100% altered.

Grind time for XRF/ICP-MS analysis: 3.5 minutes

Sample Site Location: McDonald Reservoir

GPS Coordinates: N 47° 25' 35.8", W 113° 59' 04.1"

Strike and dip measurements:

(Taken from host rock)

Strike	Dip	Strike	Dip	Strike	Dip	Strike	Dip
154°	22	163°	14	100°	19	145°	10

Sample Name: MT-MR-01

50-60% Plagioclase 0.5 –0.75 mm

30-40% Pyroxene 0.5 –0.75 mm

1-5% Magnetite/ilmenite – altered to limonite

10-15% Epidote, hornblende, chlorite, apatite

1-2% quartz

Textures

Plagioclase and pyroxene grains are equigranular. Almost all plagioclase have undergone sericitization, all pyroxene grains have some uralitization. Micrographic texture is common in this sample.

Grind time for XRF/ICP-MS analysis: 3.5 minutes

Sample Site Location: McDonald Reservoir

GPS Coordinates: N 47° 25' 35.8", W 113° 59' 04.1"

Strike and dip measurements:

(Taken from host rock)

Strike	Dip	Strike	Dip	Strike	Dip	Strike	Dip
154°	22	163°	14	100°	19	145°	10

Sample Name: MT-MR-02

50-55% Plagioclase 1.5 –2 mm

40-50% Pyroxene 1-2 mm

1-5% Magnetite/ilmenite – altered to limonite

10-15% Epidote, hornblende, chlorite, apatite

Textures

Plagioclase not greatly affected by alteration. Almost all pyroxene grains have some uralitization. Micrographic and graphic textures are common in this sample.

Grind time for XRF/ICP-MS analysis: 3.5 minutes

Sample Site Location: Rogers Pass East (RPE)

GPS Coordinates: N 47° 07' 22.4", W 112° 21' 03.3"

Strike and dip measurements:

Strike	Dip	Strike	Dip	Strike	Dip
110°	22	100°	34	114°	38

Sample Name: MT-RPE-04

50-60% Plagioclase

30-35% Pyroxene – augite/pigeonite

1-5% Magnetite/ilmenite

15-20% Epidote, hornblende, biotite, apatite

Textures

Plagioclase and pyroxene grains are equigranular. While most plagioclase grains have undergone minor sericitization, all pyroxene grains have undergone severe uralitization in their cores and in most cases only remnants are left. The alteration minerals, epidote, hornblende and biotite are strongly associated with the pyroxene remnants.

Grind time for XRF/ICP-MS analysis: 2.0 minutes

Sample Site Location: Rogers Pass East (RPE)

GPS Coordinates: N 47° 07' 22.4", W 112° 21' 03.3"

Strike and dip measurements:

Strike	Dip	Strike	Dip	Strike	Dip
110°	22	100°	34	114°	38

Sample Name: MT-RPE-22

50-60% Plagioclase

30-35% Pyroxene – augite/pigeonite

1-5% Magnetite/ilmenite – limonite on some edges.

15-20% Epidote, hornblende, biotite, chlorite, apatite

Textures

Pigeonite has a 2V of 2-3 degrees and low birefringence. The pyroxenes are slightly altered and there are rare lamellae of pigeonite in Augite. Micrographic textures are common in this sample.

Grind time for XRF/ICP-MS analysis: 2.0 minutes

Sample Site Location: Rogers Pass Middle (RPM)

GPS Coordinates: N 47° 05' 13.6", W 112° 22' 14.6"

Strike and dip measurements:

Strike	Dip	Strike	Dip	Strike	Dip
313°	20	321°	19	310°	28

Sample Name: MT-RPM-01

40-50% Plagioclase – 1 mm in size, slightly altered to mica

30-40% Pyroxene – pigeonite lamellae – low 2V angle

1-5% Magnetite/ilmenite – fine-grained

5-10% Hornblende, biotite, chlorite, apatite

Groundmass

60-70% plagioclase of which 50 % has undergone sericitization.

30-40% pyroxene of which 90-80% has undergone sericitization.

Textures

Microporphyritic, subophitic. Limonite lines some fractures. Alteration occurs throughout sample, mostly in groundmass.

Grind time for XRF/ICP-MS analysis: 3.5 minutes

Sample Site Location: Rogers Pass Middle (RPM)

GPS Coordinates: N 47° 05' 13.6", W 112° 22' 14.6"

Strike and dip measurements:

Strike	Dip	Strike	Dip	Strike	Dip
313°	20	321°	19	310°	28

Sample Name: MT-RPM-02

35-45% Plagioclase – 1 mm in size, slightly altered to mica, some reverse zoning

30-40% Pyroxene

Augite – high birefringence, large 2V angle

Pigeonite – low birefringence, small 2V

1-5% Magnetite/ilmenite – limonite around edges

5-10% Epidote, hornblende, chlorite, apatite

Textures

Subophitic. Alteration occurs throughout sample, but also in localized zones of complete alteration. These zones are not associated with fractures.

Grind time for XRF/ICP-MS analysis: 3.0 minutes

Quartz Sample Blank

Sample Name: QTZ-01

Quartz blank used for analysis of contamination during sample preparation. Sample consists of pure coarse-grained quartz.

Grind time for XRF/ICP-MS analysis: 2.0 minutes

Granophyre

Sample Site Location: Turah

GPS Coordinates: N 46° 49' 39.13", W 113° 48' 20.32"

Sample Name: MT-TU-01

55-65% Plagioclase

15-20% Quartz

10-15% Feldspar

<1% Pyroxene

10-20% epidote, hornblende, biotite

Textures

The plagioclase is almost entirely altered to clay minerals, graphic intergrowths of quartz and feldspars and relic myrmekitic intergrowths of plagioclase and quartz are very common. The hornblende and epidote appear to be secondary alteration products. A few rare remnants of pyroxene are also present.

Granophyre

Sample Site Location: Holland Lake

GPS Coordinates: N 47° 24' 0.0", W 113° 34' 54"

Strike and dip measurements:

(Taken from host rock)

Strike	Dip	Strike	Dip	Strike	Dip
326°	28	336°	36	340°	30

Sample Name: MT-HL-13

55-65% Plagioclase 1 mm

25-35% Quartz

10-15% Feldspar

<1 % Pyroxene

1-5% Epidote, hornblende, biotite, apatite

Textures

Plagioclase grains have undergone almost 100 percent alteration, quartz, graphic and myrmekitic textures are very common, altered microcline and fresh quartz grains are also present.

Granophyre

Sample Site Location: Rogers Pass East (RPE)

GPS Coordinates: N 47° 07' 22.4", W 112° 21' 03.3"

Strike and dip measurements:

Strike	Dip	Strike	Dip	Strike	Dip
110°	22	100°	34	114°	38

Sample Name: RP-KRC-02-2

50-60% Plagioclase

15-20% Quartz

10-15% Feldspar

<1% Pyroxene

5-10% hornblende, biotite

Textures

Alteration of this sample is almost 100 percent and only faint grain boundaries remain, with, in rare cases, original twin extinction preserved in plagioclase and feldspars.

Remnant pyroxenes are present, but rare. Graphic and myrmekitic textures are very common.

Appendix II
Geochemical Data

		MT	MT	MT	MT	MT	MT	MT	MT	MT	MT	MT
	QTZ01	ALE01	ALE02	KF01	KF02	KF02	MR01	MR02	RPE04	RPE21	RPM01	RPM02
Date	9-Jul-03	9-Jul-03	9-Jul-03	9-Jul-03	9-Jul-03	9-Jul-03	10-Jul-03	10-Jul-03	10-Jul-03	10-Jul-03	10-Jul-03	10-Jul-03
	Unnormalized Major Elements (Weight %):										Unnormalized Major Elements (Weight %):	
SiO2	98.22	50.00	52.42	48.43	48.16	48.05	49.67	50.41	50.03	50.61	50.19	50.03
Al2O3	0.09	13.48	13.38	15.36	15.47	15.04	12.23	12.25	12.40	12.92	12.35	12.35
TiO2	0.000	2.498	2.019	2.928	2.515	2.835	2.859	2.555	2.872	2.245	2.872	2.844
FeO	0.02	14.61	11.17	14.21	13.66	13.73	16.00	15.33	15.97	14.22	16.07	15.79
MnO	0.000	0.216	0.215	0.190	0.192	0.207	0.249	0.237	0.231	0.223	0.232	0.235
CaO	0.21	9.74	7.25	6.70	8.08	8.77	9.48	9.78	9.21	9.98	9.32	8.99
MgO	0.04	4.98	6.95	4.09	4.55	4.29	5.00	5.50	4.85	5.82	4.89	4.85
K2O	0.01	0.73	1.58	1.90	2.30	1.34	0.76	0.77	0.70	0.65	0.72	0.83
Na2O	0.02	2.45	2.89	2.58	2.79	3.26	2.33	2.24	2.33	2.33	2.29	2.37
P2O5	0.000	0.224	0.210	0.514	0.471	0.531	0.256	0.225	0.252	0.212	0.255	0.252
Total	98.61	98.93	98.08	96.90	98.19	98.06	98.83	99.30	98.84	99.21	99.19	98.54
	Normalized Major Elements (Weight %):										Normalized Major Elements (Weight %):	
SiO2	99.60	50.54	53.45	49.98	49.05	49.00	50.26	50.77	50.62	51.01	50.60	50.77
Al2O3	0.09	13.63	13.64	15.85	15.76	15.34	12.37	12.34	12.55	13.02	12.45	12.53
TiO2	0.000	2.525	2.059	3.022	2.561	2.891	2.893	2.573	2.906	2.263	2.895	2.886
FeO*	0.02	14.77	11.38	14.67	13.91	14.01	†16.19	†15.44	†16.15	14.33	†16.20	†16.02
MnO	0.000	0.218	0.219	0.196	0.196	0.211	0.252	0.239	0.234	0.225	0.234	0.238
CaO	0.21	9.85	7.39	6.91	8.23	8.94	9.59	9.85	9.32	10.06	9.40	9.12
MgO	0.04	5.03	7.09	4.22	4.63	4.38	5.06	5.54	4.91	5.87	4.93	4.92
K2O	0.01	0.74	1.61	1.96	2.34	1.37	0.77	0.78	0.71	0.66	0.73	0.84
Na2O	0.02	2.48	2.95	2.66	2.84	3.32	2.36	2.26	2.36	2.35	2.31	2.41
P2O5	0.000	0.226	0.214	0.530	0.480	0.542	0.259	0.227	0.255	0.214	0.257	0.256

Table 1. XRF data.

		MT	MT	MT	MT	MT	MT	MT	MT	MT	MT	MT	
	QTZ01	ALE01	ALE02	KF01	KF02	KF02	MR01	MR02	RPE04	RPE21	RPM01	RPM02	
Date	9-Jul-03	9-Jul-03	9-Jul-03	9-Jul-03	9-Jul-03	9-Jul-03	10-Jul-03	10-Jul-03	10-Jul-03	10-Jul-03	10-Jul-03	10-Jul-03	
	Unnormalized Trace Elements (ppm):											Unnormalized Trace Elements (ppm):	
Ni	6	50	137	27	28	31	52	55	54	62	51	50	
Cr	0	70	299	44	37	35	67	101	65	108	66	63	
Sc	3	40	26	29	23	33	48	42	42	40	42	41	
V	0	422	308	222	183	209	480	467	470	417	463	470	
Ba	2	133	631	769	929	603	155	173	197	109	144	236	
Rb	2	25	45	55	60	40	25	26	28	20	28	34	
Sr	5	153	202	306	368	410	160	149	153	158	151	162	
Zr	18	167	162	256	236	255	185	180	186	156	189	199	
Y	1	42	28	43	40	42	46	43	47	41	47	47	
Nb	2.7	11.3	12.9	26.5	24.3	27.2	12.6	11.9	12.9	10.4	13.8	12.2	
Ga	1	26	20	26	25	29	22	26	23	24	24	23	
Cu	2	†303	123	17	20	72	†386	†241	†356	†275	†315	†366	
Zn	7	142	169	133	140	149	149	127	144	125	138	142	
Pb	0	5	5	4	6	0	16	6	6	4	4	8	
La	12	15	31	38	46	38	87	64	21	18	7	35	
Ce	19	55	48	88	74	76	40	33	39	24	52	25	
Th	0	2	5	6	3	4	6	2	6	2	5	2	
	Major elements are normalized on a volatile-free basis, with total Fe expressed as FeO.										Major elements are normalized on a volatile-free basis, with total Fe expressed as FeO.		
	"†" denotes values >120% of our highest standard.											"†" denotes values >120% of our highest standard.	

Table 1 continued.

Sample ID	La ppm	Ce ppm	Pr ppm	Nd ppm	Sm ppm	Eu ppm	Gd ppm
BUR QTZ-01	0.21	0.47	0.03	0.11	0.02	0.01	0.03
BUR MT-ALE-01	14.44	33.45	4.50	21.33	6.64	2.13	7.48
BUR MT-AL-02	20.19	43.20	5.35	23.80	6.23	1.77	6.15
BUR MT-KF-01	41.09	77.01	9.95	43.10	9.93	2.98	9.24
BUR MT-KF-02	37.93	72.77	9.39	39.77	9.32	2.86	8.77
BUR MT-KF-03	40.31	81.84	9.86	42.77	9.95	3.27	9.35
BUR MT-MR-01	16.08	36.76	4.92	23.91	7.32	2.28	8.60
BUR MT-MR-02	14.70	33.80	4.52	21.88	6.75	2.08	7.85
BUR MT-RPE-04	15.57	35.58	4.81	23.01	7.12	2.22	8.37
BUR MT-RPE-21	12.67	29.31	3.98	19.00	5.92	1.87	6.83
BUR MT-RPM-01	15.74	36.17	4.88	23.44	7.34	2.26	8.46
BUR MT-RPM-02	15.65	36.04	4.82	23.15	7.17	2.23	8.32
BUR MT-RPE-04 ®	15.22	34.86	4.63	22.48	7.00	2.13	8.12

Table 2. ICP-MS data.

Sample ID	Tb ppm	Dy ppm	Ho ppm	Er ppm	Tm ppm	Yb ppm	Lu ppm
BUR QTZ-01	0.00	0.02	0.01	0.02	0.00	0.03	0.01
BUR MT-ALE-01	1.34	8.11	1.66	4.35	0.63	3.78	0.58
BUR MT-AL-02	0.97	5.53	1.09	2.72	0.38	2.21	0.34
BUR MT-KF-01	1.44	8.43	1.67	4.35	0.60	3.59	0.58
BUR MT-KF-02	1.36	7.94	1.54	4.04	0.56	3.34	0.52
BUR MT-KF-03	1.46	8.40	1.68	4.29	0.60	3.52	0.56
BUR MT-MR-01	1.50	9.28	1.90	4.93	0.70	4.29	0.67
BUR MT-MR-02	1.38	8.61	1.75	4.63	0.65	4.03	0.62
BUR MT-RPE-04	1.46	8.95	1.83	4.82	0.68	4.17	0.65
BUR MT-RPE-21	1.23	7.62	1.53	4.13	0.58	3.51	0.54
BUR MT-RPM-01	1.50	9.20	1.89	4.96	0.71	4.28	0.66
BUR MT-RPM-02	1.46	9.14	1.85	4.97	0.70	4.26	0.67
BUR MT-RPE-04 ®	1.44	9.01	1.81	4.83	0.69	4.16	0.65

Table 2 continued.

Sample ID	Ba ppm	Th ppm	Nb ppm	Y ppm	Hf ppm	Ta ppm	U ppm
BUR QTZ-01	1	0.07	2.51	0.19	0.54	4.69	1.19
BUR MT-ALE-01	137	2.75	10.70	42.31	4.60	1.06	0.69
BUR MT-AL-02	617	3.83	11.14	27.42	4.39	0.99	0.92
BUR MT-KF-01	765	3.64	25.64	43.94	6.38	1.69	0.52
BUR MT-KF-02	920	3.35	23.51	41.12	5.96	1.61	0.50
BUR MT-KF-03	609	3.57	26.31	42.80	6.39	1.73	0.52
BUR MT-MR-01	161	3.07	12.16	48.51	5.22	1.33	0.77
BUR MT-MR-02	159	2.94	11.25	45.13	5.03	1.32	0.72
BUR MT-RPE-04	198	3.06	11.83	46.73	5.13	1.01	0.70
BUR MT-RPE-21	119	2.61	9.86	39.48	4.30	1.50	0.64
BUR MT-RPM-01	144	3.12	12.08	48.32	5.31	1.15	0.80
BUR MT-RPM-02	226	3.21	12.30	47.16	5.49	1.13	0.73
BUR MT-RPE-04 ®	196	3.14	12.00	47.12	5.24	1.01	0.71

Table 2 continued.

Sample ID	Pb ppm	Rb ppm	Cs ppm	Sr ppm	Sc ppm	Zr ppm
BUR QTZ-01	0.45	0.3	0.00	3	0.0	16
BUR MT-ALE-01	5.82	26.0	2.06	154	43.4	160
BUR MT-AL-02	5.35	45.4	1.94	202	31.3	157
BUR MT-KF-01	3.99	55.6	0.92	310	32.7	251
BUR MT-KF-02	6.57	60.4	0.86	374	29.4	231
BUR MT-KF-03	6.01	39.0	0.34	422	33.1	250
BUR MT-MR-01	10.73	25.6	1.39	163	46.6	181
BUR MT-MR-02	4.58	26.8	1.22	150	48.5	176
BUR MT-RPE-04	4.36	28.1	4.21	153	46.0	179
BUR MT-RPE-21	4.03	21.5	1.07	157	46.6	147
BUR MT-RPM-01	5.06	27.6	1.90	153	46.4	184
BUR MT-RPM-02	6.66	33.5	2.90	160	45.7	191
BUR MT-RPE-04 ®	4.36	28.5	4.21	154	45.4	180

Table 2 continued.

	Line Numbers	"Na2O Oxide Percents"	Al2O3 Oxide Percents	FeO Oxide Percents	K2O Oxide Percents	CaO Oxide Percents
Un 7 MTMR01cr3 coreplag	111	5.34	24.76	0.52	0.52	8.05
	112	6.14	27.18	0.51	0.56	8.78
	113	6.01	27.49	0.34	0.76	8.54
Un 9 MTMR01cr4 corepig [actually kspar]	117	0.75	19.09	0.28	15.68	0.16
Un 12 MTMR01cr6 coreplag	120	5.33	24.55	0.45	0.43	7.74
Un 15 MTMR01cr8 coreplag	123	6.06	27.09	0.39	0.49	9.19
Un 19 MTMR01cr9 coreplag	126	4.48	27.24	0.45	0.47	10.35
Un 20 MTMR01cr11 coreplag	127	4.10	27.79	0.71	0.45	11.05
Un 23 MTRPM01 cr01 plag	136	5.83	27.74	0.61	0.55	9.59
Un 25 MTRPM01 cr02 coreplag	138	4.31	29.58	0.50	0.29	12.22
Un 29 MTRPM01 cr08 coreplag	142	3.96	29.98	0.52	0.18	13.25
Un 30 MTRPM01 cr06 coreplag	143	4.65	28.18	0.56	0.30	11.69
Un 33 MTRPM01 cr11 coreplag	146	4.69	28.46	0.63	0.42	11.32
Un 35 MTRPE22 cr01 coreplag	148	4.12	28.68	0.53	0.26	12.76
Un 39 MTRPE22 cr03 core plag	151	4.30	30.58	0.56	0.27	12.26
Un 44 MTRPE22 cr08 coreplag	159	4.18	28.81	0.61	0.26	12.64
Un 45 MTRPE22 cr09 coreplag	160	4.28	27.49	0.61	0.23	12.08
Un 48 MTRPM02 cr01 coreplag	172	4.90	29.19	0.62	0.35	11.31
Un 54 MTRPM02 cr06 coreplag	178	5.00	28.79	0.60	0.29	11.31
Un 55 MTRPM02 cr05 coreplag	179	5.24	28.64	1.01	0.45	10.66
Un 58 MTRPM02 cr03 coreplag	182	5.23	28.98	0.59	0.40	10.76
Un 59 MTRPM02 cr03 rimplag	183	4.89	29.53	0.50	0.28	11.55
Un 63 MTRPM02 cr01 coreplag	187	5.67	28.61	0.59	0.40	9.91
Un 64 MTRPM02 cr01 coreplag2	188	5.12	29.34	0.72	0.34	11.16
Un 74 MTALE01 cr07 coreplag	198	4.36	29.58	0.61	0.27	12.78
Un 75 MTALE01 cr08 coreplag	199	4.26	30.14	0.70	0.27	12.91
Un 76 MTALE01 cr09 coreplag	200	5.45	28.15	0.63	0.36	10.52
Un 77 MTALE01 cr10coreplag	201	5.11	28.66	0.71	0.32	11.18
Un 78 MTRPE04 cr01 coreplag	202	3.83	30.74	0.70	0.25	13.17
	203	3.71	30.41	0.59	0.20	13.43
Un 80 MTRPE04 cr03 coreplag	205	4.86	29.57	0.46	0.49	11.39
Un 81 MTRPE04 cr04 coreplag	206	4.89	29.31	0.60	0.40	11.12
Un 84 MTRPE04 cr07 coreplag	209	3.07	27.73	0.89	0.30	12.12
Un 88 MTRPE04 cr07 rimplag	213	4.65	28.15	0.92	0.37	11.45
Un 90 MTMR02 cr02 coreplag	215	4.61	29.65	0.53	0.33	11.51
	216	3.26	21.61	0.38	0.25	8.63
Un 91 MTMR02 cr03 coreplag	217	4.57	30.19	0.37	0.25	12.03
Un 95 MTMR02 cr07 coreplag	222	4.58	29.63	0.47	0.34	10.75

Table 3. Electron microprobe data for plagioclase.

	SiO2 Oxide Percents	MgO Oxide Percents	MnO Oxide Percents	TiO2 Oxide Percents	Cr2O3 Oxide Percents	Oxide Totals
Un 7 MTMR01cr3 coreplag	58.94	0.00	0.00	0.00	0.00	98.14
	56.32	0.00	0.00	0.00	0.00	99.49
	56.03	0.00	0.00	0.00	0.00	99.17
Un 9 MTMR01cr4 corepig [actually kspar]	63.82	0.00	0.03	0.01	0.01	99.85
Un 12 MTMR01cr6 coreplag	59.17	0.00	0.00	0.00	0.00	97.67
Un 15 MTMR01cr8 coreplag	56.42	0.02	0.00	0.10	0.01	99.76
Un 19 MTMR01cr9 coreplag	56.69	0.00	0.00	0.00	0.00	99.67
Un 20 MTMR01cr11 coreplag	54.53	0.00	0.00	0.00	0.00	98.62
Un 23 MTRPM01 cr01 plag	56.21	0.05	0.01	0.17	0.00	100.77
Un 25 MTRPM01 cr02 coreplag	52.87	0.00	0.00	0.00	0.00	99.76
Un 29 MTRPM01 cr08 coreplag	51.92	0.00	0.00	0.00	0.00	99.81
Un 30 MTRPM01 cr06 coreplag	54.37	0.00	0.00	0.00	0.00	99.74
Un 33 MTRPM01 cr11 coreplag	53.71	0.00	0.00	0.00	0.00	99.23
Un 35 MTRPE22 cr01 coreplag	53.03	0.00	0.00	0.00	0.00	99.37
Un 39 MTRPE22 cr03 core plag	51.96	0.00	0.00	0.00	0.00	99.94
Un 44 MTRPE22 cr08 coreplag	53.72	0.00	0.00	0.00	0.00	100.24
Un 45 MTRPE22 cr09 coreplag	55.29	0.00	0.00	0.00	0.00	99.99
Un 48 MTRPM02 cr01 coreplag	52.97	0.00	0.00	0.00	0.00	99.34
Un 54 MTRPM02 cr06 coreplag	53.64	0.00	0.00	0.00	0.00	99.63
Un 55 MTRPM02 cr05 coreplag	53.77	0.00	0.00	0.00	0.00	99.76
Un 58 MTRPM02 cr03 coreplag	54.10	0.00	0.00	0.00	0.00	100.06
Un 59 MTRPM02 cr03 rimplag	53.09	0.00	0.00	0.00	0.00	99.84
Un 63 MTRPM02 cr01 coreplag	54.81	0.00	0.00	0.00	0.00	100.00
Un 64 MTRPM02 cr01 coreplag2	53.64	0.00	0.00	0.00	0.00	100.32
Un 74 MTALE01 cr07 coreplag	52.25	0.00	0.00	0.00	0.00	99.86
Un 75 MTALE01 cr08 coreplag	51.99	0.00	0.00	0.00	0.00	100.28
Un 76 MTALE01 cr09 coreplag	55.09	0.00	0.00	0.00	0.00	100.19
Un 77 MTALE01 cr10coreplag	54.22	0.00	0.00	0.00	0.00	100.20
Un 78 MTRPE04 cr01 coreplag	51.28	0.00	0.00	0.00	0.00	99.97
	50.79	0.00	0.00	0.00	0.00	99.12
Un 80 MTRPE04 cr03 coreplag	53.41	0.00	0.00	0.00	0.00	100.18
Un 81 MTRPE04 cr04 coreplag	53.66	0.00	0.00	0.00	0.00	99.98
Un 84 MTRPE04 cr07 coreplag	55.91	0.00	0.00	0.00	0.00	100.02
Un 88 MTRPE04 cr07 rimplag	56.16	0.00	0.00	0.00	0.00	101.71
Un 90 MTMR02 cr02 coreplag	52.65	0.00	0.00	0.00	0.00	99.29
	52.61	0.00	0.00	0.00	0.00	86.72
Un 91 MTMR02 cr03 coreplag	52.73	0.00	0.00	0.00	0.00	100.13
Un 95 MTMR02 cr07 coreplag	50.90	0.00	0.00	0.00	0.00	96.67

Table 3 continued.

	Line Numbers	Na2O Oxide Percents	MgO Oxide Percents	Al2O3 Oxide Percents	FeO Oxide Percents	MnO Oxide Percents	
Un 4	MTMR01cr01 corepig	109	0.18	17.68	3.07	14.47	0.31
Un 5	MTMR01cr02 coreaug	110	0.31	13.97	2.80	12.66	0.25
Un 8	MTMR01cr4 coreaug	115	0.19	15.61	3.01	13.26	0.31
Un 9	MTMR01cr4 corepig	116	2.66	0.11	15.68	0.55	0.00
Un 10	MTMR01cr4 corepig	118	0.18	6.75	1.31	25.86	0.54
Un 11	MTMR01cr5 coreaug	119	0.29	15.15	2.98	12.15	0.28
Un 13	MTMR01cr7 coreaug	121	0.17	8.47	1.45	23.40	0.48
Un 14	MTMR01cr7 corepig	122	0.58	12.86	3.52	22.39	0.41
Un 17	MTMR01cr8 corepig	124	0.28	14.68	3.16	11.73	0.24
Un 18	MTMR01cr9 laminaug	125	0.25	8.05	1.17	16.36	0.34
Un 22	MTRPM01 cr01coreaug	135	0.33	12.05	2.29	13.17	0.28
Un 24	MTRPM01 cr02 pig	137	0.32	14.96	2.75	11.91	0.25
Un 26	MTRPM01 cr03 laminaug	139	0.20	14.24	1.93	13.75	0.35
Un 27	MTRPM01 cr04 lcore pig	140	0.18	17.08	2.91	14.60	0.40
Un 28	MTRPM01 cr05 core pig	141	0.24	16.17	2.97	14.79	0.33
Un 31	MTRPM01 cr07 coreaug	144	0.26	15.49	2.56	13.61	0.27
Un 32	MTRPM01 cr09 corepig	145	0.24	14.11	2.13	11.17	0.36
Un 34	MTRPM01 cr12 laminaug	147	0.27	15.55	2.97	13.94	0.33
Un 37	MTRPE22 cr02 coreaug	149	0.21	15.18	2.10	11.67	0.22
Un 38	MTRPE22 cr02 corepig	150	0.07	14.93	1.95	26.16	0.48
Un 40	MTRPE22 cr04 coreaug	152	0.15	15.00	1.82	16.20	0.35
Un 41	MTRPE22 cr05 corepig	153	0.12	12.94	1.06	22.60	0.47
Un 42	MTRPE22 cr06 coreaug	154	0.24	14.83	1.99	13.63	0.32
Un 43	MTRPE22 cr07 coreaug	155	0.31	12.75	2.36	12.15	0.24
Un 49	MTRPM02 cr02 corepig	173	0.16	15.03	2.15	18.20	0.41
Un 50	MTRPM02 cr02 coreaug	174	0.24	14.70	3.13	12.62	0.28
Un 51	MTRPM02 cr08 corepig	175	0.20	15.79	2.10	15.58	0.34
Un 52	MTRPM02 cr08 coreaug	176	0.24	14.84	2.41	13.05	0.30
Un 53	MTRPM02 cr07 laninaug	177	0.53	15.33	2.56	17.73	0.37
Un 56	MTRPM02 cr04 laminaug	180	0.10	17.38	0.95	23.43	0.49
Un 57	MTRPM02 cr04 coreaug	181	0.24	15.74	2.45	12.32	0.28
Un 60	MTRPM02 cr02 coreaug	184	0.20	15.19	1.84	15.60	0.33
Un 61	MTRPM02 cr02 corepig	185	0.71	12.58	5.33	20.75	0.35
Un 62	MTRPM02 cr01 corepig	186	0.17	15.82	2.12	16.41	0.39
Un 66	MTALE01 cr01 laminaug	190	0.26	12.86	1.62	17.73	0.40
Un 67	MTALE01 cr01 coreaug	191	0.22	13.77	2.02	16.76	0.37
Un 68	MTALE01 cr02 coreaug	192	0.29	14.37	2.72	13.60	0.33
Un 69	MTALE01 cr03 coreaug	193	0.23	13.46	1.80	16.98	0.33
Un 70	MTALE01 cr04 corepig	194	0.06	13.81	1.02	29.02	0.60
Un 71	MTALE01 cr04 corepig2	195	0.10	17.59	1.20	22.46	0.46
Un 72	MTALE01 cr06 coreaug	196	0.28	13.50	3.12	13.15	0.28
Un 73	MTALE01 cr06 corepig	197	0.08	17.31	1.48	20.85	0.45
Un 79	MTRPE04 cr02 coreaug	204	0.21	16.20	2.80	14.27	0.33
Un 82	MTRPE04 cr05 coreaug	207	0.21	15.60	3.11	13.95	0.29

Table 4. Electron microprobe data for pyroxene.

	Line Numbers	Na2O Oxide Percents	MgO Oxide Percents	Al2O3 Oxide Percents	FeO Oxide Percents	MnO Oxide Percents
Un 83 MTRPE04 cr06 corepig	208	0.16	15.32	2.64	13.58	0.30
Un 85 MTRPE04 cr08 coreaug	210	0.21	15.89	2.73	14.54	0.34
Un 86 MTRPE04 cr010 laminaug	211	0.09	18.64	1.95	16.32	0.37
Un 87 MTRPE04 cr010 coreaug	212	0.31	14.84	3.44	11.61	0.23
Un 89 MTMR02 cr01 coreaug	214	0.37	10.91	3.46	22.49	0.42
Un 92 MTMR02 cr04 coreaug	218	0.49	10.32	3.91	22.46	0.33
Un 93 MTMR02 cr05 coreaug	219	0.51	9.02	3.29	22.52	0.37
Un 94 MTMR02 cr06 coreaug	220	0.30	3.18	1.43	5.73	0.11
	221	0.20	12.80	2.77	10.74	0.23
Un 97 MTMR02 cr06 coreaug,rpt aft re-coating	223	0.88	6.64	5.96	25.66	0.38
	224	0.57	6.68	4.81	26.23	0.34

Table 4 continued.

	TiO2 Oxide Percents	K2O Oxide Percents	CaO Oxide Percents	SiO2 Oxide Percents	Cr2O3 Oxide Percents	Oxide Totals
Un 4 MTMR01cr01 corepig	1.01	0.00	12.36	50.40	0.11	99.59
Un 5 MTMR01cr02 coreaug	0.88	0.01	18.18	50.26	0.02	99.34
Un 8 MTMR01cr4 coreaug	0.95	0.02	11.89	54.26	0.14	99.65
Un 9 MTMR01cr4 corepig	0.09	0.35	6.46	67.91	0.00	93.81
Un 10 MTMR01cr4 corepig	0.71	0.01	12.33	49.57	0.00	97.27
Un 11 MTMR01cr5 coreaug	0.91	0.00	17.33	50.35	0.05	99.49
Un 13 MTMR01cr7 coreaug	0.52	0.01	15.78	49.16	0.00	99.43
Un 14 MTMR01cr7 corepig	0.84	0.11	9.65	48.64	0.02	99.01
Un 17 MTMR01cr8 corepig	0.81	0.00	15.75	51.90	0.07	98.61
Un 18 MTMR01cr9 laminaug	0.53	0.01	7.89	65.10	0.04	99.73
Un 22 MTRPM01 cr01coreaug	0.69	0.06	13.27	56.50	0.08	98.71
Un 24 MTRPM01 cr02 pig	0.85	0.01	17.78	52.10	0.13	101.08
Un 26 MTRPM01 cr03 laminaug	0.59	0.02	8.88	60.26	0.02	100.25
Un 27 MTRPM01 cr04 lcore pig	0.86	0.00	12.89	51.21	0.13	100.27
Un 28 MTRPM01 cr05 core pig	0.76	0.01	13.17	51.80	0.03	100.27
Un 31 MTRPM01 cr07 coreaug	0.80	0.00	15.89	52.02	0.08	100.99
Un 32 MTRPM01 cr09 corepig	0.68	0.03	11.98	56.65	0.11	97.47
Un 34 MTRPM01 cr12 laminaug	0.83	0.01	15.34	51.34	0.03	100.62
Un 37 MTRPE22 cr02 coreaug	0.76	0.01	17.57	52.14	0.08	99.95
Un 38 MTRPE22 cr02 corepig	0.54	0.03	5.61	50.21	0.03	100.02
Un 40 MTRPE22 cr04 coreaug	0.66	0.00	15.16	51.62	0.09	101.05
Un 41 MTRPE22 cr05 corepig	0.51	0.01	10.47	50.53	0.02	98.72
Un 42 MTRPE22 cr06 coreaug	0.75	0.01	16.55	52.16	0.06	100.52
Un 43 MTRPE22 cr07 coreaug	0.76	0.03	14.94	53.99	0.09	97.62
Un 49 MTRPM02 cr02 corepig	0.96	0.01	13.02	50.44	0.03	100.39
Un 50 MTRPM02 cr02 coreaug	0.88	0.00	16.84	50.70	0.10	99.49
Un 51 MTRPM02 cr08 corepig	0.84	0.00	13.31	51.15	0.10	99.40
Un 52 MTRPM02 cr08 coreaug	0.89	0.01	17.34	50.92	0.08	100.09
Un 53 MTRPM02 cr07 laninaug	0.67	0.07	9.87	50.85	0.01	97.98
Un 56 MTRPM02 cr04 laminaug	0.43	0.00	5.63	51.89	0.00	100.30
Un 57 MTRPM02 cr04 coreaug	0.75	0.00	16.72	51.49	0.12	100.10
Un 60 MTRPM02 cr02 coreaug	0.64	0.00	14.96	51.59	0.01	100.36
Un 61 MTRPM02 cr02 corepig	0.51	0.53	10.03	48.40	0.02	99.21
Un 62 MTRPM02 cr01 corepig	0.73	0.04	11.18	52.08	0.05	98.98
Un 66 MTALE01 cr01 laminaug	0.99	0.00	15.91	50.73	0.00	100.49
Un 67 MTALE01 cr01 coreaug	0.90	0.00	16.02	50.83	0.03	100.95
Un 68 MTALE01 cr02 coreaug	0.97	0.01	16.79	50.35	0.08	99.51
Un 69 MTALE01 cr03 coreaug	0.96	0.00	15.43	50.91	0.01	100.11
Un 70 MTALE01 cr04 corepig	0.57	0.00	5.00	50.65	0.02	100.73
Un 71 MTALE01 cr04 corepig2	0.53	0.02	6.21	51.66	0.04	100.28
Un 72 MTALE01 cr06 coreaug	1.22	0.00	18.90	50.13	0.07	100.64
Un 73 MTALE01 cr06 corepig	0.55	0.00	7.79	51.44	0.02	99.96
Un 79 MTRPE04 cr02 coreaug	0.82	0.01	14.37	51.15	0.11	100.27
Un 82 MTRPE04 cr05 coreaug	0.90	0.00	15.56	50.69	0.11	100.43

Table 4 continued.

	TiO2 Oxide Percents	K2O Oxide Percents	CaO Oxide Percents	SiO2 Oxide Percents	Cr2O3 Oxide Percents	Oxide Totals
Un 83 MTRPE04 cr06 corepig	0.78	0.00	16.67	51.45	0.11	101.01
Un 85 MTRPE04 cr08 coreaug	0.96	0.00	14.68	50.49	0.06	99.90
Un 86 MTRPE04 cr010 laminaug	0.64	0.00	9.93	51.95	0.09	99.99
Un 87 MTRPE04 cr010 coreaug	1.04	0.02	18.03	50.69	0.15	100.35
Un 89 MTMR02 cr01 coreaug	0.41	0.10	9.43	51.73	0.06	99.39
Un 92 MTMR02 cr04 coreaug	0.46	0.11	10.09	49.73	0.08	97.97
Un 93 MTMR02 cr05 coreaug	0.10	0.20	10.33	49.89	0.00	96.22
Un 94 MTMR02 cr06 coreaug	0.13	0.07	3.96	34.31	0.00	49.22
	0.65	0.00	12.82	44.68	0.09	84.98
Un 97 MTMR02 cr06 coreaug,rpt aft re-coating	0.50	0.35	10.82	47.82	0.01	99.02
	0.35	0.12	10.89	49.61	0.00	99.60

Table 4 continued.

Oxide	1	2	3	4	5	6	7	8
SiO ₂	45.44	44.81	48.27	45.5	48.28	51.91	47.00	47.49
TiO ₂	2.43	2.55	2.20	3.1	.82	1.25	3.60	3.29
Al ₂ O ₃	13.69	13.96	8.58	15.0	9.36	15.31	16.44	14.54
Fe ₂ O ₃	6.06	3.75	4.06	3.5	2.14	0.98	3.31	3.36
FeO	15.12	16.66	22.89	10.4	11.54	9.36	12.34	11.80
MnO	0.21	0.17	0.26	0.2	0.12	0.08	0.04	n.d.
MgO	7.60	5.54	1.12	8.1	17.48	7.52	3.32	6.10
CaO	6.15	8.53	7.42	8.7	7.00	9.71	9.57	9.70
Na ₂ O	2.20	3.35	2.65	2.6	1.59	2.30	3.38	2.60
K ₂ O	0.70	0.33	0.34	0.4	0.41	0.79	0.67	1.12
H ₂ O	0.24	0.34	1.13	1.7	0.99	0.93	n.d.	n.d.
H ₂ O -	0.07	0.19	0.37	1.0	0.06	0.15	n.d.	n.d.
P ₂ O ₅	Tr.	0.08	0.65	0.3	0.11	0.18	0.33	n.d.
CO ₂	0.1
Total	99.97	100.26	100.03	99.99	99.90	100.42	100.0	100.0

- 1.) Milltown Dam ferrodiabase.
- 2.) Hortonolite ferrograbbro, Wager and Deer, 1939, Skaergaard.
- 3.) Fayalite ferrograbbro, Wager and Deer, 1939, Skaergaard.
- 4.) Average plateau basalt, Mull, 1924.
- 5.) Olivine diabase, Palisade sill, N.J., Walker, 1940.
- 6.) Average undifferentiated diabase, Walker, 1940.
- 7.) Diabase dike, Sudbury, Ontario, T. L. Walker, 1897.
- 8.) Diabase dike, Rockport, N.Y., Washington, 1899.

Table 5. Geochemical data from wet geochemical analysis. (Eisenbeis, 1958).

[Columns 3, 4, and 8: rapid rock analyses by P. L. D. Elmore, S. D. Elmore, S. D. Botts, I. H. Barlow, and G. W. Chloé, U.S. Geol. Survey, July 28, 1961; Columns 1, 2, 5, 6, and 7: rapid rock analyses by P. L. D. Elmore, L. Artis, G. W. Chloé, J. Kelsey, S. D. Botts, J. E. Glenn, and H. Smith, U.S. Geol. Survey, December 5, 1967]

	1	2	3	4	5	6	7	*8
Laboratory No. -----	W169254	W169258	158041	158042	W169259	W169240	W169257	158039
Field No. -----	WC64-4	WC65-3	WC60-5	WC60-15	WC66-3	WC59-10	WC65-2	WC59-14
SiO ₂ -----	43.0	49.3	50.8	52.8	62.4	65.8	69.7	76.1
Al ₂ O ₃ -----	14.2	13.9	16.7	16.0	17.8	15.4	16.6	13.3
Fe ₂ O ₃ -----	7.1	14.6	5.4	3.9	1.7	1.4	.84	.42
FeO -----	6.3	2.4	4.4	3.4	2.3	.96	.14	.23
MgO -----	5.6	3.0	4.4	6.1	1.5	1.9	.09	.13
CaO -----	11.3	7.5	7.0	5.1	5.7	3.9	.84	.31
Na ₂ O -----	4.6	2.6	3.3	4.8	3.9	4.8	4.6	4.1
K ₂ O -----	1.1	.65	3.1	2.7	2.2	3.8	5.5	4.1
H ₂ O+ -----	2.7	2.4	3.3	2.0	1.7	.92	.85	.72
H ₂ O- -----	.19	.16						
TiO ₂ -----	2.2	2.7	.60	1.1	.36	.50	.10	.04
P ₂ O ₅ -----	.88	.40	.44	.74	.00	.26	.04	.03
MnO -----	.18	.25	.18	.12	.11	.04	.07	.06
CO ₂ -----	.61	.10	<.05	<.05	.15	.08	.42	<.05
Total -----	99.96	99.96	99.62	98.76	100.06	100.04	99.94	99.54

1. Analcime gabbro; dike intruding western facies of Two Medicine Formation, 200 feet northeast of Dearborn River, in SW1/4 sec. 23, T. 17 N., R. 5 W., Comb Rock quadrangle.

2. Gabbro; sill intruding Empire Formation of Belt Supergroup, 0.25 mile west of Greenpole Creek, in NW1/4 sec. 21, T. 15 N., R. 5 W., Roberts Mountain quadrangle.

3. Augite trachybasalt; dike intruding eastern facies of Two Medicine Formation, 1 mile northwest of Nohrgang Ranch, in SE1/4 sec. 36, T. 16 N., R. 4 W., Wolf Creek quadrangle.

4. Hornblende monzonite; dike intruding Adel Mountain Volcanics of Lyons (1944), 0.1 mile east of Sevenmile Road, in SW1/4 sec. 29, T. 18 N., R. 3 W., Wolf Creek quadrangle.

5. Rhyolite porphyry; sill intruding Spokane Formation of Belt

Supergroup, 1.5 miles east of Rogers Mountain, in SW1/4 sec. 31, T. 15 N., R. 4 W., Roberts Mountain quadrangle.

6. Quartz monzonite porphyry; sill intruding sedimentary member of western facies of Two Medicine Formation, north side of Deadman Coulee Road, in SW1/4 sec. 8, T. 16 N., R. 4 W., Comb Rock quadrangle.

7. Quartz monzonite porphyry; sill intruding Helena Dolomite and Empire Formation of Belt Supergroup, 0.4 mile southeast of Rogers Mountain, in NE1/4 sec. 2, T. 14 N., R. 5 W., Roberts Mountain quadrangle.

8. Rhyolite; dike or sill intruding Kevin Member of Marias River Shale, crest of Black Rock, in NE1/4 sec. 7, T. 17 N., R. 4 W., Comb Rock quadrangle.

Table 6. Geochemical data from Schmidt (1978)

	Group IIIA								
	MBT-3	-5	-22	-23	-24	-30	-51	-81	-109
SiO ₂	51.34	52.28	51.87	52.52	52.32	52.42	52.85	52.14	51.79
Al ₂ O ₃	11.89	12.43	11.84	12.39	12.46	12.54	12.6	12.7	13.5
Fe ₂ O ₃ *	16.19	15.94	16.45	16.01	16.74	16.87	17.31	17.32	17.57
MgO	4.46	4.50	4.59	4.51	4.47	4.61	4.90	4.75	4.80
CaO	7.82	8.24	8.33	8.38	8.37	8.44	8.61	8.84	9.16
TiO ₂	2.85	2.90	2.86	2.85	2.86	2.87	2.85	2.64	2.87
Na ₂ O	2.60	3.24	2.48	2.56	2.50	2.66	3.19	2.49	2.49
K ₂ O	1.19	1.14	1.04	1.12	1.07	1.01	.95	.969	.883
H ₂ O	1.7		1.4	.5	.6	.53			
Σ	100.04		100.86	100.84	101.39	101.95			
Rb	52	44	43	47	42	38	45	32	28
Sr	188	168	174	168	175	181	194	186	171
K/Rb	190	215	201	198	211	221	175	251	262
Rb/Sr	.28	.26	.24	.28	.24	.21	.23	.17	.18
K/Sr	52	56	49	55	51	46	41	43	43
U	1.1	.92	1.2	.93	1.0	1.7	3.7		
Th	4.6	5.0	4.5	4.6	5.1	4.1	8.9		
Th/U	4.2	5.4	3.7	4.9	5.1	2.4	2.4		

Table 7. Geochemical data from Mueller (1971).